ISBN 978-82-471-2737-7 (printed ver.)
ISBN 978-82-471-2738-4 (electronic ver.)
ISSN 1503-8181

Doctoral theses at NTNU, 2011:102

Limin Yang

Stochastic dynamic system analysis of wave energy converter with hydraulic power take-off, with particular reference to wear damage analysis

Limin Yang
Doctoral Thesis

NTNU
Norwegian University of
Science and Technology

Doctoral theses at NTNU, 2011:102

NTNU
Norwegian University of
Science and Technology

NTNU
Norwegian University of
Science and Technology
Thesis for the degree of
philosophiae doctor
Faculty of Engineering Science and Technology
Department of Marine Technology

NTNU
Norwegian University of
Science and Technology

Limin Yang

Stochastic dynamic system analysis of wave energy converter with hydraulic power take-off, with particular reference to wear damage analysis

Thesis for the degree of philosophiae doctor

Trondheim, May 2011

Norwegian University of
Science and Technology
Faculty of Engineering Science and Technology
Department of Marine Technology

NTNU
Norwegian University of
Science and Technology

NTNU
Norwegian University of Science and Technology

Thesis for the degree of philosophiae doctor

Faculty of Engineering Science and Technology
Department of Marine Technology

ISBN 978-82-471-2737-7 (printed ver.)
ISBN 978-82-471-2738-4 (electronic ver.)
ISSN 1503-8181

Doctoral Theses at NTNU, 2011:102

Printed by Tapir Uttrykk

Abstract

The study of the renewable energy has drawn increasing attention in the recent years. Wave energy with its relatively high power density is a major resource that has remained untapped until recently. Different types of wave energy converters have been proposed for extracting the energy from the waves. In this thesis, a heaving semi-submerged buoy, moving relative to a fixed reference to drive hydraulic power take-off, was studied.

To meet stringent in-service and operational requirements, the components of a wave energy converter (WEC) need to have high levels of reliability and availability. Hence, it is necessary to develop mathematical models that enable a numerical solution with sufficient accuracy and computational efficiency, and apply these models to assess the energy capture and the safety and availability of the system based on relevant reliability theory.

The studied wave energy converter system consists of several subsystems, i.e., a floating buoy, a hydraulic pump, check valves, transmission lines, accumulators, a hydraulic motor and an electric generator, where energy is converted between several energy domains, and each belongs to a different engineering discipline. An integrated dynamic model in the state space form was established for this system of components. The dynamic characteristic of the considered wave energy converter system was studied, with particular reference to high frequency oscillations (HFO) of the buoy and the transient pressures in the pipelines.

High frequency oscillations (HFOs), as defined in this thesis, refer to the motions of the buoy that oscillates at frequencies much higher than those of the incident waves. HFOs were observed in the time interval when no fluid was pumped or sucked between the hydraulic pump and accumulators. This type of motion is mainly caused by the fluid compressibility of the hydraulic pump. The analytical solutions of the oscillating frequencies, which depend on the hydraulic cylinder parameters, were derived in this study. The results show that the HFOs contribute significantly to the wear damage of the hydraulic pump, especially to the wear loss of cylinder bore. Because of the notable effect on the wear estimation, a dynamic wave energy converter model that can describe the HFOs is developed in the thesis.

The transient pressure in the pipeline, which accompanies any sudden change in the rate of fluid flow, was another detrimental load studied in the thesis. The magnitudes of the transient pressures can be many times larger than the normal operating pressure and may cause fatigue and catastrophic failures. This fact raises the question of how to predict and mitigate the pressure pulsations. In this study, pipeline dynamics were taken into account in the form of modal representations. In addition, to predict the opening and closing times of the valve operation, which directly affect the magnitude of the transient pressures, a dynamic model of the check valves is also introduced. By combining the subsystem models of pipelines and check valves with the models of other subsystems employed in the wave energy converter system, the transient pressures were calculated numerically. Moreover, the effect of the pipelines connected between the hydraulic pump and check valves on the electric power production is also investigated in this research work.

The hydraulic pump, which converts the kinetic energy of the buoy into hydraulic energy of the working fluid, plays an important role in the proposed wave energy converter system. Wearing of the piston rings and cylinder bore significantly contribute to hydraulic pump failure. This research focuses on wear damage of the piston rings and cylinder bore under random sea state conditions. An abrasive wear model that considers the effect of the sealed pressure, lubrication condition, surface roughness, material properties, relative velocity and the cutting efficiency was developed. Based on the wear model and hypothesis of linear cumulative loss, a $\dot{W} - T_f$ approach (wear work rate versus time duration for wear damage growth till failure) was provided to estimate the piston ring wear resistance. By taking into account the occurrence probability of each sea state, a long-term wear damage estimation model was finally derived and given in the thesis. Because it is very time consuming to calculate the wear damage by considering all of the sea states, focus should be on the sea states that represent the most significant contribution to wear. In this thesis, the relative contribution of wear for the piston ring and cylinder bore from different sea states was calculated. The primary sea states contributing to wear can be found easily from the obtained figures.

The last topic of this research work is to construct modal bond graphs for the transmission lines. To model a pipeline with fluid pressures and flow rates at its two ends (i.e., the upstream side and downstream side) as input-output variables, four possible boundary conditions—pressure inputs at both ends, flow rate inputs at both ends and the two cases of mixed inputs—should be taken into account. The pipeline dynamics can be approximately modelled with modal models, which can be represented in the bond graph forms. To derive the modal models, two methods, separation of variables (SOV) and rational transfer function (RTF*) may be used. In

this thesis, modal bond graph representations were reviewed and new bond graph models were proposed for combinations of the solution methods and input-output configurations not yet presented in the literature, which include a bond graph for the two mixed input cases developed using the SOV technique and bond graphs for the other two cases (i.e., pressure inputs or flow rate inputs) constructed based on RTF solutions. It is found that the modal models derived by SOV and RTF have the same accuracy when the same number of modes is employed. With the developed bond graph models, the pipelines which are coupled with any other dynamic elements and systems can be modelled and analysed straightforwardly.

RTF* is used herein to represent the modal approximation method developed by Hullender et al. (1981). The basic idea of this method is to represent the transcendental transfer functions of the pipeline model in the Laplace domain as finite sum approximations of low-order rational transfer functions. In this research, the abbreviation “RTF” is used to represent this method.

Acknowledgements

The research work in this thesis was supported by the Research Council of Norway (RCN) through the Centre for Ships and Ocean Structures (CeSOS) at the Norwegian University of Science and Technology (NTNU).

Most of all, I wish to thank my supervisor, Professor Torgeir Moan. Thank you for giving me the opportunity to perform this work in Norway. During the past years, Prof. Moan taught me to identify and perform research, which are the most valuable things I gained in my PhD period. His innovative ideas and insightful understanding in the field of marine engineering form the solid basis of this thesis; his supervision and advice have always been useful for keeping me on track when my ideas have been diverging; his continuous encouragement has always been the best and most effective method to motivate me to overcome the difficulties I have met. It is my great pleasure to be one of his students.

I would also like to acknowledge my collaborator, Dr. Jørgen Hals, for the pleasant discussions, valuable comments and helpful suggestions. His broad knowledge of renewable energy laid a solid foundation for my research. It is only because of him that I have gone so far.

Sincere thanks are extended to Associate Professor Zhen Gao for his useful advice on stochastic simulations, structural reliability and system risk analysis. Thanks also go to Associate Professor Eilif Pedersen, who helped me in the early stages of developing the WEC model by using bond graph method. I am also very grateful to Professor Emeritus Hallvard Engja for his timely help and valuable guidance for this work. In addition, Professor Emeritus Kristan Tønder and Professor Roy Johnsen also gave me great help in the wear damage analysis of the seals. Their kind help is greatly appreciated.

All of the people at CeSOS and the Department of Marine Technology worked together to create an international, competitive and cooperative research environment, which made my PhD life pleasant and unforgettable. I would like to thank all the professors and my colleagues for their kind help in the past several years, including Professor Emeritus Johannes Falnes, Professor Dag Myrhaug, Sigrid Bakken Wold,

Karelle Gilbert, Marianne Kjølås, Linda Grønstad, Dr. Yanlin Shao, Dr. Muk Chen Ong, Dr. Huirong Jia, Zhenhui Liu, Suji Zhu, Decao Yin, Wenbin Dong, Shaoji Fang, Bo Zhao, Øyvind Ygre Rogne and many others. Special thanks to my roommate Biao Su, who shared my PhD life throughout this study period.

Finally, I want to give my special thanks to my parents and sister in China. Their motivation and emotional support have been the main support for me to study and live abroad during these years.

Trondheim, December, 2010
Limin Yang

Nomenclature

General Rules:

Bold symbols denote vectors or matrices. Dots over symbols represent differentiation with respect to time. In the symbol list, the units of dimensionless variables are represented by [].

Symbols:

β	[Pa]	bulk modulus of fluid
ς	[]	position ratio of valve stem/stroke
$\xi(t)$	[]	modal general coordinate of the flow rate in the pipe
$\eta(t)$	[]	modal general coordinate of the pressure in the pipe
σ	[m]	root-mean-square value of surface height
λ	[]	dimensionless film thickness
ρ	[kg/m^3]	density
γ	[]	ratio of specific heat
υ_0	[m^2/s]	kinetic viscosity of fluid
ω	[rad/s]	angular frequency
B	[1/s]	fluid friction coefficient
Ω	[]	open area ratio of valve
Δ	[]	ring wear damage at failure
A, B, C	[]	state-space matrices
a	[m/s]	acoustic velocity
A	[m^2]	cross sectional area
A_∞	[kg]	added mass coefficient at infinite frequency
B	[N·s/m]	damping coefficient
C_d	[]	discharged coefficient of the valve
D	[m]	diameter
E	[Pa]	Young's modulus
F	[N]	force
$F(x,t)$	[N/m]	externally applied force on the pipeline fluid per length
g	[m/s^2]	acceleration of gravity
$G(x)$	[]	mode shape of flow rate

$H(x)$	[]	mode shape of fluid pressure
H_s	[m]	significant wave height
k	[m^2/N]	wear coefficient
K	[N/m]	stiffness coefficient
$K(\lambda)$	[]	modified wear factor related to λ
K_0	[m^2/N]	wear coefficient at boundary lubrication regime
$K(t)$	[N/m]	retardation function
L	[m]	length
m	[kg]	mass
N	[N]	normal load
P	[Pa]	pressure
Q	[m^3/s]	fluid flow rate
R	[m]	radius
RaK	[]	ratio of the stiffness coefficients
Re	[]	Reynolds number
s	[m]	sliding distance
S	[N/m]	hydrostatic coefficient
$S_Q(x,t)$	[m^2/s]	volume flow into the pipe per length
t	[s]	time
t_c	[s]	valve closure time
t_R	[m]	ring thickness
T	[s]	time interval of operation
T_c	[]	dimensionless valve closure time
T_f	[s]	ring life duration during steady state operation
T_p	[s]	spectral peak wave period
T_r	[s]	return period of the propagation wave in the pipe
T_w	[s]	propagating time of the wave pressure in the pipe
T	[]	transfer function matrix
u	[m/s]	fluid velocity in the pipeline
V	[m^3]	geometric volume
w	[kg/s]	mass flow
WeV	[m^3]	wear volume loss
$\dot{W}$	[N/m·s]	instantaneous wear work rate
X	[m]	position coordinate
z	[]	additional state-space vector

Abbreviations:

FDM	frequency domain modification method
FORM	first order reliability method
HFO	high frequency oscillation
LFO	low frequency oscillation
ODE	ordinary differential equation

PDE	partial differential equation
PTO	power take-off
R&D	research and development
RTF	rational transfer function method
SORM	second order reliability method
SOV	separation of variables
SSC	steady state correction
WEC	wave energy converter

Superscripts:

PP	[P_{up}, P_{down}] as output
PQ	[P_{down}, Q_{up}] as output
QQ	[Q_{up}, Q_{down}] as output

Subscripts:

0	initial or default value
A, B	upper/lower cylinder chamber
c	hydraulic cylinder bore
cyl	hydraulic cylinder
down	downstream end of a pipeline
end	end stopper
exc	exciting wave force
f	friction
fluid	working fluid in the WEC system
gen	electric generator
hm	hydraulic motor
HP	high-pressure accumulator
in	inlet fluid flow
le	external leakage
li	internal leakage
line	transmission line
LP	low-pressure accumulator
out	outlet flow
p	piston
r	rod
R	radiation force
t	tubing
tr	threshold Reynolds number of transient flow
up	upstream end of a pipeline
val	check valve
wp	water pressure

List of appended papers

This thesis is presented in the form of a collection of five papers that are reported in Appendix A.

Paper A: Yang, L., Hals, J., and Moan, T., Analysis of dynamic effects relevant for the wear damage in hydraulic machines for wave energy conversion, Ocean Engineering, Vol. 37, No. 13, pp. 1089-1012, 2010.

Paper B: Yang, L., and Moan, T., Cylinder bore wear damage analysis of a heaving-buoy wave energy converter with hydraulic power take-off, In the Proceedings of the ASME 29th International Conference of Offshore Mechanics and Arctic Engineering, OMAE2010-20164, Shanghai, China, June 6-11, 2010.

Paper C: Yang, L., and Moan, T., Numerical modeling of wear damage in seals of a wave energy converter with hydraulic power take-off under random loads, Tribology Transactions, Vol. 54, No. 1, pp. 44-56, 2011.

Paper D: Yang, L., and Moan, T., Dynamic analysis of wave energy converter by incorporating the effect of hydraulic transmission lines, Submitted for publication, 2010.

Paper E: Yang, L., Hals, J., and Moan, T., Comparative study of bond graph models of hydraulic transmission lines with transient flow dynamics, Submitted for publication, 2010.

The following paper worked out during the study is not included in the thesis because it overlaps somewhat with **Paper A**.

Paper F: Yang, L., Hals, J., and Moan, T., A wear model for assessing the reliability of wave energy converter in heave with hydraulic power take-off, In the Proceedings of 8th European Wave and Tidal Energy Conference, Uppsala, Sweden, pp. 874-881, September 7-10, 2009.

Contents

1. Introduction

1.1. Background on wave energy

Wave energy is a nonpolluting and renewable source of energy that is converted naturally from wind energy above the oceans. The study of wave power is said to have started hundreds of years ago, and the first patent was registered in 1799 (David, 1995). As petroleum became the most important modern energy, the interest in wave energy utilisation faded after the First World War (Falnes, 2007). Modern research into exploiting energy from waves was stimulated by the oil crisis in 1973 (Salter, 1974) and then almost ceased due to the falling oil price in the 1980s. Recently, because of continuously increasing energy consumption and the rising level of CO_2, harnessing energy from waves is once again an important area of study. A detailed description of the historical development of wave energy can be found in the literature (e.g., Drew et al., 2009; Falnes, 2007; Hals, 2010; Thorpe, 1999).

The worldwide potential of wave power resources is on the order of 1–10 TW (1 terawatt=10^{12} W) (Panicker, 1976 and Thorpe, 1999), a quantity that is comparable to the primary world energy consumption. Although wave energy is only a small portion of solar and wind energy, sea waves offer the highest energy density among these three energy sources and are much more persistent (Falnes, 2007). Thus, there are good prospects for developing commercial wave-power plants, which may become a significant power resource for many coastal nations in the future.

The energy of sea waves can be transformed into electrical power or used to drive desalination plants etc by wave energy converters (WEC). Today, the majority of wave converters are used to produce electricity, although some concepts for pumping seawater, e.g., in sea farming, have also been developed. Various types of wave energy converters are being investigated, but many are in the research and development (R&D) stage. Generally, WECs are classified into three types: point absorber, terminator and attenuator (Cruz, 2008). A point absorber is a device that possesses small physical dimensions relative to the incident wave length (e.g., a type supplied by Ocean Power Technology); a terminator WEC is positioned in the sea with its dominant direction perpendicular to the incident wave direction, and Salter's Duck, developed at the University of Edinburgh, is one example of this type (Cruz,

2008, Chapter 2). The last WEC type, an attenuator, is a device that lies parallel to the incident wave direction with its beam much smaller than its length. An example of this type of WEC is Pelamis, which is developed by Ocean Power Delivery Ltd (Cruz, 2008, Section 5.4).

In this thesis, point absorbers are used to capture the energy from the sea waves. Compared with the other two types of absorbing devices, point absorbers possess a large power-to-volume ratio, which implies a large ratio of absorbed power to submerged buoy volume (Hals et al., accepted for publication). It is also attractive in terms of modelling because the scattered wave field can be neglected and forces on the submerged buoy are only due to the incident waves (Cruz, 2008). Moreover, due to its relatively small physical dimensions, wave direction is not important for this type of absorber.

The point-absorbing WECs have been studied since the 1970s in Norway. Two main contributors are Kjell Budal and Johannes Falnes. They studied oscillating wave-power-absorption theoretically in 1975 (Budal and Falnes, 1975) and 1978 (Falnes and Budal, 1978). Their proposed latching method for phase control and advocated reasonable small buoys are admitted and used as the basic concept for wave energy studies. Relevant research, including testing at the laboratory scale and under real-sea conditions, on this type of WEC has been carried out by many researchers (e.g., Evans, 1981; French and Bracewell, 1986; Pizer, 1993; Vantorre et al., 2004).

The main mechanism that can be implemented to convert waves into mechanical and/or electrical energy is called a power take-off (PTO) or power conversion system. The three main PTOs are air turbines, direct-coupled electric generators and hydraulic pumps (Cruz, 2008). The hydraulic pump system is generally known as hydraulic power take-off and includes a hydraulic cylinder, a motor, gas accumulators and an electric generator. This type of PTO converts the oscillatory motion of the buoy into hydraulic power through the use of a hydraulic pump, which then drives the shaft with a hydraulic motor connected to a generator (Falcão, 2007). This configuration is used by many researchers for energy conversion (e.g., Bjarte-Larsson and Falnes, 2006; Eidsmoen, 1995; Falcão, 2008; Hals et al., 2007). Comparing the three converters, hydraulic PTOs have some special properties such as the relatively smaller size, less weight and better energy storage (Mueller, 2002). In this thesis, an oil-hydraulic system is adopted due to the advantages mentioned above.

The research in this work focused on a heaving semi-submerged sphere absorber moving relative to a fixed reference and equipped with hydraulic power take-off for energy conversion. Figure 1.1 shows a sketch diagram of this wave energy converter

system. During operation, the oscillating motion of this floating buoy is converted into the flow of a liquid (oil is used here) at high pressure through the use of a hydraulic cylinder. The pumped fluid then flows into a high-pressure accumulator for short-term energy storage. A hydraulic motor uses this high-pressure fluid from the high-pressure accumulator to drive a connected electric generator. Hence, this power conversion system includes different energy domains, such as wave energy, hydraulic energy, electric energy and mechanical energy. In order to reduce the complexity of the WEC system model, it is useful to divide the whole system into several subsystems: a wave-buoy, a hydraulic pump, pipelines, check valves, accumulators, a hydraulic motor and an electric generator. The models of these subsystems are based on basic physical laws in the relevant domain and are dispersed in different publications. Hence, developing a complete WEC model by combining the interactions of the subsystems with correct energy flow comes to the first objective of this research.

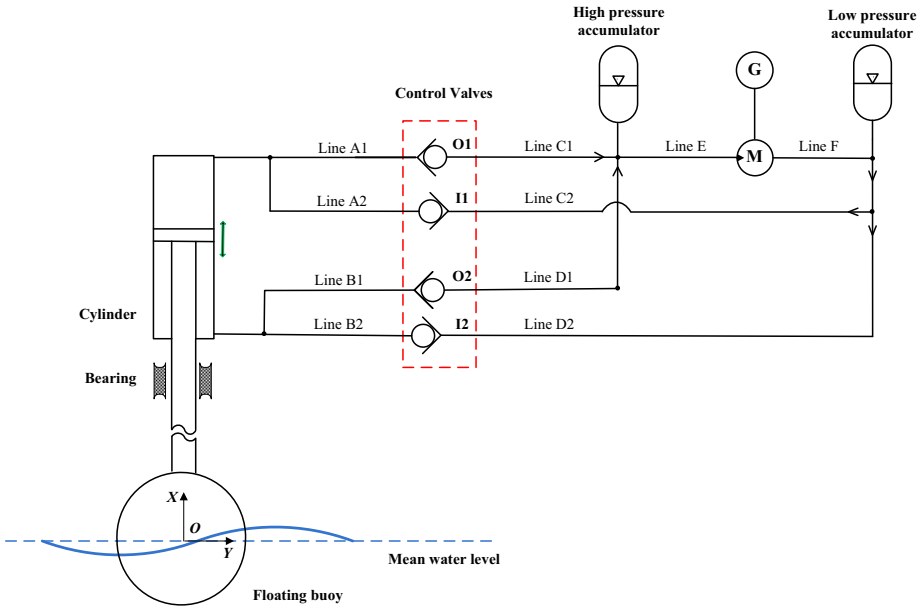

Figure 1.1: Sketch of a wave energy converter consisting of a heaving sphere connected to the hydraulic power take-off. The hydraulic PTO includes a hydraulic pump, gas accumulators, check valves, hydraulic pipelines and a motor. An electric generator is connected to the hydraulic PTO. The bearings are used to restrict the buoy motion. The coordinate system is fixed with respect to the mean position of the buoy with positive X vertically upwards, and the origin is set in the plane of the undisturbed surface.

1.2. Pipeline dynamics

Hydraulic pipelines, which are used to transport the working fluid between the hydraulic pump and motor, are important components in the wave energy converter system. These lines play a significant role in achieving the desired energy conversion efficiency and durability of the wave energy converter system. Because of the compressibility and inertia of the fluid, the fluid pressure waves propagate at the speed of sound, which is about a=1000 m/s for oil. For a pipeline with length L_{pipe}, the time for the pressure waves to propagate through the pipeline is $T_w=L_{pipe}/a$. Consequently, if the pipeline is short, e.g., L_{pipe} =1 m, the corresponding propagation time is 1 ms (one thousandth of a second). Thus, the pressure differences in the pipeline will disappear after 1 ms. In this case, it is reasonable to assume that the pipeline is a static device. However, for long pipelines, the propagation time introduces a time delay that may be significant if the exciting input frequency approaches the resonance frequency of the pipelines (Egeland and Gravdahl, 2002; Van Schothorst et al., 1994). With this time delay, both the pressures and fluid flows at the upstream side of the pipeline have to be distinguished from those at the downstream side.

In addition to problems associated with the time delays, a severe problem is that the wave pressure may be reflected at the end of the pipeline (Pierre, 2010), which may cause strong pressure fluctuations in the system and increase the failure probabilities for both the pipelines and the system. This pressure fluctuation (in some literature, this induced pressure is also called water hammer pressure) can be generated by, for instance, sudden valve actuation or pump failure. A typical pressure wave temporal trace for a water hammer event resulting from a sudden valve closure is shown in Fig. 1.2. The water hammer pressures in the pipeline are a source of noise and may significantly influence the reliability and performance of the system. Consequently, in the design of the pipeline, both normal operating pressures as well as water hammer pressures need to be considered.

The power take-off system shown in Fig. 1.1 employs four self-acting check valves to control the fluid flow. In this system, no feedback signals are supplied. This kind of PTO can be considered to be a passive hydraulic power take-off (Hals et al., 2007). These check valves connected to the pipelines are dynamic boundaries during their actuation, i.e., opening or closing, and represent one of the main causes of fluid transients. The transient flow from one steady state to another can cause water hammer pressures. Depending on the time interval of the transient, pressure waves can easily generate enough energy to damage the system (Záruba, 1993). Estimating the magnitude of the water hammer pressure with reasonable accuracy by

incorporating the dynamic responses of the absorber is another topic examined in this research.

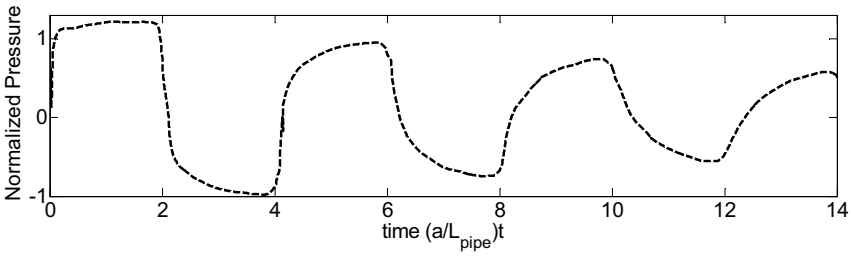

Figure 1.2: Results of a water hammer experiment that are reproduced from Holmboe and Rouleau (1967). In this figure, the pressure response is normalised by $\rho g \Delta u$, where ρ is fluid density, g is acceleration of gravity and u is the initial fluid velocity in the pipe.

Iberall (1950) seems to have developed the first analytical solutions of the fluid dynamic behaviour in the rigid circular pipelines. Later, extensive studies have been done on describing the fluid pressure wave propagation of the transmission lines. Many scientific publications and books are available for characterising the fluid transients and in developing proper modelling techniques. The pressure propagation can be modelled by mass, momentum and energy conservation equations (Chevary and Mathieu, 1993). However, energy conservation is commonly neglected due to the rapidness of the transient phenomenon (Ghidaoui et al., 2007). By applying the mass and momentum balance equation, the pipeline system can be described as partial differential equations (PDE) in the form of the wave equation (Stecki and Davis, 1986). For a single line with length L_{pipe} and radius R_{pipe} as described in Fig. 1.3, a one-dimensional wave equation of the pipeline can be expressed in terms of fluid pressure P and flow rate Q (Karnopp, 1975):

$$\frac{\partial P(x,t)}{\partial t} + \frac{\rho a^2}{A_{pipe}} \frac{\partial Q(x,t)}{\partial x} = \frac{\rho a^2}{A_{pipe}} S_Q(x,t) \tag{1.1}$$

$$\frac{\partial Q(x,t)}{\partial t} + \frac{A_{pipe}}{\rho} \frac{\partial P(x,t)}{\partial x} = \frac{F(x,t)}{\rho} \tag{1.2}$$

where A_{pipe} is the cross section area of the pipe, ρ is the fluid density, $F(x,t)$ is any externally applied force per length and $S_Q(x,t)$ represents volume flow into the pipe per length. Finite wall stiffness can be taken into account by correcting the fluid bulk modulus β and corresponding acoustic velocity a, as shown by Wylie et al. (1993), but this effect is neglected in this thesis. With the assumption of laminar flow, the

fluid friction losses can be modelled using the Hagen-Poiseuille equation (White, 1999): $F_f(x,t) = \rho \mathrm{B} Q(x,t)$. The friction coefficient B depends on the fluid kinematic viscosity υ_0 and the effective radius of the pipeline R_{pipe} and can be expressed as $\mathrm{B} = 8\upsilon_0 / R_{pipe}^2$.

The partial differential equations (1.1) and (1.2) can be formulated analytically in the frequency domain by applying the Laplace transform (Iberall, 1950; Karam and Franke, 1967; Nichols, 1962). The dissipative viscosity and heat transfer effects can be included directly. The pipeline model in the frequency domain, which relates the signals at the ends of pipelines, can handle arbitrary pipeline boundary conditions and is proved to be a useful tool for the analysis and design of hydraulic pipelines. However, for simulation in system synthesis or analysis, time domain solutions are often desirable.

The method of characteristics is a simple and accurate method for transmission line transient analysis (Wylie et al., 1993) in the time domain and has been widely used in many practical applications for numerical simulation purposes (e.g., Streeter, 1971; Pierre, 2010). The disadvantage of this method is that it is based on a fixed discretisation in the time-distance plane. It is not easy to incorporate the model into a coupled simulation system with variable time steps (Mäkinen et al., 2000).

To avoid the weakness of the method of characteristics, modal approximation methods based on the infinite product representation of a hyperbolic transfer function (Oldenburger and Goodson, 1964) were developed by Hullender and co-workers (Hullender and Healy, 1981; Hullender and Hsue, 1983; Hsue and Hullender, 1983). Using this model approximation technique, the transmission line dynamics can be characterised as a series of damped resonance modes. Each mode of the transmission line can be represented in a linear state space form (Yang and Tobler, 1991; Van Schothorst, 1997; Ayalew and Kulakowski, 2005) that can be added directly to Ordinary-Differential-Equation (ODE)-based simulation systems. This modal approximation model, in which the physical structure and parameters are preserved, is quite useful for modelling a complex fluid system. Moreover, compared with other approximate approaches, the modal method has its own advantages, such as being numerical stability, ease of use and high accuracy (Watton and Tadmori, 1988). Because of these features, the approximation model is widely used in different hydraulic systems, e.g., hydraulic servo-systems (Jelali and Kroll, 2003).

Another alternative modal approach, based on normal modes in which distributed parameter components can be represented approximately by a finite number of normal modes, was introduced by Karnopp (1975) for a pipeline model with no friction losses. By using the separation of variables (SOV) technique, a set of

decoupled ordinary differential equations can be obtained for each of the normal modes. Each normal mode equation can be solved separately in the time domain. Considerable work has also been reported by Lebrun (1984, 1985) and Skarbø and Engja (1990), for example.

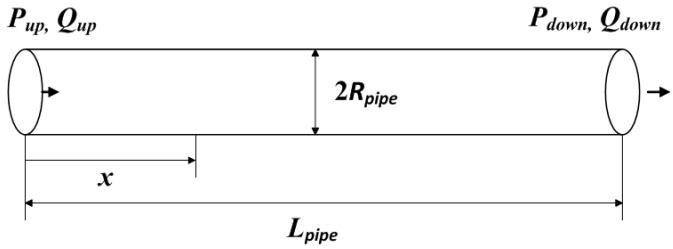

Figure 1.3: Schematic of a one-dimensional fluid transmission line. The line has length L_{pipe} and radius R_{pipe}, and P and Q are the fluid pressure and flow rate, respectively. The subscripts "up" and "down" refer to the upstream and downstream ends.

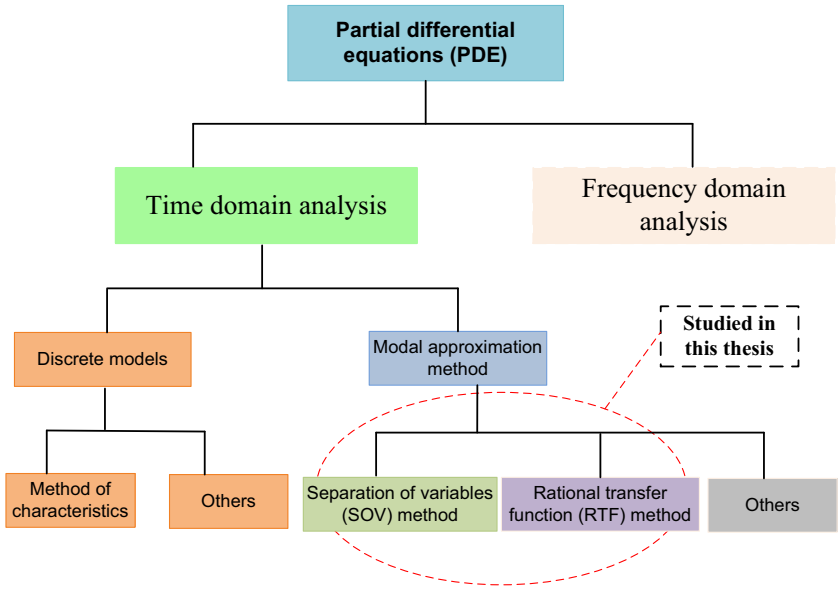

Figure 1.4: Chart showing different methods for solving the transmission line problem.

Other approximation methods, e.g., Viersma's Discrete Model (Viersma, 1980) and Pawlik's Discrete Model (Jelali and Kroll, 2003), may also be used to solve the partial differential equations of the pipelines. However, these methods are not discussed further in this thesis. An overview of different approaches for analysis of the transmission line problem is given in Fig. 1.4. Taking the complexity and

nonlinearity of the studied wave energy converter system into account, the two modal models mentioned above (one developed by Hullender et al. (1983) and the other by Karnopp (1975)) are adopted to develop the WEC system model. In this research, the Hullender's approximate model is simply represented as "RTF" (rational transfer function), while the modal model suggested by Karnopp is denoted as "SOV" (separation of variables).

1.3. Safety assessment – wear in the WEC

It is important that the WEC produces power and survives under extreme and repetitive environmental loads. Therefore, wave energy converter systems need to have a high level of reliability and availability to meet stringent in-service and operational requirements. Assessing the safety of a wave energy converter is essential to the design of a conversion system, which leads to the third purpose of this thesis.

Large systems can fail if their components fail. The hydraulic power take-off system considered herein consists of a large number of basic components, such as hydraulic cylinders, pistons, piston rings, nonreturn check valves, hydraulic pipelines etc. The failure modes mainly include fatigue, wear and overload.

Generally, the design strength of marine structures, e.g., platforms, has to fulfil the ultimate and fatigue criteria (Moan, 2008). The corresponding limit state criteria are defined by limit states for ultimate failure (ULS–ultimate limit state) and fatigue failure (FLS–fatigue limit state), respectively. Ultimate limit states are generally based on extreme load effects, while fatigue failure is mainly caused by repetitive loading. For the wave energy converter, another failure mode, wear, is also very important. The focus of this thesis is on wear loss analysis of the hydraulic pump used in this WEC system.

Wear occurs when the surfaces of engineering components are loaded together and subjected to sliding and/or rolling (Archard, 1980). The reciprocating motion of the piston in the hydraulic cylinder can cause wear damage both on the piston rings, which are normally used for sealing the working fluid, and the cylinder bore. According to previous studies, wear is the prevailing failure mode of the hydraulic piston rings (Dahlheimer, 1972; Peterson and Winer, 1980) and cylinder bore (Becker and Ludema, 1999; Giorgio et al., 2007). For this wave energy converter system, piston rings are used in a double-acting cylinder to prevent leakage between the upper and lower chambers with different fluid pressures (Fig. 1.5). Contact surface wear loss can cause leakage, which may result in the following:

a. Loss in system power;

b. Lack of control and loss of sensitivity and accuracy in response;

c. Loss in volumetric efficiency;

d. Resultant system malfunction.

Therefore, it is very important to determine the wear limit state (WLS) for the WEC system in design. In this research, only WLS was studied for the hydraulic pump components. A detailed introduction of the wear in a hydraulic pump is supplied in Chapter 4.

Since only few papers about the structural risk and reliability analysis for the WEC system have been published in the recent decades, I hope this research will increase knowledge of safety evaluations for WEC systems related to different sea states and close the gap between theory and practice by combining various science disciplines. The results from this research are expected to increase knowledge in both scientific and technical areas, and the long term aim is to enhance interdisciplinary collaboration.

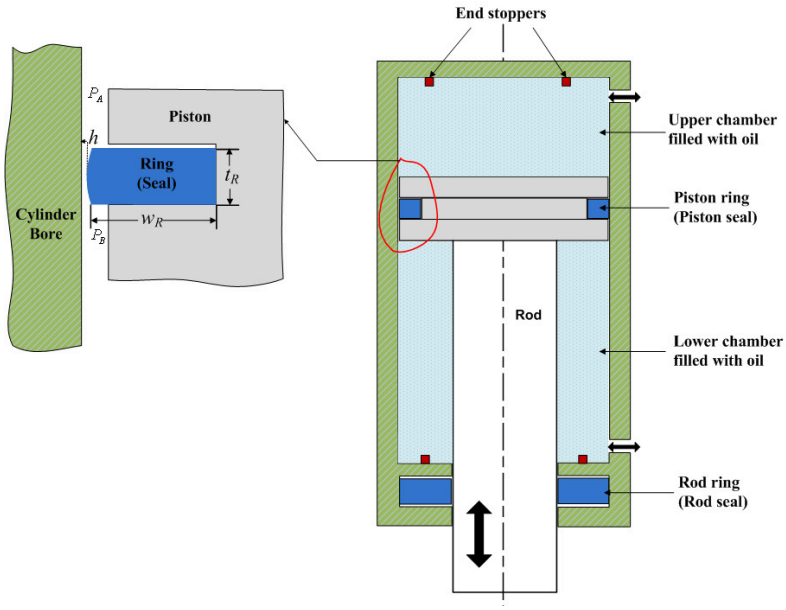

Figure 1.5: Sketch of a piston pump with sealing elements and end stoppers. The pump consists of a hydraulic cylinder filled with oil, a piston, a piston rod and seals. In the figure, P_A and P_B are the oil pressures of the chambers; h is the clearance between the ring and cylinder bore; and t_R and w_R are the thickness and width of the ring, respectively.

1.4. Thesis

1.4.1. Objectives and scope of work

Until now, the application of electricity transformed by the waves is still in the pre-commercial stage. The development of wave energy technology, unlike other forms of renewable sources, has resulted in a wave energy converters which relies heavily on results from numerical simulations and experiments with scale models, which leads to the overall objectives and main scope of this research:

- Develop a mathematical model for the wave energy converter system. The wave energy converter system consists of a number of subsystems: a heaving buoy, a hydraulic pump, hydraulic pipelines, check valves, accumulators, hydraulic motor and an electric generator. To obtain insight into various subsystems that play a role in the behaviour of the wave energy converter system, an integrated model is desirable. The goal is to establish a system model using inter-linked models of each subsystem that enable a numerical solution with sufficient accuracy and computational efficiency.
- Establish an abrasive wear model for hydraulic piston rings for steady state operation considering the relevant parameters. Estimate the piston ring wear loss by incorporating the established wear model and the random dynamic responses of the wave energy converter system in time domain when the buoy is exposed to irregular incident waves.
- Estimate the wear damage along the cylinder bore by taking bore wear into account the dynamic characteristics of WEC system and lubrication analysis. Predict the position of the cylinder bore where the maximum wear occurs.
- Investigate the effect of fluid compressibility on the wear damage of the piston ring and cylinder bore. Identify design parameters to reduce the wear damage induced by the compressible fluid.
- Take into account the pressure transients in the WEC system. Predict the pressure pulsations by incorporating random sea states.

1.4.2. Thesis structure

This thesis is based on articles listed in Appendix A and Chapters 2-5 which summarise the main aspects of the work.

Chapter 2 presents the studied WEC system with its corresponding dynamic model. The modelling studies of the wave energy converter are described in Papers A and D. An integrated bond graph model of the WEC system is outlined in Chapter 3.

Bond graph models of the transmission lines are presented in Chapter 3. The chapter mainly focuses on how to construct modal bond graphs for pipelines using the separation of variables technique and method of rational transfer function. Bond graph representations are shown in this chapter. A detailed study is reported in Paper E.

Chapter 4 addresses the wear damage of the hydraulic piston rings and cylinder bore. Analysis of the wear damage is one of the core issues in this PhD thesis. The long term wear damage to both the piston rings and cylinder bore is predicted in this part. Papers B and C are the relevant detailed studies.

The conclusions and main contributions of this thesis and recommendations for future work are summarised in Chapter 5. The relationships among the appended papers are given in Fig. 1.6.

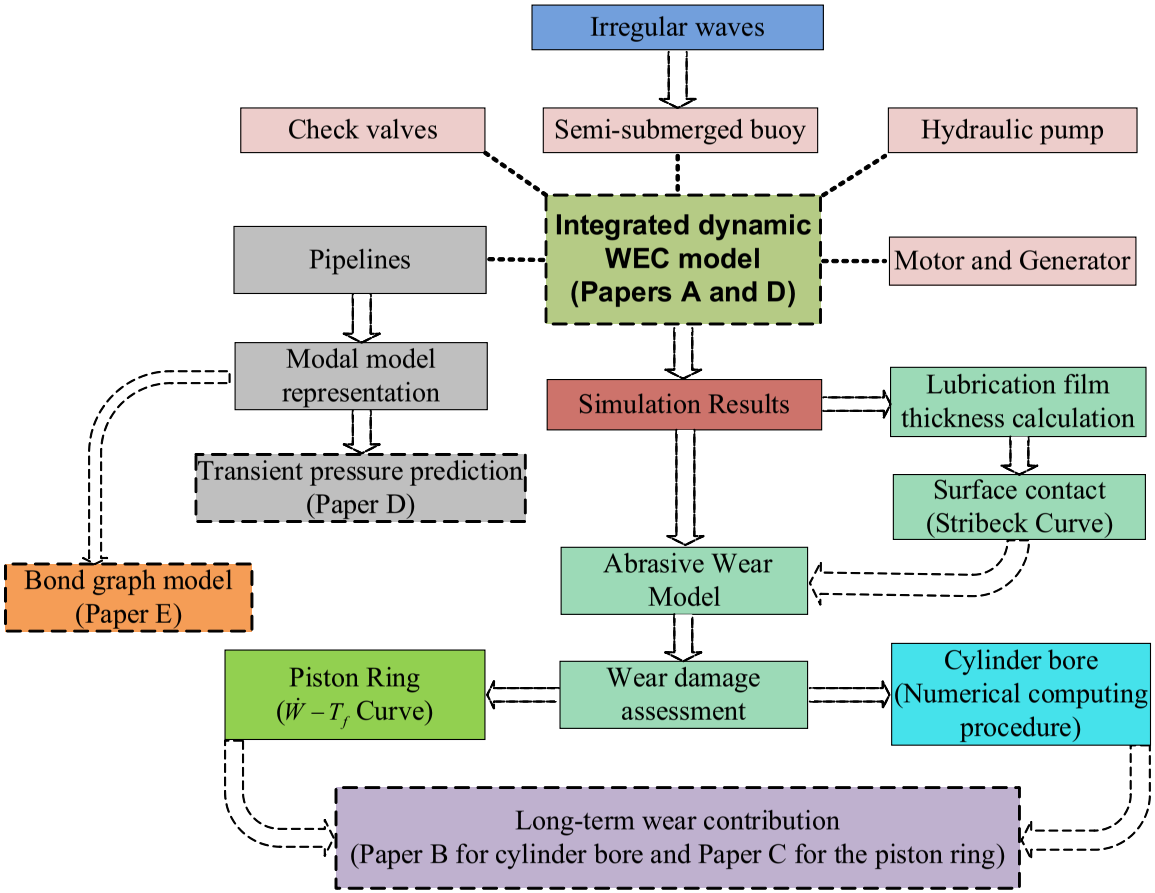

Figure 1.6: Scope of the thesis and relationships among the appended papers.

2. Modelling the wave energy converter

2.1. General

The studied wave energy converter system depicted in Fig. 1.1 can be divided into the following subsystems:

Buoy: Hydrodynamic theory describes the interaction between free surface waves and a floating buoy. The conversion of energy from the gravity waves to the hydraulic power take-off is governed by the interaction between the pressure acting on the wetted surface and the buoy motion.

Hydraulic pump: The role of the hydraulic pump is to convert the buoy motion into fluid flows at high pressure. It consists of two chambers separated by a piston. The physical model of this device can be derived by applying the mass balance law to the compressible fluid in each chamber. The kinetic power is transformed to hydraulic power in this step.

Hydraulic pipelines: The working fluid is transported circularly between the hydraulic pump and motor with pipelines. Dynamic models of pipelines are governed by the mass and momentum balance laws. Long pipelines will cause pressure propagation with time delay and strong pressure pulsations. Therefore, in this thesis, dynamic models of the transmission lines are included in the WEC system. Modelling pipelines are not mentioned in this chapter; however, a detailed description of the pipeline models using bond graph representations is given in Chapter 3.

Check valves: The self-acting check valves can be considered to be a control mechanism in this wave energy converter system. They can be modelled using conditional statements and functions that relate pressure and flow. Dynamic check valve responses are taken into account in this thesis because they represent one of the main reasons for fluid transients.

Hydraulic motor: The fluid pumped from the hydraulic chambers flows into the hydraulic motor and forces the motor shaft to rotate. The rotated shaft can drive the electric generator connected to the motor. The dynamic model of the hydraulic motor

is quite similar to the model of a hydraulic pump, i.e., both the models are governed by the mass balance law. The hydraulic motor converts the hydraulic power into mechanical power.

Accumulators: Two gas-loaded accumulators, mounted at the upstream and downstream of the hydraulic motor, are employed in this WEC system for energy storage and to maintain a constant flow to the motor. Isentropic pressure-volume law is applied to approximate the relationship between the gas pressure and volume.

Electric generator: This device is used to transform mechanical energy into electric energy. In this thesis, the generator is simplified as a dissipative element.

The input-output behaviour of the components and the interconnections between them are shown in Fig. 2.1.

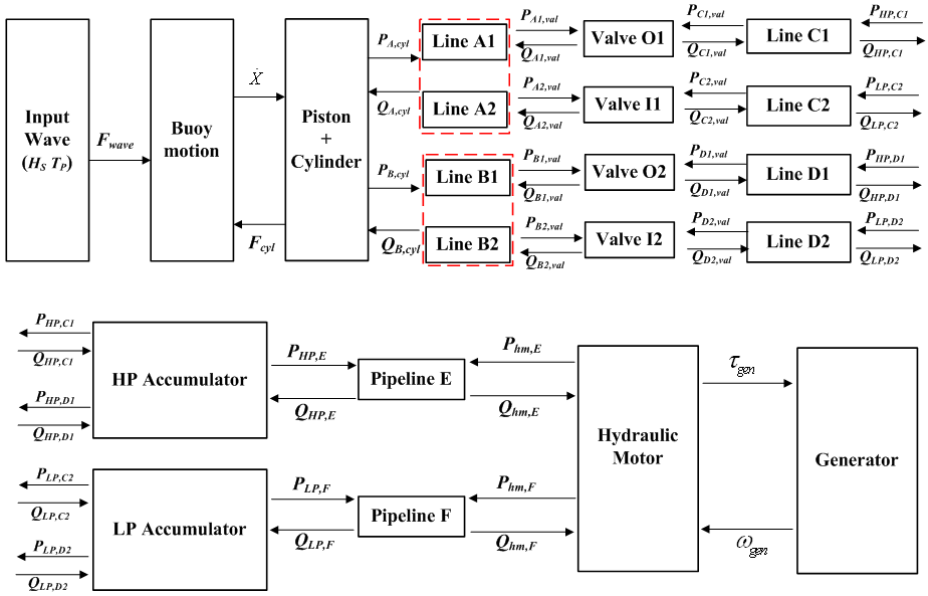

Figure 2.1: Subsystems of a wave energy converter with interconnections. The input-output relations between the connected subsystems are shown with single direction arrows. The representations of the symbols are listed in the nomenclature.

2.2. Model of the buoy

Wave, current and wind forces act on the buoy. Here, only the wave forces are considered. The oscillating buoy is modelled by assuming that the waves have small amplitudes, relative to both the wave length and water depth and that the motion

amplitudes of the buoy were also small. With these two basic assumptions, linear wave theory is adopted. Then the forces induced by the waves can be approximated as follows:

$$F_{wp}(t) = F_{exc}(t) + F_R(t) + F_{hs}(t) \tag{2.1}$$

where $F_{wp}(t)$ is the force due to the water pressure on the wetted surface of the buoy. The exciting force $F_{exc}(t)$ in the linear approximation may be decomposed into two parts: (1) a force due to the undisturbed pressure field of the incident wave, known as the Froude-Krylov force, and (2) a correction force due to the diffracted wave (Newman, 1977). The radiation force $F_R(t)$ is a force applied to the buoy by the dynamic water pressure due to the waves caused by the buoy oscillation. In a regular wave, this force can be described with two components:

$$F_R = A(\omega)\ddot{X} + B(\omega)\dot{X} \tag{2.2}$$

where $\ddot{X}$ and $\dot{X}$ are the acceleration and velocity of the oscillation buoy, respectively; $A(\omega)$ and $B(\omega)$ are the added mass and radiation damping coefficients (Faltinsen, 1990). For irregular wave cases, the radiation force must be represented in time domain by a convolution term to govern the fluid memory effect (Cummins, 1962):

$$F_R(t) = -A_\infty \ddot{X}(t) - \int_{-\infty}^{t} K(t-\tau)\dot{X}(t)d\tau \tag{2.3}$$

where A_∞ is the added mass of the buoy in the limit of infinite frequency, and $K(t)$ is the radiation force kernel. This method was adopted in the wave energy converter study by Jefferys (1980).

The frequency-dependent added mass, radiation damping and the excitation force for the buoy can be calculated numerically using the software package WAMIT (2006).

The hydrostatic force $F_{hs}(t)$ in Eq. (2.1) depends on the buoy deviation X from its equilibrium position and can be written as $F_{hs}=SX$, where S is the hydrostatic coefficient.

Detailed discussion about the linear approximation used herein can be found in Newman (1977), Faltinsen (1990) and Falnes (2002). In addition, only a single degree of freedom, i.e., heaving oscillation, is considered. For the general case of a freely floating rigid body, six motion modes—surge, sway, heave (translation) and roll, pitch and yaw (rotational)—are available. For systems with more than one degree of freedom, the decomposition of the wave forces can be extended using the

vector and matrix expressions instead of the scatter terms employed in the one-degree-of-freedom case mentioned above (Falnes, 2002).

The viscous forces on the buoy can in principle be estimated using the Morison equation (Morison et al., 1980), which represents a semiempirical relation between the drag force and the relative velocity between the fluid and body for the case of steady flow. Lopes et al. (2009) and Hals (2010) investigated the effects of viscous forces on the oscillating buoy of a WEC. They found that viscous forces are small compared to the hydrodynamic wave forces and the damping implied by the PTO. Hence, the viscous forces are neglected in this research work.

We now take into account the radiation force formulated in Eq. (2.3). Computing the convolution term by numerical integration directly is time consuming. To increase the calculation efficiency, a reasonably accurate state-space approximation model is desirable. Recently, considerable efforts have been made by several authors (e.g., Jefferys, 1984; Yu and Falnes, 1995; Kristiansen et al., 2005; Taghipour et al., 2008) to approximate the convolution term using a linear state space model, both for marine structure and wave energy converter studies. According to their results, the radiation force kernel K(t) can be calculated from the radiation damping coefficient $B(\omega)$ as follows:

$$K(t) = \frac{2}{\pi}\int_0^\infty B(\omega)\cos(\omega t)d\omega \tag{2.4}$$

The convolution integral can then be represented by

$$\dot{\mathbf{z}}(t) = \mathbf{A}\mathbf{z}(t) + \mathbf{B}\dot{X}(t) \text{ with } \mathbf{z}(0) = \mathbf{0} \tag{2.5}$$

and

$$\int_{-\infty}^{t} K(t-\tau)\dot{X}(\tau)d\tau \approx \mathbf{Cz(t)} \tag{2.6}$$

where $\mathbf{z}(t) = \left[z_1(t), z_2(t)\cdots, z_n(t)\right]^T$ is the state vector of the radiation force approximation. In this thesis, realisation theory, described by Kristiansen et al. (2005) and Taghipour et al. (2008), is adopted to deduce the state space model, and their coefficients **A**, **B** and **C**, were calculated using the Matlab function *imp2ss* (2006).

2.3. Model of the hydraulic pump and motor

In the present WEC system, the hydraulic cylinder together with the rod converts the mechanical power into fluid power. This hydraulic pump is a source of flow to the connected hydraulic motor, which converts fluid power into mechanical power so that rotation of the output shaft can take place against an opposing torque load (Chapple, 2003). By taking into account the fluid compressibility with an effective bulk modulus β, the hydraulic pump/motor can be modelled by employing the mass balance law for a volume V, which can be expressed as follows (Egeland and Gravdahl, 2002):

$$\frac{d}{dt}(\rho V) = w_{in} - w_{out} \tag{2.7}$$

Here, $w_{in}=\rho Q_{in}$ and $w_{out}= \rho Q_{out}$ are the mass flow into and out of the volume with the corresponding volumetric fluid flow rates Q_{in} and Q_{out}.

Applying the mass balance law to the respective hydraulic pump chambers gives state space equations for the chamber pressures $P_{A,cyl}$ and $P_{B,cyl}$, which are written as follows:

$$\begin{aligned}
\dot{P}_{A,cyl} &= \frac{\beta}{A_p\left(L_{cyl} - X\right)}(Q_{A,cyl} - Q_{li} + A_p\dot{X}) \\
\dot{P}_{B,cyl} &= \frac{\beta}{\alpha A_p\left(L_{cyl} + X\right)}(Q_{B,cyl} + Q_{li} - Q_{le} - \alpha A_p\dot{X})
\end{aligned} \tag{2.8}$$

where A_p is the cross-sectional area of the piston; α is the area ratio, which equals $(A_p\text{-}A_r)/A_p$; and A_r is the cross-sectional area of the rod. The flow rates into and out of the respective cylinder chambers are denoted by $Q_{A,cyl}$ and $Q_{B,cyl}$, while Q_{li} and Q_{le} are the internal leakage flow and external leakage flow, respectively. The half length of the cylinder is denoted by L_{cyl}. In this thesis, the piston is set in the middle of the cylinder when the buoy is in calm water. The buoy and piston are assumed to be one rigid body, which implies that the buoy motion X can be used to represent the vertical distance of the piston from the midpoint of the cylinder.

The piston position and velocity are obtained from the equation of piston motion by adopting Newton's second law:

$$M_p\ddot{X} = F_{wp} + \alpha A_p P_{B,cyl} - A_p P_{A,cyl} - F_f - F_{end} \tag{2.9}$$

where M_p is the inertia of the piston, which can include the mass of the buoy (including the added mass), piston, rod and the fluid in the chambers. The friction force F_f opposes the piston velocity and can be determined from the Stribeck friction curve by considering the lubrication conditions (Jelali and Kroll, 2003) (see also Fig. 4.1 in Chapter 4). The last force component considered here is F_{end}, a force given by the end stoppers when the excursion of the buoy exceeds the limit value of the designed cylinder dimensions. This force can be approximated by using a very stiff spring and has been formulated previously (see Paper A).

The models of the hydraulic motor are quite similar to that of the hydraulic pump and are not given here. Detailed information can be found in Chapple (2003).

2.4. Model of check valves

Self-acting valves are used to control the direction of the fluid flow and can be considered as resistances that cause pressure drops when the fluid flows across them. Given the pressure drop ΔP, the fluid flow Q can usually be calculated by the orifice equation derived from Bernoulli's energy equation for an incompressible flow:

$$Q = C_d A_{val} \sqrt{\frac{2}{\rho}|\Delta P|}\,\mathrm{sign}(\Delta P) \tag{2.10}$$

where C_d is the discharged coefficient and A_{val} is the cross section area of the valves. The formula describes the flow rate with good accuracy for turbulent flow conditions with a constant discharged coefficient value, which in practice, can be in the range of 0.60–0.65 for orifices with sharp edges and 0.8–0.9 for the rounded edge sections. However, the square root characteristic of Eq. (2.10) may create numerical problems because the derivative of the flow with regard to the pressure drop is infinite when the pressure drop ΔP approaches zero. Given this background, Borutzky et al. (2002) proposed a single empirical flow formula for the valves. In their model, an approximate relationship between the measured discharge coefficient C_d and the square root of the Reynolds number given by Merritt (1967) was used to smooth the transition from the laminar to turbulent region. The derived flow equation is as follows:

$$Q = \left(C_d A_{val} \sqrt{\frac{2}{\rho}|\Delta P| + \left(\frac{\upsilon_0 \,\mathrm{Re}_{tr}}{2 C_d D_{val}} \right)^2} - A_{val} \upsilon_0 \frac{\mathrm{Re}_{tr}}{2 D_{val}} \right) \mathrm{sign}(\Delta P) \tag{2.11}$$

where υ_0 is the kinetic fluid viscosity, D_{val} is the effective diameter of the valves (in this research, a valve with a circular cross section is assumed) and Re_{tr} is the

threshold Reynolds number to limit the laminar and transient regions. This check valve model can be successfully applied to the present WEC model without any simulation problems. The dissipative power induced by the check valves can be estimated. To predict the converted power of the WEC system, this model is accurate enough.

However, the self-acting valves represent dynamic boundaries of the connected pipelines during their actuation and represent one of the main causes of rapid pressure transients. The pressure transient amplitude can be approximated by Joukowski's expression (Wylie et al., 1993):

$$\Delta P = \rho a \Delta u \tag{2.12}$$

where ΔP is the pressure change generated by a flow velocity change, Δu. Joukowski's equation approximates pressure transient amplitudes for complete closure or opening within critical time T_r, where T_r is the return period of the pressure propagation within a pipeline with length L_{pipe} and defined as $T_r = 2L_{pipe}/a$.

However, partial valve actuations, i.e., the case when the valve closure time t_c is larger than T_r, are also responsible for transient phenomena. Time-dependent pressure transient magnitudes can be calculated from valve actuation functions derived from geometric considerations and valve actuation time (Wood and Jones, 1973). To illustrate this relationship, a plot of the maximum transient pressure amplitudes for different valve closure times is shown in Fig. 2.2. A global valve type with uniform stem motion was adopted to calculate the transient pressure. For convenience, a dimensionless time T_c, which is defined as t_c/T_r, was used. The results plotted in the figure clearly show how the maximum transient pressure amplitude varies with the valve actuation. Thus, the dynamic behaviour of the check valves with fluid interaction is desirable for predicting the transient pressures.

In practice, several types of check valves are available to be employed in this WEC model, and each of them has their own features and configurations. The dynamic models of the valves are different. Here, a spring-loaded valve is used as an example to obtain the insight of the valve performance in the WEC system. For this type of check valve, the valve stroke displacement x_{val} can be governed with the model proposed by Johnston (1991). The model calculates the acceleration of the valve stroke by calculating the net forces acting upon it. This model is used to predict the pressure pulsations of the pipelines and is given in detail in Paper D.

By incorporating the temporal performance of the valve stroke, a flow equation for the check valves can be rewritten by employing a time-dependent A_{val} to model the open area of the valve. According to the valve type, the actuation function,

represented as a relationship between Ω, the ratio of open valve area to total possible flow area, and the stroke position ratio ς, has different forms (Wood and Jones, 1973). Taking the valve model into account, the flow equation can then be written as follows:

$$Q = \left(C_d A_{val} \Omega(t) \sqrt{\frac{2}{\rho}|\Delta P| + \left(\frac{\upsilon_0 \mathrm{Re}_{tr}}{2 C_d D_{val}} \right)^2} - A_{val} \Omega(t) \upsilon_0 \frac{\mathrm{Re}_{tr}}{2 D_{val}} \right) \mathrm{sign}(\Delta P)$$

$$\Omega(t) = f(\varsigma), \quad \text{with} \quad \varsigma = \frac{x_{val}(t)}{x_{val,stop}}. \tag{2.13}$$

Here, $x_{val,stop}$ is the maximum displacement that the valve stroke reaches.

The valve model Eq. (2.13) can capture the current valve performance, which is important when estimating the pressure pulsation. The transient pressure phenomenon is illustrated in detail when it is combined with the pipeline dynamic model in Chapter 3.

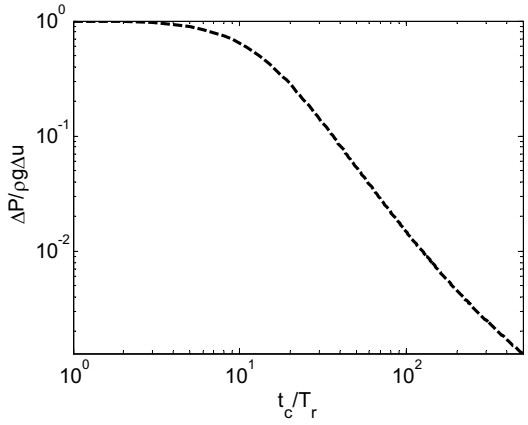

Figure 2.2: Maximum transient pressure amplitudes verses a dimensionless valve closure time.

2.5. Model of accumulators

The hydraulic power take-off contains one high-pressure accumulator and one low-pressure accumulator (Fig. 1.1). Both of them are gas-compressed bladders with precharged pressure, and they are used to reduce pressure peaks in the system and to store energy. The nonlinear capacitance relationship between the compressed gas

pressure and the volume of each accumulator can be characterised using the ideal gas pressure-volume law (Tisza, 1966):

$$PV^{\gamma} = P_0 V_0^{\gamma} = \text{constant} \tag{2.14}$$

In this equation, γ is the ratio of the specific heat at constant pressure and volume (for air at atmospheric pressure, $\gamma \approx 1.4$).

When the hydraulic fluid flows into or out of the accumulator, the gas is compressed or expanded. By integrating the hydraulic fluid rate Q with respect to time t, the gas volume can be obtained as follows:

$$V = V_0 - Q = V_0 - \int_0^t Q dt \tag{2.15}$$

Here, the compressibility of the hydraulic fluid is neglected.

The governing equations for the two accumulators can then be yielded by combining their physical parameters and equations (2.14) and (2.15):

$$\begin{aligned} P_{HP} &= \left(P_{0\_HP} V_{0\_HP}^{\gamma}\right) \Big/ \left(V_{0\_HP} - \int_0^t Q_{HP} dt\right)^{\gamma} \\ P_{LP} &= \left(P_{0\_LP} V_{0\_LP}^{\gamma}\right) \Big/ \left(V_{0\_LP} - \int_0^t Q_{LP} dt\right)^{\gamma} \end{aligned} \tag{2.16}$$

The subscripts “HP” and “LP” represent high-pressure accumulator and low-pressure accumulator, respectively.

The modelling of the hydraulic pipelines is described in detail in Chapter 3 and hence is not addressed here. The electric generator is simplified as a dissipative resistance in this project. This choice of the electric generator model does not influence the effects studied in this thesis. However, a detailed model of the generator can be added in the WEC system if it is necessary.

2.6. Discussion of the models

The above-mentioned models for the subsystems can be integrated into a system model to investigate the system dynamics. The WEC system model, which neglects the pipeline effects, can be found in Paper A, while the model that takes into account the dynamics of pipelines is developed in Paper D. To develop the model, some assumptions are made. Analysis of the influence of these assumptions is given below:

- Linear water wave theory underlies the whole hydrodynamic theory of the studied wave energy converter. This linear theory is only valid for a buoy operating in small waves with small wave height and motion amplitudes. For waves with large wave height, e.g., storm conditions, nonlinear water wave theory is desirable. The aim of this thesis is to investigate the performance of the WEC system in normal operating conditions and the accumulated damage for the relevant components. Extreme sea states are not considered herein. Therefore, linear theory, adopted here, is supposed to be a reasonable model for this study.

- The mass of the piston-rod and hydraulic fluid in the cylinder can be neglected in this studied WEC case, which employs a sphere buoy with a radius of 5 m. Compared with the buoy mass m (2.7×10^5 kg) and its added mass at infinite frequency A_∞ (1.35×10^5 kg), the mass of the piston-rod and working fluid in the chambers (only hundreds of kilograms) is very small and can be neglected. Hence, the mass M_p defined in Eq. (2.9) can be approximated as (m+ A_∞) in the simulation model. This approximation was adopted in Papers A and D.

- Fluid compressibility is modelled within the hydraulic chambers as a linear spring with constant bulk modulus β. This bulk modulus is defined as the change in pressure divided by the fractional change in volume and could be a function of several parameters, such as the applied pressure, elastic of the cylinder tubing and gas entrance. However, for common pressures (P<45 MPa) and temperatures ($[-40,120]^\circ$C), one may use a mean value for this variable (Jelali and Kroll, 2003). In this research, the operation conditions are within these boundaries. Thus, the bulk modulus is taken as a constant value 1×10^9 Pa, a value which is commonly suggested for the hydraulic system (Totten, 2000).

- The entropy of the gas in the accumulators is to be constant for this simulation model. In reality, the gas entropy changes due to heat transfer. Such changes are likely to be significant over time intervals longer than a few hours. In a short time period, e.g., the 3000-second simulation time period in the studied case, it is reasonable to consider that gas compression and expansion inside the accumulator is approximately isentropic.

- The hydraulic cylinder tubing is assumed to be rigid. In this WEC system, the hydraulic tubing can be considered as a fluid capacitor. The deformation of the hydraulic tubing describes a relationship between a pressure and the integral of a flow rate, which may contribute to the compliance coefficient. For a thin-walled hydraulic tubing with constant cross sectional area A_t, this relationship can be written as follows (Karnopp et al., 2006)**:**

$$\Delta P = \frac{t_t E_t}{D_0 V_0} \Delta V \tag{2.17}$$

where ΔP and ΔV are the changes in fluid pressure and volume, respectively. The thickness of the tube is denoted as t_t, and E_t is the Young's modulus, D_0 is the nominal diameter and V_0 is the initial volume of the tube.

The changes of the force ΔF applied on the piston and its corresponding displacement ΔX are as follows:

$$\begin{aligned} \Delta F &= \Delta P \cdot A_t \\ \Delta V &= \Delta X \cdot A_t \end{aligned} \tag{2.18}$$

Combining Eqs. (2.17) and (2.18) yields the following:

$$\Delta F = \frac{t_t E_t}{D_0 V_0} A_t^2 \Delta X \tag{2.19}$$

In Eq. (2.19), an equivalent stiffness coefficient K_t caused by the deformation of hydraulic tubing can be obtained as follows:

$$K_t = \frac{t_t E_t}{D_0 V_0} A_t^2 \tag{2.20}$$

Another equivalent stiffness caused by the fluid compressibility K_{fluid} in this hydraulic tubing can be written as follows (Eq. (21) in Paper A):

$$K_{fluid} = \frac{\beta}{V_0} A_t^2 \tag{2.21}$$

The ratio between the two induced stiffness coefficients K_{fluid} and K_t, denoted as *RaK*, can now be expressed as follows:

$$RaK = \frac{K_{fluid}}{K_t} = \frac{\beta}{E_t} \cdot \frac{D_0}{t_t} \tag{2.22}$$

For hydraulic tubing with $\frac{D_0}{t_t} = 10$, i.e., a limit value for the thin-walled tubing, and $E_t = 2.1 \times 10^{11}$ Pa, the value of *RaK* is about 5%. This value is even smaller for thick-walled tubing.

Thus, the total equivalent stiffness K can be written as:

$$\frac{1}{K} = \frac{1}{K_{fluid}} + \frac{1}{K_t} \approx \frac{1}{K_{fluid}}, \text{i.e.,} K \approx K_{fluid} \tag{2.23}$$

Compared with the compressibility of the working fluid in the hydraulic chambers, the elasticity of the hydraulic tubing can be neglected. This procedure can also be followed to illustrate the reasons to neglect the elasticity of the accumulator tube and the compressibility of the working fluid within the accumulators.

It is important to realise that no system can be modelled exactly (Karnopp et al., 2006). A good model should be as simple as possible (that is efficient) and provide results relevant for power capture and integrity assessment with satisfactory accuracy. To estimate the converted electric power and wear damage of the piston ring and cylinder bore, the established system model with the above assumptions can provide simulation results with satisfactory accuracy. The wear damage is described in detail in Chapter 4.

3. Bond graph model of transmission lines

3.1. General

3.1.1. Bond graph model of WEC

A bond graph is a graphical representation of a physical dynamic system, which is introduced by Henry M. Paynter, professor at MIT & UT Austin. It is a multidisciplinary and unified approach for modelling of multi-energy domain systems. The main applications of bond graphs are to physical systems in which power and energy interactions are important. These multi-energy domain interactions are characteristic of wave energy converter system and therefore, well suited for bond graph modelling (Engja and Hals, 2007).

Bond graph modelling of a wave energy converter with different hydraulic power take-off has been investigated by several researchers (Marré, 2006; Engja and Hals, 2007; Hals, 2010; Yang et al., 2009). The construction procedure is not included in this thesis. An introduction to bond graph modelling vocabulary can be found in the textbook by Karnopp et al. (2006). Following the rule of bond graph language, the governing equations given in Chapter 2 can be represented in the bond graph form (Paper F).

In the aforementioned studies, the pipelines employed in the WEC system were either neglected or included as an equivalent dissipative component. The transient flow problems in the pipeline have not yet been included in the WEC bond graph models. In the following, the bond graph representation will be used in the discussion of the fluid dynamic behaviour of hydraulic pipelines.

3.1.2. Bond graph model of pipelines

The one-dimensional distributed parameter model of the transmission line, shown schematically in Fig. 1.3, has four possible sets of boundary conditions: a symmetric boundary condition with (I) pressure inputs [P_{up}, P_{down}] or (II) flow rate inputs [Q_{up}, Q_{down}] and mixed boundary conditions with (III) [P_{up}, Q_{down}] or (IV) [P_{down}, Q_{up}] as

inputs. Here, we adopt the name *admittance* model for configuration (I) and *impedance* model for configuration (II) and refer to these as *symmetric* boundary conditions. The words *mixed* or *hybrid* may be used to refer to configurations (III) and (IV) (Fig. 3.1).

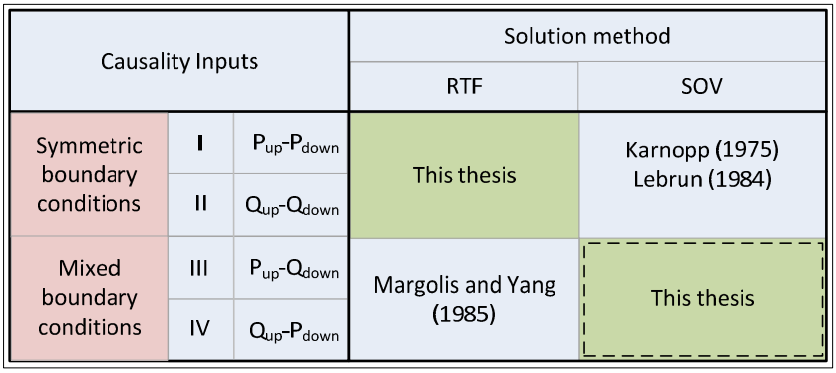

Figure 3.1: The diagram shows solution methods used to establish bond graph representations for a hydraulic transmission line that are divided between the four different causal inputs (left column).

By taking advantage of the bond graph approach (Karnopp et al., 2006), Margolis and Yang (1985) developed modal bond graph representations for the transmission lines using the rational transfer function (RTF). In their study, the mixed causality configurations with [P_{up}, Q_{down}] or [P_{down}, Q_{up}] as inputs were considered. Karnopp (1975) introduced the bond graph representation using the separation of variables technique for a pipeline with no friction loss and with corresponding symmetric conditions, and later, Lebrun (1984) made a model by considering the same configuration case with linear friction assumption. Although considerable effort has been devoted to construct the model bond graphs for the distributed pipelines, the bond graph representations for the symmetric inputs using the RTF model and mixed boundaries based on SOV have not been developed. These model graphs were developed by the author and co-workers of this study (Paper E). Figure 3.1 shows which solutions have been represented earlier and which are investigated in this thesis. In the following sections, an overview of establishing bond graph models using RTF and SOV, will be given. All four input-output configurations are mentioned. The result of this research work is eight bond graph structures.

3.2. Bond graph representations using SOV

The partial differential equations (1.1) and (1.2) can be combined in two ways to form a forced wave equation. With suitable second derivations for time t and space x, pressure or flow can be eliminated:

$$\frac{A_{pipe}}{\rho a^2}\frac{\partial^2 P(x,t)}{\partial t^2}=\frac{A_{pipe}}{\rho}\frac{\partial^2 P(x,t)}{\partial x^2}-\frac{1}{\rho}\frac{\partial F(x,t)}{\partial x}+\frac{\partial S_Q(x,t)}{\partial t} \tag{3.1}$$

$$\rho\frac{\partial^2 Q(x,t)}{\partial t^2}=\rho a^2\frac{\partial^2 Q(x,t)}{\partial x^2}-\rho a^2\frac{\partial S_Q(x,t)}{\partial x}+\frac{\partial F(x,t)}{\partial t} \tag{3.2}$$

To yield normal mode representation in bond graph form, the separation of variables technique is used. This method begins by temporarily setting the boundary inputs to zero and assuming that the variables $P(x,t)$ or $Q(x,t)$ can be separated into a product of two functions: one is x dependent, and one is t dependent:

$$P(x,t)=\sum_{i=0}^{\infty}H_i(x)\eta_i(t) \tag{3.3}$$

$$Q(x,t)=\sum_{i=0}^{\infty}G_i(x)\xi_i(t) \tag{3.4}$$

where $\eta_i(t)$ and $\xi_i(t)$ represent modal general coordinates of the pressure P and flow rate Q, respectively; $H_i(x)$ and $G_i(x)$ are the mode shapes for the pressure P and flow rate Q, respectively.

The boundary conditions compatible with the input causalities are the following:

$$\frac{\partial P}{\partial x}(0,t)=\frac{\partial P}{\partial x}(L_{pipe},t)=0 \qquad \left[Q_{up},Q_{down}\right]\text{as input} \tag{3.5}$$

$$\frac{\partial Q}{\partial x}(0,t)=\frac{\partial Q}{\partial x}(L_{pipe},t)=0 \qquad \left[P_{up},P_{down}\right]\text{as input} \tag{3.6}$$

$$\begin{cases}P(0,t)=\dfrac{\partial P}{\partial x}(L_{pipe},t)=0\\ \dfrac{\partial Q}{\partial x}(0,t)=Q(L_{pipe},t)=0\end{cases} \qquad \left[P_{up},Q_{down}\right]\text{as input} \tag{3.7}$$

For the symmetric input conditions, the mode shapes $H_i(x)$ or $G_i(x)$ can be obtained by solving Eq. (3.1) or Eq. (3.2) with the corresponding spatial boundary conditions

of Eq. (3.5) or (3.6). The mode shapes $H_i(x)$ or $G_i(x)$ are cosines with arbitrary amplitudes which are normally set to unity:

$$H_i(x) = G_i(x) = \cos\left(\frac{\omega_i}{a}x\right) = \cos\left(\frac{i\pi x}{L_{pipe}}\right) \qquad i = 0,1,2\cdots \tag{3.8}$$

The corresponding resonant frequencies are the following:

$$\omega_i = \frac{i\pi a}{L_{pipe}} \tag{3.9}$$

Because the mode shape functions are orthogonal, a set of decoupled ordinary differential equations can then be obtained for each normal mode. These ODEs can be represented elegantly in the bond graph forms. For the model with fluid pressure P as input and flow rate Q as output, the bond graph model is given in Fig. 3.2, while for the case with flow rate Q as input and fluid pressure P as output, the modal bond graph is shown in Fig. 3.3. The inertial, capacitance and resistance parameters for each mode are supplied by Karnopp (1975) and Lebrun (1984).

The mixed configuration condition with [P_{up}, Q_{down}] as input is more complex than the cases with symmetric input conditions because of the mixed output variables, i.e., the normal mode equations for both the pressure P and flow rate Q must be determined. However, the basic idea for obtaining the modal bond graph is similar to that for the symmetric input cases. The mode shapes $H_i(x)$ are sinusoidal functions:

$$H_i(x) = \sin\left(\frac{(2i-1)\pi}{2L_{pipe}}x\right) \qquad i = 1,2,3\cdots \tag{3.10}$$

For $G_i(x)$, the expressions are cosines:

$$G_i(x) = \cos\left(\frac{(2i-1)\pi}{2L_{pipe}}x\right) \qquad i = 1,2,3\cdots \tag{3.11}$$

The above two equations (3.10) and (3.11) imply that the ith mode shape of the pressure P and flow rate Q have different forms. However, the corresponding resonant frequencies are the same and can be expressed as follows:

$$\omega_i = \frac{(2i-1)\pi}{2L_{pipe}}a \tag{3.12}$$

Using the orthogonality property of the mode shape, two sets of bilaterally decoupled ODEs—one is relevant to $\eta_i(t)$, and the other is relevant to $\xi_i(t)$—can be obtained for

each of the normal modes $H_i(x)$ and $G_i(x)$, respectively. The bond graph model for the ith mode is shown in Fig. 3.4. A detailed derivation for constructing the bond graph forms and the elements coefficients is given in Paper E.

For the mixed configuration with [Q_{up}, P_{down}] as input, the corresponding bond graph can be obtained by simply interchanging the **0**- and **1**- junctions along with the **I**, **C** and **R** elements of Fig. 3.4. The bond graph representation for this case is also reported in Paper E.

The above analysis shows that the boundary conditions play a dominant role in the construction of the bond graphs. These input variables with different combinations can affect the mode shape and its resonant frequencies. In particular, attention should be paid to when considering the stability of the system, i.e., as the exciting force frequency approaches the mode frequency of the pipeline.

The pipe models shown in Figs. 3.2–3.4 contain an infinite number of frequencies, which is clearly impractical in a computer simulation. The models have to be truncated after a finite number of modes. For a coupled system, the frequency band of interest is assumed to be known. The pipe models should contain all modes up to the maximum frequency of interest. From a safety point of view, a few extra modes may also be included (Skarbø and Engja, 1990). By observing that the truncated modes with resonant frequencies that greatly exceed the interest frequency are stiffness- or inertia-controlled, the contribution to the output made by these high frequency modes can be taken into account as residual **I** or **C** elements. The residual coefficient matrix can be found in Lebrun (1984) for the symmetric input configurations, and for the mixed input case, they are reported in Paper E. Because this modification method is based on the frequency domain, in this research, it is defined as the frequency domain modification (FDM) method.

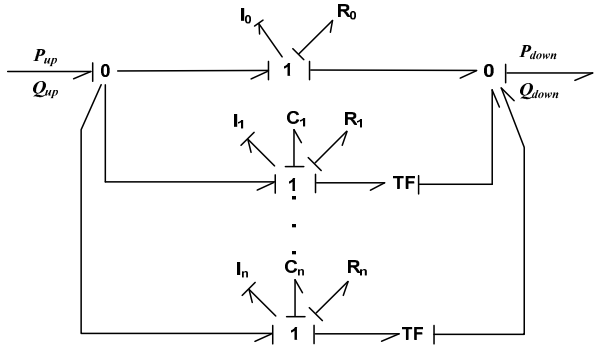

Figure 3.2: Bond graph representation determined using SOV when pressure inputs are considered with *n* modes (Reproduced from Lebrun (1984)). Here **I**, **C**, **R**, **0**, **1** and **TF** are standard bond graph elements (e.g., Karnopp et al., 2006).

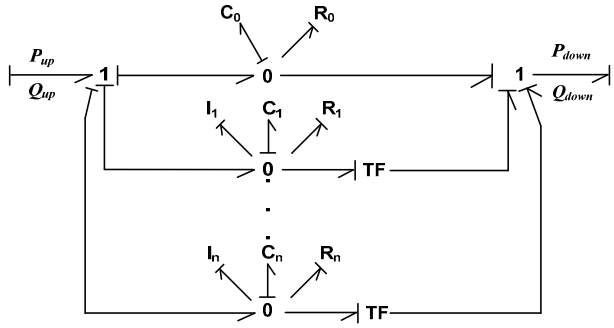

Figure 3.3: Bond graph representation found using SOV when flow rate inputs are considered with *n* modes (Reproduced from Lebrun (1984)).

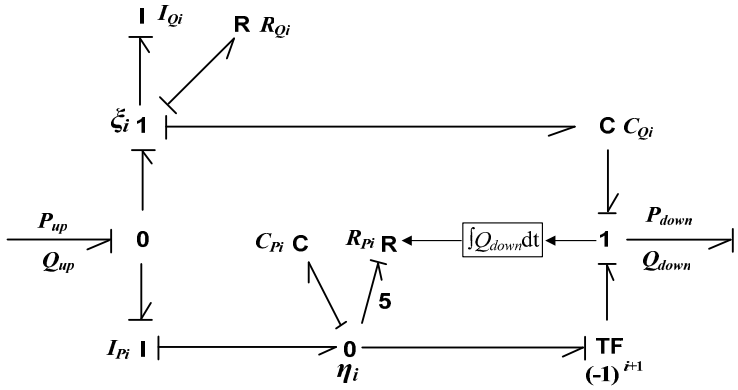

Figure 3.4: The bond graph representation of the *i*th mode for the pipeline with [P_{up}, Q_{down}] as inputs (Paper E).

3.3. Bond graph representations using RTF

The one dimensional partial differential equations (1.1) and (1.2) have analytical solutions in the Laplace domain, which can be expressed in a two-port matrix form. The input-output boundary conditions determine the form of the transfer matrix **T,** which can be found in Goodson and Leonard (1972). The transfer matrix includes hyperbolic functions, which can be represented as finite-sum approximations of low-order polynomial functions, i.e., $\mathbf{T} = \sum_i \mathbf{T}_i$. The transmission line model can then be approximated as follows:

$$\begin{bmatrix} P_{up} \\ P_{down} \end{bmatrix} = \sum_i \begin{bmatrix} P_{up,i} \\ P_{down,i} \end{bmatrix} = \sum_i \mathbf{T}_i^{\mathrm{PP}} \begin{bmatrix} Q_{up} \\ Q_{down} \end{bmatrix} \tag{3.13}$$

$$\begin{bmatrix} Q_{up} \\ Q_{down} \end{bmatrix} = \sum_i \begin{bmatrix} Q_{up,i} \\ Q_{down,i} \end{bmatrix} = \sum_i \mathbf{T}_i^{\mathrm{QQ}} \begin{bmatrix} P_{up} \\ P_{down} \end{bmatrix} \tag{3.14}$$

$$\begin{bmatrix} P_{down} \\ Q_{up} \end{bmatrix} = \sum_i \begin{bmatrix} P_{down,i} \\ Q_{up,i} \end{bmatrix} = \sum_i \mathbf{T}_i^{\mathrm{PQ}} \begin{bmatrix} P_{up} \\ Q_{down} \end{bmatrix} \tag{3.15}$$

For a linear friction model, the representations of transfer functions $\mathbf{T}_i^{\mathrm{PP}}$, $\mathbf{T}_i^{\mathrm{QQ}}$ and $\mathbf{T}_i^{\mathrm{PQ}}$ have been derived by Van Schothorst (1997), Ayalew and Kulakowski (2005), and Yang and Tobler (1991), respectively. Because the approximation pipeline model of the causal configuration with [P_{down}, Q_{up}] as input is quite similar to the case with [P_{up}, Q_{down}], it is not mentioned here. A detailed description was given by Van Schothorst (1997).

Equations (3.13), (3.14) and (3.15) govern the input-output behaviour of transmission lines in the modal form. Each of these models represents a single resonant mode of the transmission line dynamics. These models are quite similar to the modal model obtained using the SOV technique. However, as mentioned in the preceding section, using SOV ends up with a set of decoupled ordinary differential equations, while bilaterally coupled modes are obtained using RTF.

For these bilaterally coupled modes governed by Eq. (3.15), Margolis and Yang (1985) introduced a bond graph model for each mode (Fig. 3.5). A subsequent study for the transmission line model with symmetric boundary conditions, was preceded by Yang et al. (Paper E). The suggested bond graph model for the modes governed by Eq. (3.13) is given in Fig. 3.6, while the modal bond graphs for the modes with Eq. (3.14) are shown in Fig. 3.7.

With the suggested bond graph structures shown in Fig. 3.5, by applying the bond graph algebra, one can derive the state space equations for each mode of the pipeline using the physical state variables. The modal parameters and modulus used in the bond graph can be obtained by comparing the derived modal state space equations with the modal transfer functions in Eq. (3.15), respectively. The procedure for obtaining the relevant unknown parameters in Fig. 3.5 was described by Margolis and Yang (1985).

The basic ideas for constructing the modal bond graphs using RTF for the symmetric boundary conditions are the same as those for the mixed configuration. However, to calculate the unknown parameters, instead of using the modal transfer functions $\mathbf{T}_i^{PP}$ or $\mathbf{T}_i^{QQ}$, the state space equations for each pipeline modes, which have been derived by Van Schothorst (1997) and Ayalew and Kulakowski (2005), were applied. By comparing the two sets of state space equations (one set of state space equations is derived according to the suggested bond graph structure, while the other is obtained using RTF), the modal parameters and modulus can be obtained (Paper E).

With the derived bond graph model, the pipeline dynamics can be characterised approximately using a finite number of modes. The effect of the truncated modes, the same problem encountered using SOV, needs to be resolved. For the RTF method, studies have primarily focused on recovering the accuracy of steady state behaviour. The nonzero contribution to the steady state gain of theoretical model delivered by the truncated modes has been considered by many authors. One way of eliminating this contribution is to modify the approximate model to satisfy the steady state condition of the exact model (Hullender et al., 1983; Yang and Tobler, 1991; Van Schothorst, 1997). Based on this idea, steady state modifications are required for the line models when the input variables are [P_{up}, Q_{down}], [P_{down}, Q_{up}] or [Q_{up}, Q_{down}]. For the configuration with [P_{up}, P_{down}] as input, a first-order mode, whose gain is exactly equal to the theoretical model, is included in the approximation model (Ayalew and Kulakowski, 2005), which implies that no steady state corrections are necessary for this approximate dynamic model. The steady state correction on the modal bond graph for the causal input [P_{up}, Q_{down}] or [P_{down}, Q_{up}] was performed in Margolis and Yang (1985), and for the line model with [Q_{up}, Q_{down}] as input, the bond graph model with steady state correction was investigated in Paper E. This modification method focuses on recovering the accuracy of the pipeline behaviour at steady state conditions and is denoted as the steady state correction (SSC) method in this thesis.

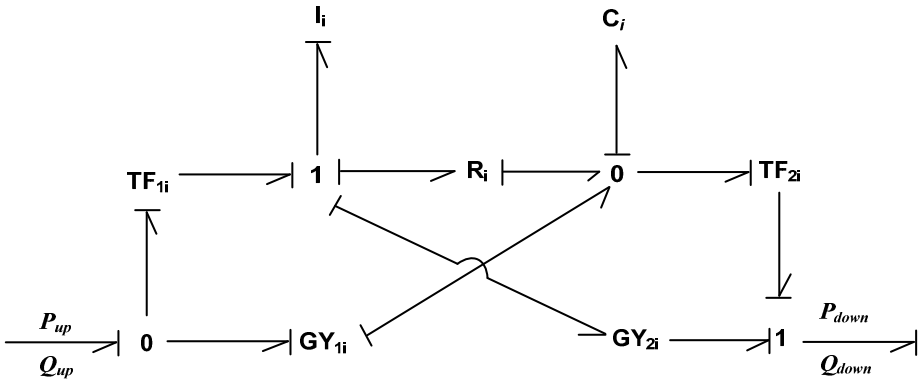

Figure 3.5: A bond graph representation of the *i*th mode for the pipeline with P_{up} and Q_{down} as inputs derived using the RTF (Reproduced from Margolis and Yang (1985)).

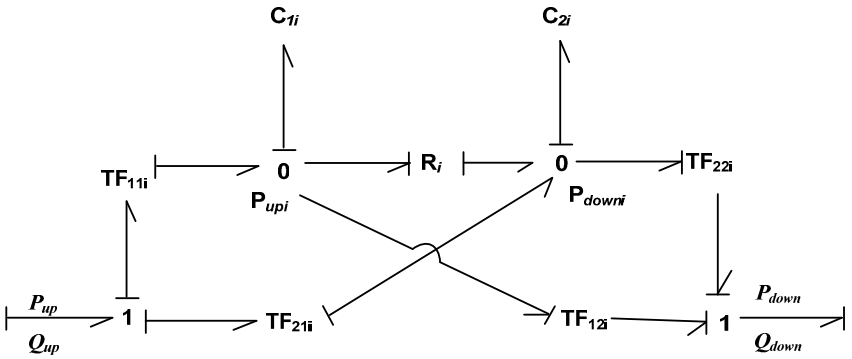

Figure 3.6: A suggested bond graph representation of the *i*th mode for the pipeline with Q_{up} and Q_{down} as inputs using RTF (Paper E).

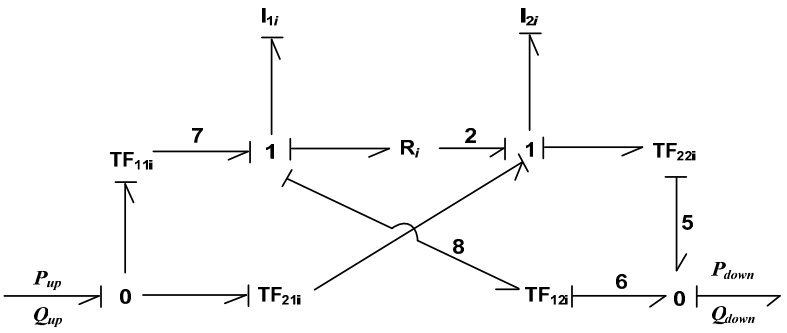

Figure 3.7: A suggested bond graph representation of the *i*th mode for the pipeline with P_{up} and P_{down} as inputs using RTF (Paper E).

3.4. Discussion of the models

Bond graph representations of distributed-parameter pipelines, which use a finite number of modes, were introduced in the preceding sections. Two alternative approaches, SOV and RTF, were employed in constructing the models. By applying the two approaches, the modal bond graphs were developed for all four possible sets of boundary input conditions, i.e., [P_{up}, P_{down}], [Q_{up}, Q_{down}], [P_{up}, Q_{down}] and [P_{down}, Q_{up}]. These models can be coupled easily with bond graph models of attached dynamic systems. Thus, difficulties arising in the modelling and analysis of fluid systems with various dynamic terminations can be eliminated. Because of these advantages, the pipeline model in the bond graph form is a preferred approach by many researchers (e.g., Lebrun, 1985; Skarbø and Engja, 1990; Aesoy and Engja, 1996) for constructing their dynamic models.

A general overview of the bond graph models developed by SOV and RTF is reported in Paper E. It is important to note that the transient properties can be preserved well, i.e., when the same finite number of modes are applied for both types of methods. Errors may appear by considering the effect of the truncated infinite high frequency modes. The contribution of these truncated modes to the pipeline model is relatively larger for the mixed input conditions than for the symmetric ones because of the magnitude of the gain for each mode. As shown by Yang and Tobler (1991), the magnitude of the gain for the ith mode at steady state condition with mixed input conditions is proportional to $1/i$, while for the symmetric case, an amplification factor $1/i^2$ controls the decreasing rate of the gain magnitude (Van Schothorst, 1997; Ayalew and Kulakowski, 2005). Thus, the converging velocity of the magnitude of the transfer function is much slower for the mixed input boundary conditions, i.e., larger errors will occur when adopting the same number of normal modes without modification for the truncated modes.

To correct or reduce the effect of the truncated modes on the pipeline behaviour, two methods, FDM and SSC, have been described in the literature. Although both of them can give reasonable corrected results for the simulation model, there are still some differences. The FDM method begins by ignoring the inertial and dissipative terms if the modes are stiffness-controlled or by neglecting the capacitive and dissipative elements when the modes are inertia-controlled. This method cannot provide an exact solution for the steady state behaviour; however, the transient behaviour affected by the high frequency modes can be described well. In contrast, SSC describes identical behaviour for the pipeline at its steady state condition; nevertheless, the effect of the truncated modes on the dynamic responses is neglected.

In addition, for the four input-output configurations, according to FDM, each of them needs a modification unless one can include all the modes in the pipeline model, which is not possible. Based on the SSC definition, if the gain of the approximate model equals the gain of the exact model at the steady state condition, no correction is desirable. Therefore, for the configuration with [P_{up}, P_{down}], no steady state correction is necessary to offset the error of truncation to a finite number of modes.

These contributions of the truncated high frequency modes are very small, and for most engineering cases, the approximation modal models give satisfactory results. In Paper E, a pipeline blocked at one end with a pressure step applied at the other end is considered. The comparison of the pressure transient response at the blocked side was established by adopting the bond graph models, as shown in Figs. 3.4 and 3.5. The simulation results show that, for this case, the bond graph model with the FDM correction method can yield satisfactory accuracy with fewer modes than the bond graph model developed by Margolis and Yang (1985) with SSC.

Finally, the modal bond graphs mentioned in this chapter were developed based on the linear friction assumption and are applicable for the pipelines with small dissipative number D_n, which can be written as $D_n = \frac{L_{pipe}\upsilon_0}{aR_{pipe}^2}$ (Goodson and Leonard, 1972). For large values of D_n, a dissipative friction model can provide more accurate results. However, the basic character of the two sets of models, the linear friction models and the dissipative friction models, is similar. Moreover, a linear friction pipeline model is much easier to establish and simulate. Consequently, the linear friction model is still widely adopted by many engineers and designers.

3.5. Model application

With the developed modal bond graphs for the pipelines considering the four possible sets of input-output configurations, the pipeline dynamics can be investigated with different coupled systems. For the proposed wave energy converter, pipelines are used to transport the working fluids and connect different components. Various input boundary conditions are included in the system (Fig. 2.1). Fortunately, bond graphs have a distinct advantage in that the subsystem can be constructed independently and stored in the computer files. These subsystem models can be assembled into a total coupled system without any difficulties and be used again and again. Thus, to develop the WEC bond graph model including the pipeline dynamics, the only thing needed to do is to choose the right pipeline model based on the causality requirement and place it in its proper position.

A bond graph model of the studied WEC (Fig. 1.1) that combines the modal bond graphs of the pipelines is given in Fig. 3.8. The corresponding interpretation of bond graph elements can be found from Table 3.1. This model can be implemented using software 20-sim, a modern modelling and simulation program that runs in Microsoft Windows.

By using this bond graph model, transient pressures induced by the pipelines and valve actuation can be predicted numerically by incorporating the interactions of other components. The numerical solution results lay a foundation for assessing the safety of the WEC system. Moreover, because the dynamic WEC system can be modelled by a set of first order ODEs, instead of using the model bond graph, one can also choose to solve these state space equations using the *ODE* solver package in Matlab (2006).

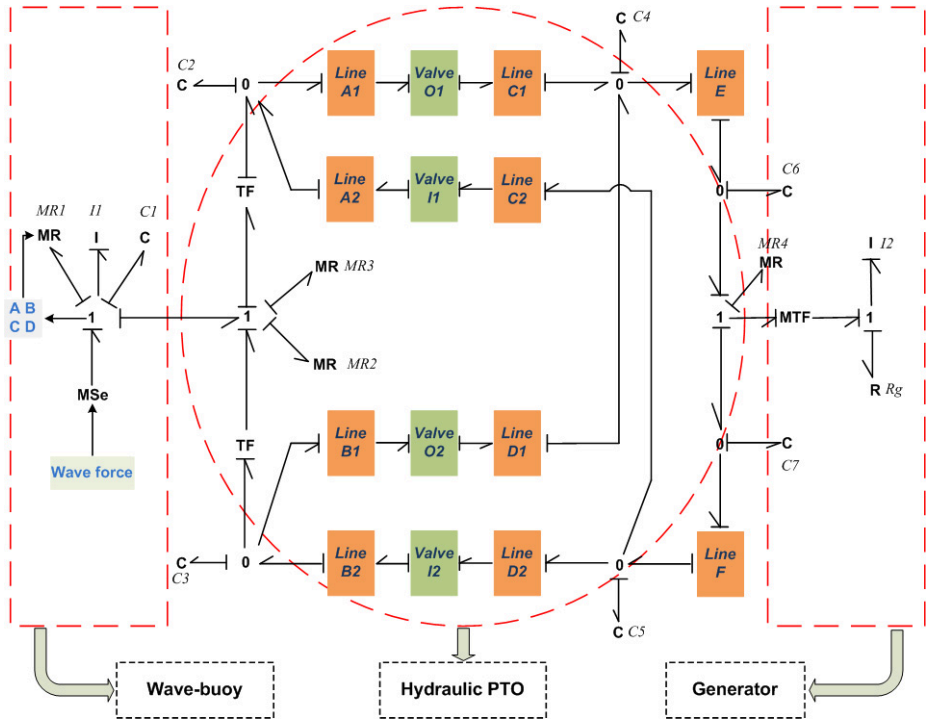

Figure 3.8: A bond graph representation for the studied wave energy converter shown in Fig. 1.1.

Table 3.1: Interpretation of the bond graph elements of the WEC system, as shown in Fig. 3.8.

Element	Interpretation
MSe	Input wave exciting force
MR1	Radiation damping force
I1	Inertia forces, $m+A_\infty$ of the buoy
C1	Restoring force of the buoy
C2	Upper cylinder chamber volume-pressure relation
C3	Lower cylinder chamber volume-pressure relation
C4	Compressed gas compliance in the high-pressure accumulator
C5	Compressed gas compliance in the low-pressure accumulator
C6	Volume-pressure relation of the inlet flow chamber of the motor
C7	Volume-pressure relation of the outlet flow chamber of the motor
MR2	Friction force in the hydraulic pump
MR3	End stopper force applied on the piston
MR4	Fluid leakage in the hydraulic motor
I2	Shaft inertia
Rg	Dissipative force of the generator

4. Wear damage of the piston ring and cylinder bore

4.1. Overview

Reciprocating engines are widely used in the modern industry. Over the years, one particular problem has prompted extensive development efforts, namely, fluid leakage between the piston and cylinder bore. This problem occurs in many types of machinery, such as hydraulic pumps, hydraulic motors and combustion engines. Initially, manufactures made an effort to manufacture the piston-cylinder assembly with a very narrow gap. This kind of sealing method has low efficiency, and the gap cannot be reduced without any limitation due to the requirement of a high degree of surface smoothness and small assembly tolerance. An effective way to solve this problem is to employ a separate element, i.e., a piston ring, to conform to the surface of the cylinder bore and thus prevent fluid leakage. This development can increase the effective pressure on the piston. In addition, because the piston is not required to seal off the fluid any more, the size of the piston can be smaller, which makes it possible to reduce the weight of the pump. Due to these advantages, various piston rings, as a new sealing concept, have developed rapidly since 1774 (Sätra, 2005), the year the piston ring was first used in a steam engine.

A common feature of the piston rings used for linear motion is that they operate against a reciprocating counter, and thus, they have to be optimised in terms of sealing ability, low friction and small wear damage. These tribological behaviour in the contacts formed by piston rings and cylinder bore has attracted significant attention over several decades. Recent studies include numerical modelling (e.g., Priest et al., 1999; Akalin and Newaz, 2001), miniaturised experiment (e.g., Papadopoulos et al., 2007; Sjödin and Olofsson, 2004) and full-scale testing (e.g., Douglas et al., 2006; Sätra, 2005).

Wear is a material removal procedure and can lead to changes in the surface quality of the contact surfaces. The most intensive wear on a piston ring and cylinder bore normally occurs in the breaking-in stage, during which the peaks of the surfaces are worn off by the counter surface (Hu et al., 1991; Priest and Taylor, 2000; Sjödin, and

Olofsson, 2003) and finally achieve an optimum mating of surfaces to control leakage (Peterson and Winer, 1980). After a “breaking-in” period of continuous operation, the wear of a piston ring and cylinder bore reaches a steady state. The wear rate, a parameter defined as material loss per second, of the respective counter surface in steady state is normally only a fraction of the level experienced in the breaking-in period (Andersson et al., 2002). However, this low wear rate can gradually change the surface quality and finally induce seal failure. Furthermore, compared with the steady state period (normally can last for years), the duration of the breaking-in stage is very small, say tens of hours. Therefore, for long-term wear damage analysis, a description of wear in the steady state period is necessary.

Several wear mechanisms, such as adhesion, abrasion, corrosion, surface fatigue and impact wear, contribute to the wear of piston rings and cylinder bore (Peterson and Winer, 1980; Becker and Ludema, 1999; Tung and Huang, 2007). Fully modelling the wear phenomenon is a very complex procedure due to the incorporation of several technical disciplines and hundreds of related variables (Ludema, 1996). Although considerable efforts have focused on developing theories and deterministic models (as Meng and Ludema (1995) mentioned, nearly 200 wear equations have been published in the literature), there is still no way to predict the tribological performance for the two loaded pairs with confidence or certainty (Williams, 1999). Consequently, to predict the wear damage of piston rings and a cylinder bore, researchers should focus on the important wear mechanisms that contribute most to the damage. According to the material properties and operating conditions, different wear types would be identified as the main wear mechanism. For the piston assembly used in the reciprocating engines, some researchers, such as Ting and Mayer (1974) and Sätra (2005), believed that adhesion wear was the dominant wear type in the system. However, because the abrasives between the contact surfaces that move relative to each other are obviously harmful, and abrasive wear could be magnitudes greater than that experienced with adhesion wear, especially when the loaded pairs work in the unclean oils, abrasive wear has been considered to be the main wear mechanism by several authors (King and Lancaster, 1980; Burr, 1982; Prehn et al., 2005; Tung and Huang, 2007).

The most commonly used model for wear on sliding contact surfaces is usually interpreted in terms of the following equation:

$$WeV = kNs \tag{4.1}$$

where WeV is the wear volume loss, N is the normal load, s is the sliding distance and k is the wear coefficient. This equation is the well-known “Archard” (Archard and Hirst, 1956) or “Rabinowicz” (Rabinowicz et al., 1961) relation. Although the

wear coefficient was initially intended to represent the probability of forming an adhesive wear particle, it could also be used to model other types of wear, such as abrasion and corrosion (Rabinowicz, 1995). This flexibility allows this law to be used widely as a quantitative formula in different domains. Often, an adoption of Archard's law depends on experimental or real measurements of the wear coefficient, k, which is the most critical term in Archard's equation.

For the hydraulic pump, the working fluids (oil or water) are also used as lubricants. A lubricant can reduce friction and wear, and provide satisfactory life for the tribo-pairs. The tribological performance of the piston assembly can only be fully understood when both lubrication and wear are considered in combination. The characteristics of a liquid lubricant can be described by the Stribeck curve. This curve was initially formulated by Stribeck for journal bearing, with the friction coefficient set against the Hersey number, a dimensionless parameter that describes the relationship among the lubricant viscosity, relative surface velocity and the normal load (Hamrock et al., 2004). Later, instead of using the Hersey number, some authors (e.g., Hutchings, 1992; Neale, 1995; Bayer, 2004) introduced another dimensionless parameter λ, the ratio between the minimum lubricant film thickness h (Fig. 1.5) and the composite surface roughness σ, i.e., the root-mean-square value of the variation of surface height (Thomas, 1999), to represent the abscissa variable in the Stribeck curve. The parameter λ, which includes the surface roughness, can depict the evolutions of the friction coefficient and wear damage quite well.

High λ values are usually related to fluid film lubrication, where the lubricating surfaces are totally separated by the lubricant, and as mentioned by Bayer (2004), wear is small and limited by fatigue mechanisms associated with pressure transmitted through the fluid. As λ decreases, mixed lubrication occurs. In this regime, contacts between the asperities are expected to occur; then, wear takes place due to physical interaction of both solid surfaces. When the λ value is small enough, say unity, the oil film thickness is very small, not fluid anymore and is related to the boundary lubrication regime, where significant wear is likely to be located. The occurrence of lubrication regimes is related to the motion type of the two lubricating surfaces (Bayer, 2004). For a sliding contact, the λ values 1 and 3 are assumed as the transition points to limit the regimes. It is widely assumed that the wear rate is constant under the boundary lubrication condition and decreases linearly as lubrication conditions change from boundary to hydrodynamic (Visscher, et al., 1998); the wear loss in the hydrodynamic lubrication region is assumed to be negligible. The lubrication regimes are indicated in Fig. 4.1 and can be inferred from the friction and wear behaviour of the sliding pairs.

The lubricant film thickness h between the piston ring and cylinder bore can be obtained by either numerically solving Reynolds equation (e.g., Akalin and Newaz, 2001; Nikas, 2003; Salant, 2007), a simplified form of Navier-Stokes equation with relevant assumptions, or by using an empirical formula, which has been derived by Hamrock et al. (2004). Generally speaking, the numerical model can yield more accurate results than the empirical model. Nevertheless, it is much more complicated and time consuming. Compared with the numerical model, the empirical model can provide satisfactory results for most cases and has been widely adopted by researchers and engineers because of its simplicity. In this thesis, the empirical model was adopted to calculate the lubrication film thickness between the piston ring and cylinder bore.

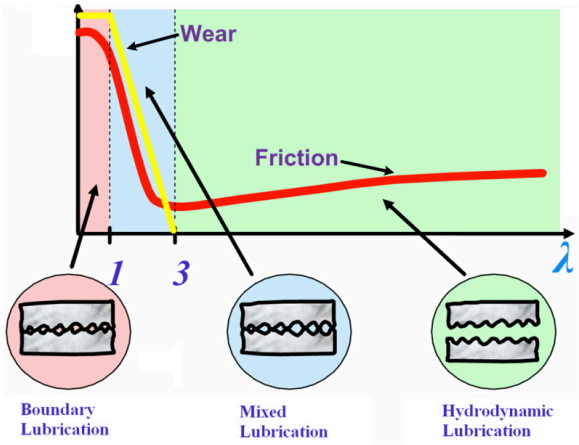

Figure 4.1: Schematic diagram of the relations among the wear, friction and lubrication regimes for sliding pairs as functions of the value λ.

Normally, the wear coefficient k can vary significantly from a very high value under aggressive conditions to very low values in more benign circumstances. To sufficiently address the wear, comprehensive programs have been implemented to investigate the relationship between wear damage and its relevant variables. Taking the abrasive wear as example, studies by different authors show that several possible factors can affect the wear coefficient k: the abrasive particle concentration and size (Hokkirigawa and Kato, 1988; Williams and Hyncica, 1992), the ratio of particle hardness to the hardness of the wearing surface (Rabinowicz et al., 1961; Kramer, 1986), the roughness of the contact surfaces (Patir and Cheng, 1978 and 1979), the oil conditions (Truhan et al., 2005), the motion type of the abrasive particles (Fang et al., 2004) and the lubrication conditions (Visscher et al., 1998; Bayer, 2004). Based on previous studies, Yang and Moan (2011) developed an abrasive wear model for the piston ring and cylinder bore during steady-state operation by considering the

effects mentioned in publications. This proposed model, in fact, is a generalisation of the Rabinowicz approach to account for the abrasive wear mechanism. However, instead of using a simple wear coefficient in the Rabinowicz's model, the wear coefficient herein is a function of several relevant variables which can represent the wear development of the piston ring and cylinder bore in detail. By incorporating the established wear model and the dynamic WEC model, the wear loss of the piston ring and cylinder bore has been estimated numerically (Papers B and C).

4.2. The wear model for the piston ring and cylinder bore

The wear analysis was determined for a hydraulic piston assembly used in the wave energy converter system (Fig. 1.5). A piston ring with a thickness t_R and a width w_R slides along the cylinder bore longitudinally with speed $\dot{X}(t)$. The piston ring has a symmetric outer crowning with a radius half the inner cylinder bore diameter D. Different types of piston rings could be used in this hydraulic pump; they could be made of elastomers (Müller and Nau, 1998) or steel (Sätra, 2005). In this thesis, elastomer and steel rings were considered in Paper C and Paper B, respectively. To derive the wear model, a uniform pressure distribution along the interface of the ring and cylinder bore was assumed. This uniform pressure $P(t)$ can be considered to be the average pressure generated by the hydrodynamic action of the lubricant on the ring face. Moreover, the pressure $P(t)$ is assumed to be approximated using the sealed pressure (Ting and Mayer, 1974; Nikas, 2003), the larger pressure of P_A and P_B, as marked in Fig. 1.5. With these assumptions, the total normal load N of Eq. (4.1) on the contact region can be written as follows:

$$N(t) = \pi D t_R P(t) = \pi D t_R \max\left[P_A, P_B\right] \tag{4.2}$$

With these basic assumptions and dimensional parameters, the wear models of the piston ring and cylinder bore can be derived, as shown in the following section.

4.2.1. The wear damage of the piston ring

A piston ring wear model has been developed in Paper C. Abrasive wear is considered to be the main wear mechanism. The wear model starts with a quantitative wear expression for an individual abrasive particle in the form of a core cutting along an abraded surface, and ends with a formula that includes the effects of lubrication, load, material properties and surface roughness (see Eq. (21) in Paper C). The proposed novel wear model is a generalisation of the Rabinowicz's relation, but it considers more variables. One can choose some or all of the affected variables

when adopting this model. The model can be simplified back to the form of Eq. (4.1) when all the effects are assumed to be addressed with wear coefficient *k*. This model is reported in Paper C.

To estimate the piston ring wear damage during the steady state period, two independent parameters are used to characterise the wear procedure: (1) the dimensional wear coefficient K_{sum} with units m^2/N and (2) the instantaneous wear work rate $\dot{W}(t)$ (Delaune, 2000), which is the product of the contact pressure $P(t)$ and piston velocity $\dot{X}(t)$. By assuming that K_{sum} is independent of time, the ring's life duration T_f during the steady state operation period at one wear work rate value $\dot{W}$ can be expressed as follows:

$$T_f = \frac{d_f}{K_{sum}} \dot{W}^{-1} \text{ (see also Eq. (25) in Paper C)} \tag{4.3}$$

where d_f is the limit wear depth loss of the ring.

The relationship between T_f and $\dot{W}$ in Eq. (4.3) can be plotted in a log-log diagram, as shown in Fig. 4.2. For various materials under different operation conditions, this curve can be established by laboratory experiments. The design check for the piston ring wear is based on the resistance defined by the $\dot{W} - T_f$ curve and the hypothesis of linear cumulative damage.

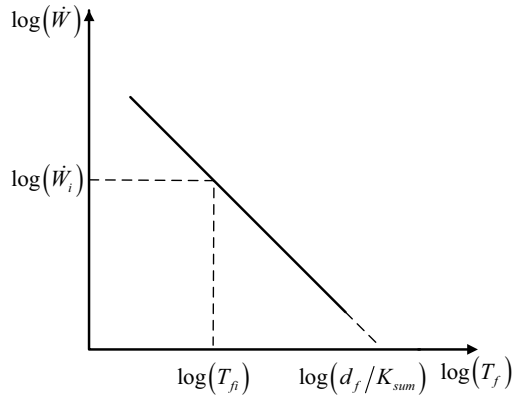

Figure 4.2: Log-log plot of the wear work rate $\dot{W}$ and ring life duration T_f.

Taking $\dot{W}$ as a random variable with its probability function $f_{\dot{W}}(\dot{W})$, the normalised accumulative ring wear damage d_R in time period T can be obtained:

$$d_R = \frac{K_{sum} T}{d_f} \int f_{\dot{W}}(\dot{W}) \dot{W} d\dot{W} \tag{4.4}$$

The long-term piston ring wear damage, taking into account different sea states described with probability density function $f_{H_s,T_p}(h_s,t_P)$, can then be expressed as follows:

$$\begin{aligned} d_R(T) &= \frac{K_{sum} T}{d_f} \int_{T_p} \int_{H_s} \int_{\dot{W}} f_{H_s,T_p}(h_s,t_P) f_{\dot{W}|H_s,T_p}\left(\dot{W}\middle|h_s,t_p\right) \dot{W} d\dot{W} dh_s dt_P \\ &= \frac{K_{sum} T}{d_f} \int_{T_p} \int_{H_s} f_{H_s,T_p}(h_s,t_P) \mathrm{E}\left[\dot{W}\middle|h_s,t_p\right] dh_s dt_P \end{aligned} \tag{4.5}$$

where H_s and T_p are the significant wave height and spectral peak wave periods, respectively. The term $f_{\dot{W}|H_s,T_p}(\dot{W}|h_s,t_p)$ is the probability density function of $\dot{W}$ conditioned upon the sea state parameters H_s and T_p, and E[•] represents the mean value of the related stochastic variable.

Then, the failure function of the piston ring due to wear damage during time interval T under steady state operation condition can be written as follows:

$$g(T) = \Delta - d_R(T) \le 0 \tag{4.6}$$

where g(T) is the limit state equation, Δ is the characterised ring wear damage at failure. Normally, a seal is said to fail when the leakage rate past the seal exceeds an acceptable design value. In this work, the leakage rate is assumed to remain reasonably constant before the quantity of surface wear reaches Δ. At the point of complete wear (Δ=d_R(T)), the seal fails and there is a sudden increase in leakage. The value of Δ depends on the consequences of failure and access for inspection and can vary between 0 and 1.

In this work, the relative frequency of the various sea states reflected in the probability density function $f_{H_s,T_p}(h_s,t_P)$ was approximated by using an appropriate scatter diagram (Gao, 2008). The wear prediction model Eq. (4.5) with an integral form can be discretized as a summation form which was reported in Paper C (Eq. (34)). The mean value of $\dot{W}$ under corresponding sea state was calculated numerically by solving the dynamic WEC model described in the preceding chapter. Long-term wear damage can be calculated by summing the short-term wear damage multiplied by the occurrence probability of each sea state during the long-term period of interest. Finally, the relative contribution of wear damage from different sea states was obtained (Fig. 13 in Paper C).

4.2.2. The wear damage of cylinder bore

When the piston-bore interface is considered to be a tribological system, the cylinder bore wear is more important than the ring wear because replacing the cylinder bore is much more expensive than replacing the ring (Arnold et al., 1960). However, because the cylinder normally possesses a relatively large diameter, e.g., tens of centimetres, and the diameter deformation due to the wear loss is very small, it is difficult to measure and detect the small changes. As a result, engines were generally operated for an extended period before measurements were taken. The postponed detection could increase the uncertainty for maintaining the cylinder assembly. Determining the postponed period may be a problem for engineers. Consequently, a wear model, which has the ability to describe the cumulative damage during operation, could be helpful for inspecting and repairing the hydraulic cylinder bore component.

Unlike the wear of the piston ring, which is a continuous material loss procedure during operation, the wear of the cylinder bore at position X (Fig. 4.3) only occurs when the ring slides through it, which can be considered a discretised procedure. To model the wear damage of the bore, one has to sum all the contributions made by each piston ring crossing. The distributed wear model along the cylinder bore is not only a function of time but also a function of space position X. Archard's equation (see Eq. (4.1)) is adopted here. To account for the lubrication effects, the wear coefficient k is modified using a factor $K(\lambda)$. The values of λ can be calculated by adopting the empirical formula given by Hamrock et al. (2004). The lubrication effect on wear is depicted in Fig. 4.1. If the linear damage rule is applicable, the cumulative cylinder bore wear depth $d_c(X)$ in the radial direction of the cylinder for a reciprocating motion during a time interval T with $n(X)$ crossings can be expressed as follows:

$$d_c(X) = K_0 \overline{P}(X) n(X) t_R \tag{4.7}$$

where K_0 is the wear factor in the boundary lubrication regime and is assumed to be a time-independent constant and $\overline{P}(X)$ is the average effective pressure, which is defined as follows:

$$\overline{P}(X) = \frac{\sum_{i=1}^{n(X)} K_i(\lambda) P_i(X)}{n(X)} \tag{4.8}$$

A detailed derivation of Eqs. (4.7) and (4.8) is reported in Paper B.

Equation (4.7) provides an expression for the wear damage of any segment of the cylinder bore as it slides by the ring during operation. The product of $n(X)$ and t_R is considered to be an equivalent sliding distance. The modified factor $K(\lambda)$, which indicates the effects of the surface roughness and lubrication, is considered in terms of the average effective pressure $\overline{P}(X)$. For the hydraulic pump used in the wave energy converter, the bore wear distribution can be estimated numerically based on the system simulation results when the buoy was exposed to irregular incident waves.

Modelling the long-term wear damage is similar to that of the ring wear. By invoking the rule of total probability, the accumulative bore wear damage can be obtained by summing the short-term wear damage multiplied by the occurrence probability of each sea state, which is expressed mathematically as follows:

$$d_c(X) = \int_{T_p}\int_{H_s} f_{H_s,T_p}(h_s,t_P)\, d_c\left(X \,|\, h_s,t_p\right) dh_s dt_p \tag{4.9}$$

The wear model Eq. (4.9) provides a way to predict the cylinder bore wear loss by incorporating the randomness of the incident waves. The sea state that contributes most to the bore wear damage can be determined using a contour plot, which could be useful for designing and planning inspection of the hydraulic cylinders.

Replacing or repairing a cylinder is generally carried out when the maximum wear of its internal surface approaches a specified limit, i.e., $d_{c,max}$. The position of the bore where the maximum wear occurs should be determined or estimated. Different parameters affect the position with maximum wear. One important issue is the dynamic characteristics of the wave energy converter system, which will be illustrated in the following section.

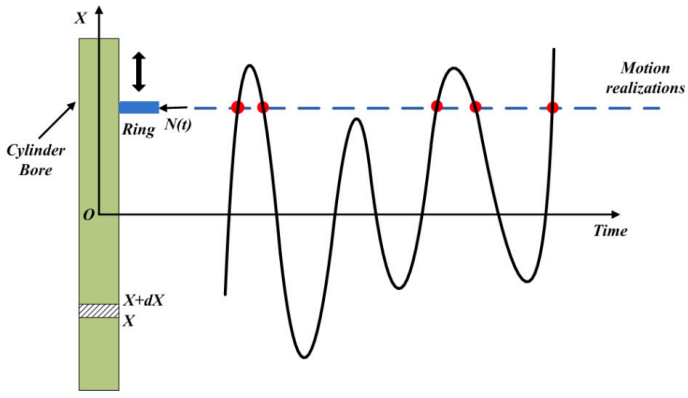

Figure 4.3: A sketch of the motion of the piston ring along the cylinder bore. The origin is set at the middle point of the cylinder bore.

4.3. The effect of the dynamic characteristics of WEC on wear estimation

In the example wave energy converter system studied in this work (Fig. 1.1), a floating buoy drives the piston, and its oscillating motion is converted into the flow of a liquid at high pressure. The randomness of the wave motion is reflected in the dynamic responses of the WEC system. Compared with the cyclic piston motion with constant amplitude in the traditional engines (e.g., internal combustion engines), the randomness of wave-induced motions increases the uncertainties and difficulties in predicting the wear damage of the piston ring and cylinder bore in the hydraulic system adopted in this WEC. In addition, because of the nonlinearities of the wave energy converter characteristics, the dynamic responses of both the piston motion and the pressure variation in the cylinder are, in principle, non-Gaussian (Yang et al., 2009). These facts make it difficult to estimate the wear damage of the piston ring and cylinder bore in the frequency domain and time-domain simulation methods need to be applied.

For the studied WEC system, the piston motion mainly includes two parts (Paper A). One part occurs when the incident wave force is sufficient to pump the fluid from the hydraulic cylinder into the HP accumulator. During this period, the single direction valves are open and the wave energy is converted into electric energy. It is found that this type of motion oscillates at or below the incident wave frequency (Yang et al., 2009) and is defined as low frequency oscillation (LFO) in this research.

The other part is related to the case with insufficient incident wave force. During this time interval, no fluid is pumped or sucked between the hydraulic pump and accumulators, i.e., the valves are closed. The buoy and piston will oscillate with small amplitudes. The oscillating frequency of this motion can be calculated by considering the fluid compressibility of the hydraulic pump to be a very stiff spring. Because this oscillating frequency is much higher than that of the incident waves, its corresponding motion is denoted as high frequency oscillation (HFO) in this work. A simulation sample for the buoy-ring motion in the time interval $1125<t<1225$ s is given in Fig. 4.4.

As reported in Paper A, the HFOs are mainly caused by the compressibility of working fluid in the hydraulic chambers, and they do not contribute to electric power production. Hence, the effect of fluid compressibility on energy absorption is negligible. However, the HFOs cannot be neglected in the study of wear damage for the reasons given below.

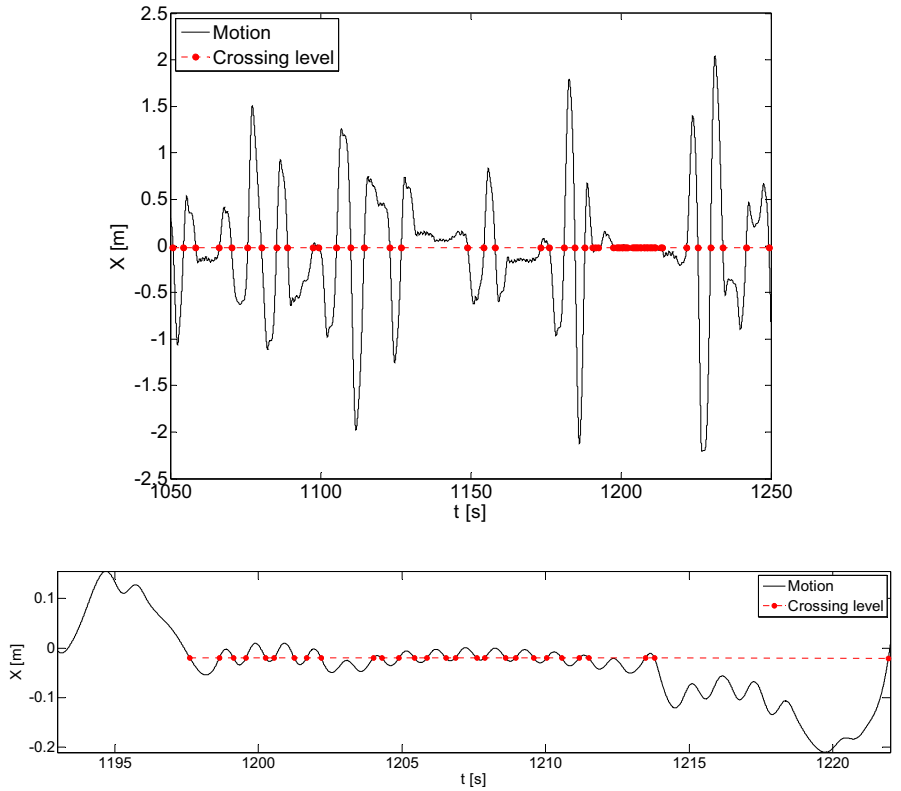

Figure 4.4: Upper plot: Time variation for the buoy-ring excursion $X(t)$ for a semi-submerged sphere with a radius 5 m. The sea state is defined by H_s = 4.25 m and T_P = 9.5 s. Compressible fluid in the hydraulic pump is considered. Both the low frequency oscillation (LFO) and high frequency oscillation (HFO) are shown in the figure. The crossings at X= -0.02 m are represented as red dots. Lower plot: Buoy-ring excursion and ring crossings for a shorter time interval to display the HFO observed in the upper plot clearly.

Archard's equation indicates that the wear volume loss is proportional to the sliding distance. The HFOs can increase the sliding distance of the piston ring, which leads to increased ring wear as the result. For the wear of the cylinder bore, as shown in Eq. (4.7), the sliding distance at piston position X is determined by the crossing number $n(X)$ and ring thickness t_R. Simulation results in Paper A show that $n(X)$ can increase significantly around the midpoint of the cylinder because of HFOs (Fig. 4.4), which, as a result, leads to an increased bore wear loss around this domain.

In addition to the increase of sliding distance, HFOs can cause poor lubrication between the contact surfaces of the piston ring and cylinder bore. At the contact area, the lubricating oil is squeezed out when the relevant velocity is small or vanishing,

which results in surface-to-surface contact, which is normally related to the boundary lubrication regime. Because a low amplitude motion, such as HFOs, does not permit the contact area to be re-lubricated, serious wear may occur on both the piston ring and cylinder bore (Fig. 4.1).

To summarise, the HFOs play a dominant role in estimating the wear damage of the piston ring and cylinder bore. In the design of the piston assembly for a wave energy converter system, both the LFOs and HFOs need to be considered. The dynamic responses of the WEC system, including the buoy motion, are reported in Paper A. The effect of the fluid compressibility and its induced high frequency buoy motion to the wear damage of the piston ring and cylinder bore is investigated in Papers A and B. By accounting for the contribution of the HFOs, long-term wear damage is reported in Paper C for the piston ring and Paper B for the cylinder bore.

4.4. Reduction of wear damage

The progressive damage and material loss of the piston ring and cylinder bore can ultimately result in poor performance and low energy conversion efficiency. The failure of the ring-bore assembly can have economic consequences that include not only the cost of replacement but also the expense involved in lost production. Hence, it is important to consider means of reducing the wear in the design of the hydraulic pump. To achieve this target, two main ways are envisaged:

1. Try to reduce the wear coefficient k as much as possible.

   This study usually belongs to the discipline of tribology. The substantial and comprehensive studies on wear with both theory and experiments in the past years are highly beneficial to understanding the material loss in reciprocating engines. These existing studies can be combined and utilised immediately in the wear damage analysis for the ring-bore pairs adopted in the WEC system. Based on previous studies in the field of tribology, some recommendations for reducing the wear coefficient include the following:

   a) Keep the lubricant as clean as possible. Both the piston ring and cylinder bore benefit from changing the oil periodically and using oil filters;

   b) Based on the working environment, choose materials for the ring and cylinder bore that are sufficiently wear resistant;

   c) Use a coating to protect the contact surfaces;

   d) Reduce the roughness of the surfaces.

2. Reduce the wear damage by choosing proper WEC parameters.

Except for the wear coefficient k, the wear volume loss of the studied ring-bore surfaces is also proportional to the sealed pressure in the cylinder and the buoy motion. The dynamic responses of the buoy motion and pressure variation in the cylinder are determined by the designed parameters of the WEC system and the operating environment. Minimising the wear damage by combining the dynamic characteristics of the WEC is a focus of this research. According to this study, this combination can be achieved in the following ways:

a) Choose an appropriate cylinder size. For the studied WEC system, the cylinder size can affect the sealed pressure and oscillating frequencies of the HFOs. It is found that there exists an optimum cylinder size that leads to minimum wear damage on the ring-bore pairs of the hydraulic pump in each sea state. By combing the probability of occurrence of each sea state, the wear losses for different types of hydraulic pumps can be calculated. An optimum pump size with minimum long-term wear damage can then be determined. A detailed analysis of this aspect is reported in Paper A.

b) The wear damage of the piston ring is directly related to the instantaneous wear work rate $\dot{W}$, which is the product of the sealed pressure and ring velocity. For the proposed WEC system, the produced electric power depends on the product of the pressure difference across the piston and the buoy velocity. The similarity between $\dot{W}$ and the produced electric power implies that there is a proportional relationship between the power conversion of the WEC and the ring wear damage. Thus, smaller buoys that convert less power also have less wear damage. From this point of view, a compact array of small buoys is advantageous over a single large buoy. This issue is described in detail in Paper C.

5. Conclusions

5.1. General

This thesis deals with the dynamic responses of a floating heaving-buoy that is equipped with hydraulic power take-off and time-domain wear damage analysis of the piston ring and cylinder bore in the hydraulic pump. The research work covers three main topics, namely:

First, a complete nonlinear mathematical model of a wave energy converter system, which consists of an absorber, a hydraulic pump, check valves, transmission lines, accumulators, a hydraulic motor and an electric generator, is developed in a state space form. The dynamic model, which spans several energy domains, where each domain belongs to different disciplines, can be solved numerically using the ODE solver package in Matlab. This topic is mainly addressed in Papers A and D.

In particular, to take advantage of bond graphs, which are graphical representations of the energy storage, dissipation and transfer among the interacting dynamic systems, modal bond graphs of the transmission lines are generated using the separation of variables technique and rational transfer function for all four possible input-output configurations. The bond graph models of the pipelines can be saved in the bond graph library, a virtual space in a computer that contains the modular bond graphs of different subsystems and be used multiple times for different coupled systems.

Finally, time-domain wear damage analysis of the piston ring and cylinder bore is performed based on the established wear model and relevant dynamic responses of the wave energy converter system. The long-term wear damage prediction is calculated by summing the short-term wear damage in each sea state and its occurrence probability, which is given in the form of a wave scatter diagram. The contribution of the wear damage from each sea state is finally obtained (Papers B and C). For the wear damage analysis, the effect of fluid compressibility and its induced high frequency oscillation is taken into account.

Based on the results and observations, the main contributions of the research work in this thesis and further recommendations for future work in these areas are presented as follows:

5.2. Summary of main contributions

The main contributions in this thesis, include:

1. Developed an integrated dynamic model for a wave energy converter system using inter-linked models of the related subsystems.
2. Investigated the effect of the fluid compressibility in the hydraulic pump and displayed the induced high frequency oscillations of the floating buoy in time series and corresponding power spectra.
3. Established an abrasive wear model for a reciprocating piston ring in a hydraulic pump by considering the effects of sealed pressure, relative velocity, material properties, time-varying environmental conditions and lubrication.
4. Derived a wear resistance curve $\dot{W} - T_f$ (wear work rate versus time duration for wear damage growth till failure) in log-log coordinates for the wear loss of a piston ring during the steady state operation period with the assumption of linear cumulative damage.
5. Developed a long-term piston ring wear damage expression by incorporating the wave scatter diagram based on the defined $\dot{W} - T_f$ curve. Calculated the contribution of the ring wear damage from each sea state in the time-domain.
6. Established a numerical wear model for the cylinder bore that accounts for the interactive dynamics, lubrication and wear and supplied a computing procedure for the time-domain bore wear estimation.
7. Estimated the wear damage along the cylinder bore based on time domain simulations and predicted the position of the bore at which the maximum accumulated wear would occur.
8. Demonstrated the long-term wear damage distribution of the cylinder bore by combining the occurrence probability of different sea states and supplied a contour plot that represents the relative contributions of bore wear damage from each sea state.

9. Emphasised the importance of the fluid compressibility in the hydraulic pump to the wear volume loss of the piston ring and cylinder bore and showed the wear difference when two dynamic wave energy converter models were adopted: one with incompressible fluid and the other with compressible fluid in the hydraulic pump.

10. Proposed possible ways to reduce the wear losses for the piston ring and cylinder bore based on the dynamic characteristics of the studied wave energy converter.

11. Investigated the effect of long transmission lines on the performance of the wave energy converter and predicted the transient pressure pulsations caused by the activity of the check valves and end stoppers.

12. Constructed bond graph models for the hydraulic pipelines for two physically realisable input-output causality relationships, i.e., upstream pressure and downstream flow rate as inputs and upstream flow rate and downstream pressure as inputs, using the separation of variables technique.

13. Developed modal bond graph representations of fluid transmission lines for the two input-output configurations, i.e., upstream and downstream pressures as inputs, upstream and downstream flow rates as inputs, using the method of rational transfer function.

5.3. Recommendations for future work

In the future, further development of the methodology and application of the approach established in this thesis is envisaged:

1. This thesis mainly focused on a heaving buoy equipped with a passive hydraulic power take-off. No control strategies, e.g., latching control or clutching control, have been attempted. Although this so called passive power take-off mechanism can attain a considerable amount of extracted power, the absorption ability of the WEC can be enhanced by applying control methods. The developed dynamic model should be extended to a model for a WEC system including proper control strategy. The stability of the system with corresponding control feedback signals could be studied further.

2. Linear wave theory was adopted in this simulation model. This theory is proved to be valid for incident waves with small wave heights and for buoy motion with small amplitudes. For extreme operation conditions, i.e., severe sea states with large wave heights, nonlinear effects should be considered, which is a topic for future study.

3. The electric generator in the developed WEC model was simplified as a linear resistance. This modelling choice did not influence the effects studied in this research. However, to obtain insight into the electric generator, which plays a role in the behaviour of the wave energy converter system, a detailed generator model, which can be directly added to the established ODE-based WEC model, is desirable.

4. Validation by laboratory test or real measurements should be carried out for the presented simulation results and observed phenomena in this research.

5. To predict piston ring wear resistance using the $\dot{W} - T_f$ curve, the wear coefficient is assumed to be time-independent. The damage obtained with this assumption is the average wear loss within a time period. In practice, wear is a random process. Extending the wear model to include the time-dependent wear coefficient could be a challenging and interesting future work.

6. The piston ring failure probability was calculated with methods such as FORM/SORM or Monte Carlo simulation by applying the failure functions given for the $\dot{W} - T_f$ approach. The randomness and uncertainty of the relevant variables should then be introduced.

7. The lubrication conditions between two contact surfaces, i.e., the piston ring and cylinder bore, are governed by Reynold's equation, which can be numerically simulated by applying the relevant boundary conditions. This feature could be taken into account in the wear model.

8. The modal bond graph representations for the transmission lines were derived based on the linear friction model with the assumption of laminar flow. For more accurate calculation, a dissipative model, which takes into account the fluid viscosity and heat transfer, would be considered.

9. The cyclic pressure variations in the hydraulic power take-off can cause fatigue damage, especially to the hydraulic cylinder and pipelines. Estimating the fatigue damage of the hydraulic cylinder and pipelines is an important issue for assessing system reliability. Damage caused by water hammer pressures should be taken into account.

10. The failure of the check valves, in addition to losing the ability to prevent backflow, can cause water hammer pressures in the hydraulic power take-off. Consequently, assessing check valves life could be important in the future.

11. Developing a methodology to assess the availability and reliability of the integrated system and providing quantitative safety measures for the studied wave energy converter system should also be studied.

References

[1]. 20-sim, version 4.1, Controllab products B.V., The Netherlands, http://www.20sim.com.

[2]. Aesoy, V., and Engja, H., 1996. Fuel injection system design, analysis and testing using bond graph as an efficient modelling tool. In Proceeding International Fall Fuels & Lubricants meeting &exposition, San Antonio, Texas, October 14-17.

[3]. Akalin, O., and Newaz, G. M., 2001. Piston ring-cylinder bore friction modeling in mixed lubrication regime: Part I-Analytical results. Journal of Tribology, Vol. 123, pp. 211-218.

[4]. Andersson, P., Tamminen, J., and Sandström,C.E., 2002. Piston ring tribology: A literature survey, Technical editing Maini Manninen.

[5]. Archard, J.F., Wear theory and mechanisms, Part II of Wear control handbook, Peterson, M.B. and Winer, W.O. editor, 1980.

[6]. Archard, J.F., and Hirst, W., 1956. The wear of metals under unlubricated conditions. Proceedings of the Royal Society of London, Series A, Mathematical and Physical Science, Vol. 236, No. 1206, pp. 397-410.

[7]. Arnold, W.C., Stonehocker, V.T., Braun, W.J., and Sunderman, D.N., 1960. Radioactive cylinders – a tool for wear research. SAE Transactions, Vol. 68.

[8]. Ayalew, B., and Kulakowski, B. T., 2005. Modal approximation of distributed dynamics for a hydraulic transmission line with pressure input-flow rate output causality. Journal of Dynamic Systems, Measurement, and Control, Vol. 127, pp. 503-507.

[9]. Babarit, A., Duclos, G., and Clement, A.H., 2004. Comparison of latching control strategies for a heaving wave energy device in random sea. Applied Ocean Research , Vol. 26, pp. 227-238.

[10]. Bayer, R.G., 2004. Mechanical wear fundamentals and testing. New York: M. Dekker, USA, ISBN 0-8247-9027-8.

[11]. Becker, E.P., and Ludema, K.C., 1999. A qualitative empirical model of cylinder bore wear. Wear, Vol. 225-229, pp387-404.

[12]. Bjarte-Larsson, T., and Falnes, J., 2006. Laboratory experiment on heaving body with hydraulic power take-off and latching control. Ocean Engineering, Vol. 33, pp. 847-877.

[13]. Bingley, M.S., and Schnee, S., 2005. A study of the mechanisms of abrasive wear for ductile metals under wet and dry three-body conditions. Wear, Vol. 258, pp.50-61.

[14]. Borutzky, W., Barnard, B., and Thoma, J., 2002. An orifice flow model for laminar and turbulent conditions. Simulation Modeling Practice and Theory, Vol.10, No.(3-4), pp. 141-152.

[15]. Budal, K., and Falnes, J., 1975. A resonant point absorber of ocean-wave power. Nature, Vol. 256, pp. 478-479.

[16]. Burr, B.H., 1982. An equation for the abrasive wear of elastomeric O-ring materials. Wear, Vol. 81, pp. 347-356.

[17]. Chapple, P.J., 2003. Principles of hydraulic system design. Oxford, Coxmoor Publishing Company, UK.

[18]. Chevary, R., and Mathieu, J., 1993. Topics in fluid mechanics. Cambridge University Press.

[19]. Cruz, J., editor, 2008. Ocean wave energy. Spring-Verlag Berlin Heidelberg.

[20]. Cummins, W., 1962. The impulse response function and ship motions. Schiffstechnik 9 (1661), pp.101-109.

[21]. Dahlheimer, J.C., 1972. Mechanical face seal handbook. Chilton, New York.

[22]. David, R., 1995. Power from the waves. Oxford: Oxford University Press, ISBN: 0-19-856511-9.

[23]. Delaune, X., Langre E. de., and Phalippou, C., 2000. A probabilistic approach to the dynamics of wear tests. Journal of Tribology, Vol. 122, pp. 815-821.

[24]. Douglas, R.M., Steel, J.A., and Reuben, R.L., 2006. A study of the tribological behaviour of piton ring/cylinder liner interaction in diesel engines using acoustic emission. Tribology International, Vol. 39, pp. 1634-1642.

[25]. Drew, B., Plummer, A.R., and Sahinkaya, M.N., 2009. A review of wave energy converter technology. In Proceedings of the Institution of Mechanical Engineers, Part A: Journal of Power and Energy, Vol. 223, No. 8, pp. 887-902.

[26]. Edge, K. A., Boston, O. P., Xiao, S., Longvill, M. J., and Burrows, C.R., 1997. Pressure pulsations in reciprocating pump piping systems Part II: experimental investigations and model validation. Part I: Journal of Systems and Control Engineering, Vol. 11, pp. 239-250.

[27]. Egeland, O., and Gravdahl, J.T., 2002. Modeling and simulation for automatic Control. Marine Cybernetics, Trondheim.

[28]. Eidsmoen, H., 1995. On the theory and simulation of heaving-buoy wave-energy converters with control. PhD thesis, NTH, Trondheim, Norway.

[29]. Engja, H., and Hals, J., 2007. Modelling and simulation of sea wave power conversion systems. In Proceedings of 7th European Wave and Tidal Energy Conference, Porto, Portugal, September.

[30]. Evans, D.V., 1981. Maximum wave-power absorption under motion constraints. Applied Ocean Research, Vol. 3, pp. 200-203.

[31]. Falcão, A.F. de O., 2007. Modelling and control of oscillating-body wave energy converters with hydraulic power take-off and gas accumulator. Ocean Engineering , Vol. 34, pp. 2021-2032.

[32]. Falcão, A.F. de O., 2008. Phase control through load control of oscillating-body wave energy converters with hydraulic PTO system. Ocean Engineering, Vol. 35, pp. 358-366.

[33]. Falnes, J., 2007. A review of wave-energy extraction. Marine Structures, Vol. 60, pp. 185-201.

[34]. Falnes, J., 2002. Ocean waves and oscillating systems. Cambridge University Press, Cambridge.

[35]. Falnes, J., and Budal, K., 1978. Wave-power conversion by point absorbers. Norwegian Maritime Research 6, pp. 2-11.

[36]. Faltinsen, O.M., 1990. Sea loads on ships and offshore structures. Cambridge University Press, Cambridge, UK.

[37]. Fang, L., Liu, W., Du, D., Zhang, X., and Xue, Q., 2004. Predicting three-body abrasive wear using Monte Carlo methods. Wear, Vol. 256, pp. 685-694.

[38]. French, M.J., and Bracewell, R., 1986. Heaving point absorbers reacting against an internal mass. In: Hydrodynamics of Ocean-Wave Energy Utilization (D.V.Evans and A.F.de O. Falcão editors), IUTAM Symposium, Lisbon, Portugal (1985), Springer Verlag, Berlin, pp. 247-255.

[39]. Gangopadhyay, A., 2000. Development of a piston ring-cylinder bore wear model. SAE paper No. 2000-01-1788.

[40]. Gao, Z., 2008. Stochastic response analysis of mooring systems with emphasis on frequency-domain analysis of fatigue duo to wide-band response process, PhD thesis, NTNU, Trondheim, Norway.

[41]. Ghidaoui, M.S., Zhao, M., McInnis, D.A., and Axworthy, D.H., 2005. A review of water hammer theory and practice. Applied Mechanics Review, Vol. 58, No. 1, pp. 49-76.

[42]. Giorgio, M., Guida, M., and Pulcini, G., 2007. A wear model for assessing the reliability of cylinder liners in marine diesel engines. IEEE Transactions on Reliability, Vol. 56, No.1, pp. 158-166.

[43]. Goodson, R.E., and Leonard R.G., 1972. A survey of modeling techniques for fluid line transients. Journal of Basic Engineering, Vol. 94, pp. 474-482.

[44]. Hals, J., 2010. Modelling and phase control of wave-energy converters. PhD thesis, NTNU, Trondheim, Norway.

[45]. Hals, J., Falnes, J., and Moan, T., A comparison of selected strategies for adaptive control of wave energy converters. Accepted for publication in Journal of Offshore Mechanics and Arctic Engineering.

[46]. Hals, J., Taghipour, R., and Moan, T., 2007. Dynamics of a force compensated two-body wave energy converter in heave with hydraulic power take-off subject to phase control. In Proceeding of 7th European Wave and Tidal Energy Conference, Porto, Portugal.

[47]. Hamrock, B.J., Schmid, S.R., and Jacobson B.O., 2004. Fundamentals of fluid film lubrication. 2nd Edition, New York: Marcel Dekker.

[48]. Henderson, R., 2006. Design, simulation, and testing of a novel hydraulic power take-off system for the Pelamis wave energy converter. Renewable Energy, Vol. 31, No. 2, pp. 271-283.

[49]. Hokkirigawa, K., and Kato, K., 1988. An experimental and theoretical investigation of ploughing, cutting and wedge formation during abrasive wear. Tribology International, Vol. 21, No. 1, pp. 51-57.

[50]. Holmboe, E.L., and Rouleau, W.T., 1967. The effect of viscous shear on transients in liquid lines. Journal of Basic Engineering, Vol. 89, No. 1, pp. 174-180.

[51]. Hsue, C., and Hullender, D., 1983. Modal approximations for the fluid dynamics of hydraulic and pneumatic transmission lines. Fluid Transmission Line Dynamics, M., Franke and T. Drzewiecki, eds. ASME, pp.51-77.

[52]. Hu, Y. Z., Li, N., and Tønder, K., 1991. A dynamic system model for lubricated sliding wear and running-in. Journal of Tribology, Vol. 113, pp. 499-505.

[53]. Hullender, D.A., and Healy, A.J., 1981. Rational transfer function for fluid transmission line models. Fluid Transmission Line Dynamics, ASME Special Publication, New York.

[54]. Hullender, D.A., and Hsue, C.Y., 1983. Modal approximations for the fluid transmission line dynamics. Fluid Transmission Line Dynamics, ASME Special Publication, New York.

[55]. Hullender, D. A., Woods, R. L., and Hsu, C. H., 1983. Time domain simulation of fluid transmission lines using minimum order state variable models. Fluid Transmission Line Dynamics, Vol. II, ASME Special Publication, New York.

[56]. Hutchings, I. M., 1992. Tribology: friction and wear of engineering materials. Edward Arnold, Great Britain.

[57]. Iberall, A.S., 1950. Attenuation of oscillatory pressures in instrument lines. Journal of Research, National Bureau of Standards, Vol. 45, pp. 85-108.

[58]. Jefferys, E.R., 1980. Device characterization. In: Count BM Power from sea waves, Academic Press, pp. 413-438.

[59]. Jefferys, E.R., 1984. Simulation of wave power devices. Applied Ocean Research, Vol. 6, No. 1, pp. 31-39.

[60]. Jelali, M., and Kroll, A., 2003. Hydraulic servo-systems: modelling, identification and control. London: Springer. ISBN: 1-85233-692-7.

[61]. Jeng, Y., 1992. Theoretical analysis of piston-ring lubrication, Part I-Fully flooded lubrication. Society of Tribologists and Lubrication Engineers, Journal of Tribology Transactions, Vol. 35, No. 4, pp. 696-706.

[62]. Johnston, D.N., 1991. Numerical modelling of reciprocating pumps with self-acting valves. Proceedings of the Institution of Mechanical Engineerings, Part I: Journal of Systems and Control Engineering, Vol. 205 (I2), pp. 87-96.

[63]. Jones, S.E., and Wood, D.J., 1972. Prediction and control of pressure surges due to valve closures. In Proceeding International Conference on Pressure Surges British Hydromechanic Research Association.

[64]. Karam, J.T. Jr., and Franke, M. E., 1967. The Frequency response of pneumatic lines. ASME Journal of Basic Engineering, Vol. 89, No. 3, pp. 371-378.

[65]. Karnopp, D., 1975. Lumped parameter models of acoustic filters using normal modes and bond graphs. Journal of Sound and Vibration, Vol. 42, No. 4, pp. 437-446.

[66]. Karnopp, D., Margolis, D.L., and Rosenberg, R., 2006. System dynamics: modeling and simulation of mechatronic systems. 4th edition, Hoboken, N.J., Wiley.

[67]. King, R.B., and Lancaster, J.K., 1980. Wear of metals by elastomers in an abrasive environment. Wear, Vol. 61, No. 2, pp. 341-352.

[68]. Kramer, B.M., 1986. Predicted wear resistances of binary carbide coatings. The Journal of Vacuum Science and Technology A, Vol. 4, No. 6**,** pp. 2870-2873,.

[69]. Kristiansen, E., Hjulstad, and Egeland, O., 2005. State-space representation of radiation forces in time-domain vessel models. Ocean Engineering, Vol. 32, pp. 2195-2216.

[70]. Lebrun, M., 1984. Normal modes in hydraulic lines. In Proceeding American Control Conference, San Diego, California, June 6-8, pp. 458-467.

[71]. Lebrun, M., 1985. The use of modal analysis concepts in the simulation of pipeline transients. Journal of the Franklin Institute, Vol. 319, No. 1/2, pp. 137-156.

[72]. Lopes, M.F.P., Hals, J., Gomes, R.P.F., Moan, T., Gato, L.M.C., and Falcão, A.F. de O., 2009. Experimental and numerical investigation of non-predictive phase-control strategies for a point-absorbing wave energy converter. Ocean Engineering, Vol. 36, pp. 386-402.

[73]. Ludema, K.C., 1996. Mechanism-based modeling of friction and wear. Wear, Vol. 200, pp. 1-7.

[74]. Mäkinen, J., Piché, R., and Ellman, A., 2000. Fluid transmission line modeling using a variable method. Journal of Dynamic Systems, Measurements, and Control, Vol. 122, pp.153-162.

[75]. Margolis, D.L., and Yang, W.C., 1985. Bond graph models for fluid networks using modal approximation. Journal of Dynamic Systems, Measurement, and Control, Vol. 107, pp. 169-175.

[76]. Marré, I.R., 2006. Modeling and simulation of a wave energy converter using a bond graph approach. Master's thesis, Department of Marine Technology, Norwegian University of Science and Technology.

[77]. Matlab, Version 7.2, The Mathworks Inc., 2006.

[78]. Meng, H. C., and Ludema, K.C., 1995. Wear models and predictive equations: their form and content. Wear. Vol. 181-183, pp. 443-457.

[79]. Merritt. H.E., 1967. Hydraulic Control Systems. John Wiley &Sons.

[80]. Moan, T., 2008. Structural risk and reliability analysis. Lecture note, CeSOS, NTNU, Trondheim.

[81]. Moan, T., Gao, Z., and Ayala-Uraga, E., 2005. Uncertainty of wave-induced response of marine structures due to long-term variation of extratropical wave conditions. Marine Structures, Vol. 18, No. 4, pp. 359-382.

[82]. Morison, J.R., O'Brien, M.P., Johnson, J.W., and Schaaf, S.A., 1950. The forces exerted by surface waves on piles. In Petroleum Transactions of AIME, Vol. 189, pp. 149-157.

[83]. Mueller, M.A., 2002. Electrical generators for direct drive wave energy converters. IEE Proceedings of Generation, Transmission and Distribution, Vol. 149, No. 4, pp. 446-456.

[84]. Müller, H.K., and Nau, B.S., 1998. Fluid sealing technology: principles and applications. New York: Marcel Dekker, USA, ISBN 0-8247-9969-0.

[85]. Naess, A., and Moan. T., Introduction to stochastic dynamics of marine structures, Lecture note, CeSOS, NTNU, Trondheim, Norway.

[86]. Neale, M.J., 1995. The Tribology Handbook. Oxford, England Boston: Butterworth-Heinemann.

[87]. Newman, J.N., 1977. Marine hydrodynamics. MIT Press.

[88]. Nichols, N.B., 1962. The linear properties of pneumatic transmission lines. Transactions of the Instrument Society of America, Vol. 1, pp.5-14.

[89]. Nikas, G.K., 2003. Elastohydrodynamics and mechanics of rectangular elastomeric seals for reciprocating piston rods, Journal of Tribology, Vol. 125, No. 1, pp. 60-69.

[90]. Ocean Power Technology. http://www.oceanpowertechnologies.com, visited in October, 2010.

[91]. Oldenburger, R., and Goodson, R.E., 1964. Simplification of hydraulic line dynamics by use of infinite products. Journal of Basic Engineering, Vol. 86, pp. 1-10.

[92]. Panicker, N., 1976. Power resource estimate of ocean surface waves. Ocean Engineering, Vol. 3, No. 6, pp. 429-439.

[93]. Papadopoulos, P., Priest, M., and Rainforth, W.M., 2007. Investigation of fundamental wear mechanisms at the piston ring and cylinder wall interface in internal combustion engines. Proceedings of the Institution of Mechanical Engineers, Part J: Journal of Engineering Tribology, Vol. 221, No. 3, pp. 333-343.

[94]. Patir, N., and Cheng, H., 1978. An average model for determining effects of three-dimensional roughness on hydrodynamic lubrication. Journal of Lubrication Technology, Vol. 100, pp. 12-17.

[95]. Patir, N., and Cheng, H., 1979. Application of average flow model to lubrication between rough sliding bearings. Journal of Lubrication Technology, Vol. 101, pp. 220-230.

[96]. PelamisWave. http://www.pelamiswave.com, visited in October, 2010.

[97]. Peterson, M.B., and Winer, W.O., 1980. Wear control handbook, New York: ASME.

[98]. Pierre, B., 2010. Pressure waves in pipelines and impulse pumping: physical principles, model development and numerical simulation. PhD Thesis, NTNU,.Norway.

[99]. Pizer, D.J., 1993. Maximum wave-power absorption of point absorbers under motion constraints. Applied Ocean Research, Vol. 15, No. 4, pp.227-234.

[100]. Prehn, R., Haupert, F., and Friedrich, K., 2005. Sliding wear performance of polymer composites under abrasive and water lubricated conditions for pump applications. Wear, Vol. 259, pp. 693-696.

[101]. Priest, M., Dowson, D., and Taylor, C.M., 1999. Predictive wear modelling of lubricated piston rings in a diesel engine. Wear, Vol. 231, pp. 89-101.

[102]. Priest, M., and Taylor, C.M., 2000. Automobile engine tribology – approaching the surface, Wear, Vol. 241, No. 2, pp. 193-203.

[103]. Rabinowicz, E., 1995. Friction and wear of materials. 2nd Edition, John Wiley and Sons, New York, USA, ISBN 0-471-83084-4.

[104]. Rabinowicz, E., Dunn, L.A., and Russell, P.G., 1961. A study of abrasive wear under three-body conditions. Wear, Vol. 4, pp. 345-355.

[105]. Rausand, M., and Høyland, A., 2004. System reliability theory: models, statistical methods, and applications. 2nd edition, Hoboken, N.J.: Wiley-Interscience.

[106]. Ross, D., 1995. Power from the waves. Oxford University Press, Oxford, UK.

[107]. Sätra, S.A., 2005. Wear of piston rings in hydrostatic transmissions. PhD Thesis, Trita-MMK-2005: Stockholm, Sweden.

[108]. Salant, R.F., Maser, N., and Yang, B., 2007. Numerical model of a reciprocating hydraulic rod seal. Journal of Tribology, Vol. 129, pp. 91-97.

[109]. Salter, S.H., 1974. Wave Power. Nature, Vol. 249, pp. 720-724.

[110]. Salter's Duck, http://tinyurl.com/saltersduck, visited in May, 2009.

[111]. Shu, J.J., Burrows, C.R. and Edge, K.A., 1997. Pressure pulsation in reciprocating pump piping systems Part I: Modelling. Proceedings of the Institution of Mechanical Engineerings, Part I: Journal of Systems and Control Engineering, Vol. 229, No. I3, pp. 229-237.

[112]. Sin, H., Saka, N., and Suh, N.P., 1979. Abrasive wear mechanisms and the grid size effect. Wear, Vol. 55, pp. 163-190.

[113]. Sjödin, U.I., and Olofsson, U.L.-O., 2003. Initial sliding wear on piston rings in a radial piston hydraulic motor. Wear, Vol. 254, pp. 1208-1215.

[114]. Sjödin, U.I., and Olofsson, U.L.-O., 2004. Experimental study of wear interaction between piston ring and piston groove in a radial piston hydraulic motor. Wear, Vol. 257, pp. 1281-1287.

[115]. Skarbø. J., and Engja, H., 1990. Modeling and simulation of a hydraulically operated gas injection valve using bond graphs. In Proceedings of 4th International Symposium on Marine Engineering, Kobe-90, Japan, 15-19, Oct..

[116]. Stecki, J., and Davis, D., 1986. Fluid transmission lines – distributed parameter models. Part I: A review of the state of the art. Proceedings of the Institution of Mechanical Engineerings, Vol. 200, pp. 215-228.

[117]. Stecki, J., and Davis, D., 1986. Fluid transmission lines – distributed parameter models. Part II: Comparison of models. Proceedings of the Institution of Mechanical Engineerings, Vol. 200, pp. 229-236.

[118]. Streeter, V.L., 1971. Unsteady flow calculations by numerical methods. ASME Paper, No. 71-WA/FE-13.

[119]. Taghipour, R., Perez, T., and Moan, T., 2008. Hybrid frequency time domain models for dynamic response analysis of marine structures. Ocean Engineering, Vol. 35, pp. 685-705.

[120]. Thomas, T., 1999. Rough surfaces. Imperial College Press, ISBN 1-86094-100-1.

[121]. Thorpe, T.W., 1999. A brief review of wave energy. Technical report No. R120, Energy Technology Support Unit (ETSU).

[122]. Ting, L. L., and Mayer, J. E., 1974. Piston ring lubrication and cylinder bore wear analysis: Part I-Theory. American Society of Mechanical Engineers, Journal of Lubrication Technology, Vol. 96, pp. 305-314.

[123]. Ting, L. L., and Mayer, J. E., 1974. Piston ring lubrication and cylinder bore wear analysis: Part II-Theory Verification. American Society of Mechanical Engineers, Journal of Lubrication Technology, Vol. 96, pp. 258-266.

[124]. Tisza, L., 1966. Generalized thermodynamics, Cambridge, MA: MIT Press.

[125]. Totten, G.E., editor, 2000. Handbook of hydraulic fluid technology. New York: Marcel Dekker.

[126]. Truhan, J.J., Qu, J., and Blau, P.J., 2005. The effect of lubricating oil condition on the friction and wear of piston ring and cylinder liner materials in a reciprocating bench test. Wear, Vol. 259, pp. 1048-1055.

[127]. Tung, S., and Huang, Y., 2007. Modeling of abrasive wear in a piston ring and engine cylinder bore system. Tribology Transactions, Vol. 47, pp. 17-22.

[128]. Van Schothorst. G., 1997. Modelling of long-stroke hydraulic servo-systems for flight-simulator motion control and system design. PhD thesis, Delft University of Technology, Netherlands.

[129]. Van Schothorst, G., Teerhuis, P.C., and Van d. Weiden, A.J.J., 1994. Stability analysis of a hydraulic servo-system including transmission-line effects. In Proceeding 3rd International Conference on Automation, Robotics and Computer Vision, Nov. 9-11, Singapore.

[130]. Vantorre, M., Banasiak, M., and Verhoeven, R., 2004. Modelling of hydraulic performance and wave energy extraction by a point absorber in heave. Applied Ocean Research, Vol. 26, pp. 61-72.

[131]. Viersma, T.J., 1980. Analysis, synthesis and design of hydraulic servosystems and pipelines. Elsevier.

[132]. Visscher, M., Dowson, D., and Taylor, C.M., 1998. The profile development of a twin-land oil-control ring during running-in. Journal of Tribology, Vol. 120, No. 4, pp. 616-621.

[133]. WAMIT. WAMIT User Manual, http://www.wamit.com, 2006, version 6.3.

[134]. Watson, M., Byington, C., Edwards, D., and Amin, S., 2005. Dynamic modeling and wear-based remaining useful life prediction of high power clutch systems. Tribology Transactions, Vol. 48, No. 2, pp. 208-217.

[135]. Watton, J., and Tadmori, M.J., 1988. A comparison of techniques for the analysis of transmission line dynamics in electrohydraulic control systems. Applied Math Modelling, Vol. 12, pp. 457-466.

[136]. White. F., 1999. Fluid mechanics. 4th editor, McGraw-Hill, New York.

[137]. Williams, 1999. Wear modelling: analytical, computational and mapping: a continuum mechanics approach. Wear, Vol. 225-229, pp. 1-17.

[138]. Williams, J.A., 2005. Wear and wear particles – some fundamentals. Tribology International, Vol. 38, pp. 863-870.

[139]. Williams, J.A., and Hyncica, A.M., 1992. Mechanisms of abrasive wear in lubricated contacts. Wear, Vol. 152, pp.57-74.

[140]. Wood, D.J., and Jones, S.E., 1973. Water-hammer charts for various types of valves. Journal of the Hydraulics Division, Vol. 99, No. 1, pp.167-178.

[141]. Wylie, E., Streeter, V., and Suo, L., 1993. Fluid transients in systems. Prentice-Hall.

[142]. Yang, L., Hals, J., and Moan, T., 2009. A wear model for assessing the reliability of wave energy converter in heave with hydraulic power take-off. In Proceedings of 8th European Wave and Tidal Energy Conference, September 7-10,, Uppsala, Sweden.

[143]. Yang, L., Hals, J., and Moan, T., 2010. Analysis of dynamic effects relevant for the wear damage in hydraulic machines for wave energy conversion. Ocean Engineering, Vol. 37, No., 13, pp. 1089-1012.

[144]. Yang, L., Hals, J., and Moan, T., 2010. Comparative study of bond graph models of hydraulic transmission lines with transient flow dynamics. Submitted to Journal of Dynamic Systems, Measurements, and Control.

[145]. Yang, L., and Moan, T., 2010. Cylinder bore wear damage analysis of a heaving-buoy wave energy converter with hydraulic power take-off. Proceedings of the ASME 29th International Conference of Offshore Mechanics and Arctic Engineering, OMAE2010-20164,June 6-11, Shanghai, China.

[146]. Yang, L., and Moan, T., 2011. Numerical modeling of wear damage in seals of a wave energy converter with hydraulic power take-off under random loads. Tribology Transactions, Vol. 54, No. 1, pp. 44-56.

[147]. Yang, L., and Moan, T., 2010. Dynamic analysis of wave energy converter by incorporating the effect of hydraulic transmission lines. Submitted to Journal of Ocean Engineering.

[148]. Yang, W.C., and Tobler, W.E., 1991. Dissipative modal approximation of fluid transmission lines using linear friction model. Journal of Dynamic Systems, Measurements, and Control, Vol. 11, pp. 152-162.

[149]. Yu, Z., and Falnes, J., 1995. State-space modelling of a vertical cylinder in heave. Applied Ocean Research, Vol. 17, No. 5, pp.265-275.

[150]. Záruba, J., 1993. Water hammer in pipe-line systems. Amsterdam: Elsevier.

Appendix A Publications

Paper A

Analysis of dynamic effects relevant for the wear damage in hydraulic machines for wave energy conversion

Published in

Ocean Engineering, Vol. 37, pp. 1089-1012, 2010.

Ocean Engineering 37 (2010) 1089–1102

Contents lists available at ScienceDirect

Ocean Engineering

journal homepage: www.elsevier.com/locate/oceaneng

Analysis of dynamic effects relevant for the wear damage in hydraulic machines for wave energy conversion

Limin Yang*, Jørgen Hals, Torgeir Moan

Centre for Ships and Ocean Structures and Department of Marine Technology, Norwegian University of Science and Technology, Otto Nielsens vei 10, NO-7491 Trondheim, Norway

ARTICLE INFO

Article history:
Received 1 December 2009
Accepted 25 April 2010
Available online 20 May 2010

Keywords:
Wave Energy Converter
Hydraulic power take-off
Irregular waves
High frequency oscillation
Piston ring and cylinder bore
Wear

ABSTRACT

The present paper deals with a mathematical model of a heaving-buoy Wave Energy Converter (WEC) equipped with high-pressure hydraulic power take-off machinery for energy conversion. This model is based on linear hydrodynamic theory, and a hybrid frequency–time domain model is used to study the dynamics of the heaving-body exposed to an irregular incident wave. For the power take-off system, end-stop devices are provided to protect the hydraulic machinery when the buoy is exposed to severe sea states. The model also takes into account the lubricated friction force and pressure drops of orifice flow through the valves in the hydraulic system. All the forces mentioned in the hydraulic power take-off machinery have non-linear features. A complete non-linear state space model for the WEC system is presented in this study.

The WEC system was numerically simulated for different cylinder lengths under a fixed volume. The effect of fluid compressibility in the cylinder has been investigated in the mathematical model. High frequency oscillations (HFOs) caused by the compressibility of the fluid are displayed in the time series and in corresponding power spectra, and variation is shown for different cylinder sizes. Piston ring and cylinder bore wear damage is estimated by using Archard's equation on the basis of the simulation results. A comparison of these results with a performance of an identical WEC system which neglects fluid compressibility has been done in this work. It shows that although the spectral power is small, HFO can make a large contribution to both the ring and cylinder bore wear. For the purpose of wear prediction, oscillations at or below the wave frequency and HFO may be equally important.

1. Introduction

Wave energy is a non-polluting and renewable source of energy, created by the natural conversion of part of the wind blowing over the oceans. Among several possible methods of capturing wave energy, point absorbers have been used for this purpose, i.e., bodies with very small extension compared to the wavelength (Falnes, Chapter 6, 2002). Point-absorbing Wave Energy Converters (WECs) have been studied since the late 1970s, including testing on the laboratory scale and under real-sea conditions. Evans (1978) obtained a solution for hydrodynamic coefficients based on the linear water wave theory for an oscillating water column (OWC) device by assuming small dimensions compared with the wavelength. Budal and Falnes (1982) described a spherical buoy only performing a heaving oscillation relative to a strut joined to an anchor on the sea bed. In their paper, the latching method for phase control was supplied with the buoy. Compared to other types of absorbers, the point absorbers possess a large power-to-volume ratio implying a large ratio of absorbed power to the submerged buoy volume. They are also attractive in terms of easy modelling because the scattered wave field can be neglected and forces on the body are only due to incident waves. A series of studies by Falnes and Budal (1978), Evans (1981), French and Bracewell (1986), Pizer (1993), Vantorre et al. (2004), Babarit et al. (2004) and others have been carried out on these devices both in regular and irregular waves.

The main mechanism that can be implemented to convert wave into mechanical and/or electrical energy is called a power take-off (PTO). The hydraulic PTO used here is a type that converts the oscillating motion of the body into hydraulic power by the use of hydraulic rams which then drive the shaft with a hydraulic motor connected to a generator, a configuration that is used by many researchers. Eidsmoen (1995) presented a tight-moored heaving-buoy WEC, with high-pressure hydraulic machinery for energy production. In his model, a linear friction force and a non-linear end-stop device were included. An estimate of the year-average power production was computed both with and without a control method for the time domain. Bjarte-Larsson and Falnes (2006) tested a heaving floating buoy with a hydraulic power take-off exposed to sinusoidal incident waves in a wave channel.

* Corresponding author. Tel.: +47 73595506; fax: +47 73595528.
E-mail address: limin.yang@ntnu.no (L. Yang).

0029-8018/$ - see front matter © 2010 Elsevier Ltd. All rights reserved.
doi:10.1016/j.oceaneng.2010.04.005

Nomenclature

α	piston area ratio
β	bulk modulus
σ	parameter for viscous friction
η	kinematic viscosity of the oil
γ	ratio of specific heat
ρ	oil density
ω	angular frequency
ω_m	angular speed of the shaft
τ	torque acted on the shaft
A_∞	added mass at infinite frequency
A	cross area
A,**B**,**C**	state-space matrices
B	damping coefficient
c	discharge coefficient
c_s	Stribeck velocity
c_{turb}	discharge coefficient for turbulent flow
C_{end}, D_{end}	force parameters of end-stop device
D	inner diameter of cylinder
D_m	motor displacement
F	force
h	wear depth
$\dot{h}$	wear rate
H_s	significant wave height
HFO	high frequency oscillation
HP	high pressure
J	shaft inertia moment
k	wear coefficient
K	stiffness
$K(t)$	retardation function
L	cylinder half length
LP	low pressure
m	buoy mass
N	normal force
P	fluid pressure
q	flow rate
Q	fluid volume
R	resistance
R_t	Reynolds number
s	sliding distance
S	hydrostatic stiffness
t_R	the height of ring
T_p	spectral peak wave period
v	velocity
V	geometric volume
WEC	Wave Energy Converter
WeV	wear volume
X	position coordinate
z	additional state-space vector

Subscripts

0	initial or default value
A, B	upper, lower chambers
b	cylinder bore
c	Coulomb friction
d	diving chamber
end	end-stop
exc	excitation force
ext	external force
f	friction
g	generator
hs	hydrostatic
m	hydraulic machinery force
min	minimum value
n	natural frequency
net	net flow
p	piston
r	rod
R	radiation
s	Stribeck friction
sum	summary
$turb$	turbulent flow
v	viscous friction
val	valve
wp	water pressure

Experimental results showed that the hydraulic power capture can be significantly increased by use of the latching control. Hals et al. (2007) used a hybrid frequency–time domain model and studied the dynamics of a two-body WEC with hydraulic power take-off. In their work (Hals et al., 2007), two kinds of hydraulic power take-offs were mentioned: a passive hydraulic system and a hydraulic system with latching control implemented by the use of shut-off valves. Flow losses in the hydraulic power take-off were also considered in the mathematical model. The most common characteristic of the three research studies mentioned above was the use of a one-way hydraulic ram which fed high pressure (HP) fluid to a hydraulic motor. Falcão (2007) used a two-way hydraulic ram to connect the oscillating body. In his paper, a time-domain analysis was presented to evaluate the performance of a buoy oscillating in heave with a hydraulic power take-off in irregular waves without phase control, and the size of the accumulators was also considered. In any case, the power loss in the hydraulic circuit was not mentioned. Later, Falcão (2008) expanded this work to consider also a phase-control method where control valves were opened only after the pressure had built up to a chosen threshold value.

The hydraulic cylinder is full of liquid (water or oil) that is slightly compressible. The compressibility of the fluid can cause pressure fluctuations during operation. Lopes et al. (2009) in their work considered the compressibility of the media (air) inside the chamber in their mathematical model for an OWC and gave an analysis of pressure variations during latched intervals. Detailed analysis of liquid compressibility in the hydraulic servo-systems is referred by Jelali and Kroll (2003). From the previous research, we can see that fluid compressibility usually introduces high frequency oscillation (HFO). This kind of oscillation makes a contribution to the piston and cylinder bore wear.

The wear of the piston ring and cylinder bore has been studied for many years within engine and motor systems (Peterson and Winer, 1980). Archard's wear law (Archard and Hirst, 1956) is commonly used in this domain. For such systems, the cyclic sliding velocity of the piston causes the film thickness to be cyclic, thus producing a squeeze film action. The film thickness varies through the engine cycle (Ting and Mayer, 1974; Priest et al., 1999). In these cases, the minimum film thickness occurs at or near the top or bottom dead centre of the cylinder bore (In a reciprocating engine, the dead centre is the maximum (top dead centre) or minimum (bottom dead centre) position of the piston (Giorgio et al., 2007)). It can be determined by transient film analysis. Due to the reduced lubrication, the wear damage on the cylinder bore becomes most severe in the region near the top or

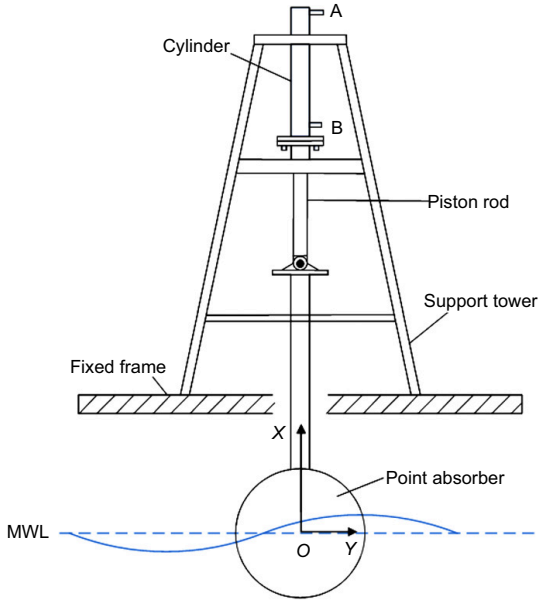

Fig. 1. Schematic illustration of Wave Energy Converter consisting of a heaving sphere connected to the hydraulic cylinder. The cylinder is rigidly attached to a frame which is fixed to the sea bed.

bottom dead centre (Giorgio et al., 2007). For the case of WEC system studied in the present work, the excitation and dynamic responses are irregular, which lead to uncertainties in the wear prediction. Compared with the wear modelling in the traditional engine and motor system, analysis of the characteristic dynamics is a key issue for wear prediction in the hydraulic power take-off system.

This paper addresses the case of a floating body oscillating in heave only. The motion of the body drives a two-way hydraulic ram connected to a hydraulic motor and generator. A simplified diagram of this body with a fixed reference and its connection to the hydraulic cylinder is shown in Fig. 1. The cylinder is connected to a high-pressure hydraulic system, and the oscillating motion of the body is converted into the flow of oil at high pressure by the hydraulic system. In the hydraulic circuit, there is a hydraulic motor which drives an electric generator, and a gas accumulator system is used to reduce pressure peaks in the system and to store energy. Fig. 2 shows this kind of power take-off system.

Random irregular waves are considered in this work, characterized by the significant wave height H_s and the peak period T_p, and deep water is assumed. A hybrid frequency–time domain model is used to study the dynamics of this WEC with a hydraulic power take-off. The governing equations for a floating body which is exposed to irregular waves, as well as for the power take-off hydraulic circuit, are presented in Section 2. Section 3 is devoted to the hydraulic natural frequency of the cylinder when considering the compressibility of the hydraulic oil. The piston is considered to be massless with fluid springs connected to each side. Simulation results for various cylinder sizes with irregular wave excitation are presented. Section 4 gives an analysis of the wear damage on the piston ring and cylinder bore. Finally, the effect of HFO on the wear of piston ring and cylinder bore is discussed based on the numerical results.

2. Non-linear dynamic model for the WEC system

We consider a WEC in the form of a heaving buoy (single degree of freedom), moving relative to a fixed reference (the coordinate is fixed with respective to mean position of the buoy with positive X vertically upwards, and the origin is set in the plane of the undisturbed surface, see Fig. 1). The fixed reference could be any offshore structure fixed to the sea bed. This structure is illustrated in Fig. 1. In this paper, we do not consider how such a fixed structure will be constructed. The design of systems providing force reference for WECs, be it fixed or moving, is a task on its own.

The governing equation for the floating buoy oscillations can be written as

$$m\ddot{X} = F_{wp}(t) + F_{ext}(t) \tag{1}$$

where m is the mass of the buoy, $\ddot{X}$ is the acceleration, F_{ext} is the external force applied on the buoy and F_{wp} is the force induced by the water pressure on the submerged body surface.

Since we are studying a small and axisymmetric device it is not necessary to consider the direction of the waves. If the amplitudes of the waves and body motions are small (giving a linear system from the viewpoint of wave hydrodynamics), the force F_{wp} can be written as follows (Faltinsen, 1990):

$$F_{wp}(t) = F_{exc}(t) + F_R(t) + F_{hs}(t) \tag{2}$$

where $F_{exc}(t)$ is the force produced by incident waves when the buoy is restrained from oscillation (excitation force), $F_{hs}(t)$ is the hydrostatic force (it is assumed to be 0 when $X=0$) and $F_R(t)$ is the hydrodynamic force due to the body oscillation which is given by Cummins (1962) as

$$F_R(t) = -A_\infty \ddot{X}(t) - \int_{-\infty}^{t} K(t-\tau)\dot{X}(t)\, d\tau \tag{3}$$

Here, $\dot{X}$ is the vertical velocity of the buoy, A_∞ is the added mass of the buoy in the limit of infinite frequency and $K(t)$ is the radiation force kernel which represents the memory effect of the body motion and can be calculated from radiation damping coefficient $B(\omega)$ by (Falnes, 2002)

$$K(t) = \frac{2}{\pi}\int_0^\infty B(\omega)\cos(\omega t)\, d\omega \tag{4}$$

With the assumption of linearity, the convolution integral in Eq. (3) can be approximated by a state-space model (Taghipour et al., 2008):

$$\dot{\mathbf{z}}(t) = \mathbf{A}\mathbf{z}(t) + \mathbf{B}\dot{X}(t) \quad \text{with } \mathbf{z}(0) = 0 \tag{5}$$

and

$$\int_{-\infty}^{t} K(t-\tau)\dot{X}(\tau)\, d\tau \approx \mathbf{C}\mathbf{z}(\mathbf{t}) \tag{6}$$

where $\mathbf{z}(t) = [z_1(t), z_2(t), \ldots, z_n(t)]^T$ is the state vector of the radiation force approximation.

In the case studied, frequency-dependent radiation damping and the excitation force for the buoy are calculated numerically by using the software package WAMIT, which is a commercially available program package developed by WAMIT Inc. (WAMIT, 2006). The radiation force kernel function $K(t)$ is approximated by a sixth-order state-space model which yields a satisfactory result as shown in Fig. 3.

The WEC is equipped with a hydraulic machinery which, as shown in Fig. 2, consists of an axial hydraulic pump with the piston rod connected to the heaving buoy, four check valves, low- and high-pressure accumulators and pipes. The pressure difference across the

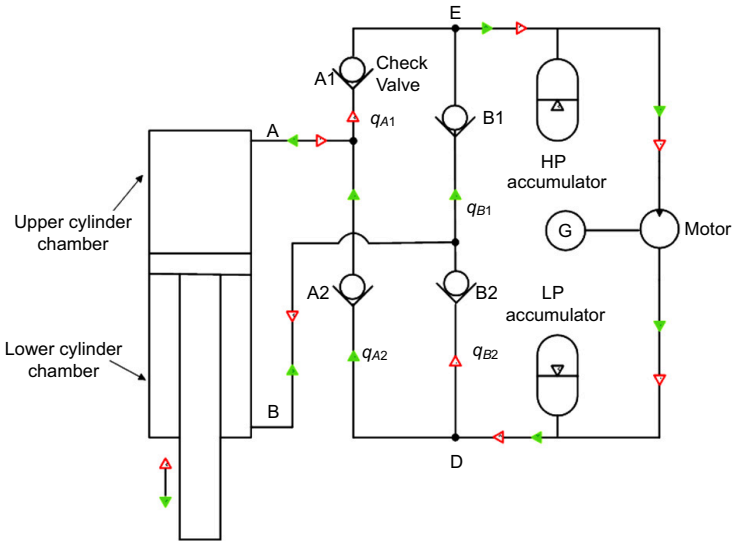

Fig. 2. Schematic diagram of the passive hydraulic system. The system consists of a hydraulic cylinder, gas accumulators (HP and LP), check valves (A1, A2, B1 and B2), a motor and a generator. When the piston is moving upwards, the flow follows the direction indicated by the red empty arrows. When the piston is moving downwards, the flow follows the direction of the green filled arrows.

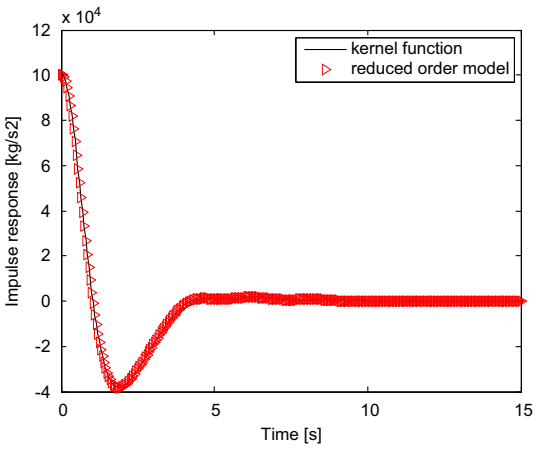

Fig. 3. The impulse response function $K(t)$ for the radiation force (line) and its state-space approximation (symbols).

piston produces a load force $F_m(t)$, which is taken to be positive when it is acting on the body in the negative X-direction (Fig. 4):

$$F_m(t) = P_A A_p - \alpha P_B A_p \tag{7}$$

Here P_A and P_B are the oil pressure of the upper and lower cylinder chambers, respectively; A_p is the piston area of the chamber, α is the piston area ratio which equals $(A_p - A_r)/A_p$ and A_r is the cross section area of the rod.

The oil in this system is slightly compressible and the pressure in the fluid will increase when the oil is compressed. A bulk modulus β is defined by the following relation (Thoma, 1970):

$$\frac{dP}{\beta} = -\frac{dV}{V} \tag{8}$$

For mineral oils, and for common pressures ($P < 450$ bar) and temperatures ($[-40, 120]$ °C), the value of the bulk modulus is about 1.4×10^9 Pa (Jelali and Kroll, 2003).

The equation for the chamber pressure can then be derived from the continuity of the mass equation (Egeland and Gravdahl, 2002):

$$\dot{P}_A = \beta \frac{q_A - \dot{V}_A}{V_A}$$
$$\dot{P}_B = \beta \frac{q_B - \dot{V}_B}{V_B} \tag{9}$$

where q_A and q_B are the net flow rates into and out of the upper and lower chambers, respectively. They are taken to be positive when the oil flows into the chambers; V_A and V_B are the volumes of the upper and lower chambers which can be written as

$$V_A = V_{A0} - x_p A_P$$
$$V_B = V_{B0} + x_p \alpha A_P \tag{10}$$

where x_p is the vertical distance of the piston from the midpoint of the cylinder (we assume the piston is in the middle of the cylinder at $X=0$), V_{A0} and V_{B0} are the fluid volumes for the upper and lower chambers with the piston at the origin location, respectively. In this paper, the piston and buoy are assumed as one rigid body, i.e., $X = x_p$. In the following, the buoy position X is used to represent the piston excursion instead of x_p.

The time derivatives of Eq. (10) are given by

$$\dot{V}_A = -A_P \dot{X}$$
$$\dot{V}_B = A_P \alpha \dot{X} \tag{11}$$

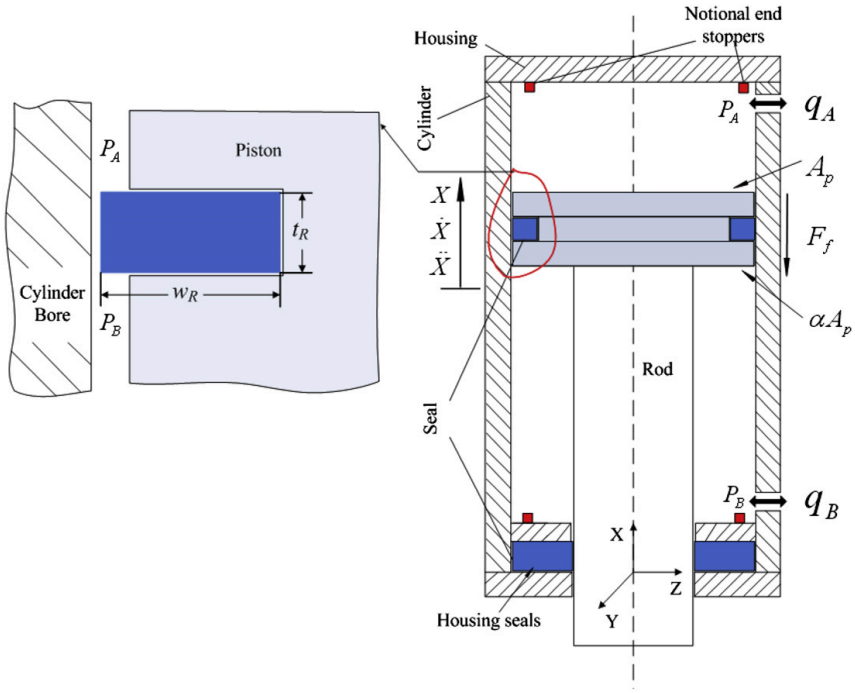

Fig. 4. Sketch of the piston pump with sealing elements and end stoppers. It consists of a hydraulic cylinder filled with oil, a piston, a piston rod and seals. In the figure, q_A and q_B are the flow rate into and out of the cylinder chambers (positive flow into the chamber and negative flow out of the chamber), P_A and P_B are the oil pressures of the chambers, A_p is the area of the piston, and F_f is the friction force. t_R and w_R are the thickness and width of the ring, respectively.

Combining Eqs. (9–11), the final derivative equations for the chambers are

$$\dot{P}_A = \frac{\beta}{(V_{A0} - A_P X)}(q_A + A_P \dot{X})$$

$$\dot{P}_B = \frac{\beta}{(V_{A0} + \alpha A_P X)}(q_B - \alpha A_P \dot{X}) \tag{12}$$

For simplification, the piston leakage and external rod leakage are neglected in Eq. (12).

The friction force F_f (Fig. 4) between the cylinder and the piston is simulated as a function of relative velocity, which is referred to as the Stribeck friction curve (Jelali and Kroll, 2003):

$$F_f(\dot{X}) = F_v(\dot{X}) + F_c(\dot{X}) + F_s(\dot{X})$$

$$= \sigma \dot{X} + \text{sign}(\dot{X})\left(F_{c0} + F_{s0}\exp\left(-\frac{|\dot{X}|}{c_s}\right)\right) \tag{13}$$

The three characteristic parts of this force are viscous friction F_v, Stribeck friction F_s and Coulomb friction F_c. The parameter σ regards viscous friction, F_{c0} is the parameter for Coulomb friction, and F_{s0} and c_s are the Stribeck friction and Stribeck velocity, respectively.

For the hydraulic system, it is necessary to include a deceleration cushion at the end of the stroke to prevent damage to the cylinder housing. This function is carried out by an end-stop device (Fig. 4). This device gently dissipates kinetic energy, thus reducing the possibility of mechanical damage to the cylinder. The force from the end-stop device in our model follows an approximate function as (Eidsmoen, 1995)

$$F_{end}(t) = D_{end}(\exp(C_{end}(X(t) - X_{end})) + \exp(-C_{end}(X(t) + X_{end})))\dot{X}(t) \tag{14}$$

where $D_{end} > 0$ and $C_{end} > 0$. When the piston position deviates more than X_{end} from the midpoint of cylinder this force will stop the motion quickly, and the WEC will lose most of its kinetic energy. Here, the parameter X_{end} is not the maximum excursion, but gives the excursion when the end-stop force becomes dominating.

The equation of the buoy motion may now be written as follows, with $F_{ext}(t) = -F_m(t) - F_f(t) - F_{end}(t)$:

$$(m + A_\infty)\ddot{X}(t) = F_{exc}(t) - \mathbf{C}\cdot\mathbf{z}(t) + F_{hs}(t) - F_m(t) - F_f(t) - F_{end}(t) \tag{15}$$

The hydrostatic force, in a linearized version, is $F_{hs}(t) = SX(t)$, where S is the hydrostatic stiffness of the buoy.

The WEC system also includes a high-pressure (HP) accumulator, a low-pressure (LP) accumulator and a hydraulic motor. The check valves prevent liquid from leaving the HP accumulator at **E** and from entering the LP accumulator at **D**. In this way, when the piston is moving upwards, the fluid flow follows the direction of the red empty arrows, otherwise it follows the green filled arrows, as shown in Fig. 2. Compared to the compressibility of gas in the accumulators, the hydraulic fluid compressibility is considered to be negligible. It compresses gas in the HP and LP accumulators and the volume of the compressed gas determines the pressure in the accumulators. Here, assuming that the peaks in the flow into or out of the accumulator are of short duration, the gas does not have time to

exchange much heat with its surroundings. Therefore, the isentropic pressure–volume law

$$PV^{\gamma} = P_0 V_0^{\gamma} = \text{constant} \tag{16}$$

is a good approximation (Karnopp et al., 2006). In this equation, γ is the ratio of the specific heats at constant pressure and volume (for air at atmospheric pressure, $\gamma \approx 1.4$). P and V are the instantaneous pressure and volume of the gas, and P_0 and V_0 are the values at the initial time. The gas volume V can be calculated by

$$V = V_0 - Q = V_0 - \int_0^t q\, dt \tag{17}$$

Here Q and q denote the net liquid volume and flow rate into the accumulator, respectively. The relationship between the two variables is $\dot{Q} = q$.

Applying Eqs. (16) and (17), the non-linear capacitance relation between P and V of each accumulators now becomes

$$\begin{aligned} P_{HP} &= (P_{0\_HP} V_{0\_HP}^{\gamma})/(V_{0\_HP} - Q_{HP})^{\gamma} \\ P_{LP} &= (P_{0\_LP} V_{0\_LP}^{\gamma})/(V_{0\_LP} - Q_{LP})^{\gamma} \end{aligned} \tag{18}$$

The subscripts HP and LP represent the high pressure accumulator and low pressure accumulator, respectively.

The last component in the WEC system is the hydraulic motor. During its operation, it will be driven by the pressure difference between the HP accumulator P_{HP} and LP accumulator P_{LP} with angular speed ω_m. The shaft is connected to an electrical generator, which is represented simply as a linear resistor in this study. (To achieve such a response in reality, the generator would have to be controlled to behave like such a resistor. This modelling choice does not influence the effects studied in this paper.) The state equation concerning the coupling between the motor and generator is

$$J_m \dot{\omega}_m = D_m(P_{HP} - P_{LP}) - R_g \omega_m - \tau_l \tag{19}$$

where J_m is the shaft inertia moment, D_m is the motor displacement, R_g is the resistance coefficient of the generator and τ_l is the equivalent torque loss of the motor which includes leakage, friction and pressure losses.

If the state variables are defined as

$$\begin{aligned} &y_1 = X, \quad y_2 = \dot{X}, \quad \mathbf{y_3} = \mathbf{z}(t), \quad y_4 = P_A, \quad y_5 = P_B, \quad y_6 = \omega_m, \\ &y_7 = Q_{HP}, \quad y_8 = Q_{LP} \end{aligned} \tag{20}$$

then the complete non-linear state space model for the WEC system can be written as

$$\begin{aligned} \dot{y}_1 &= y_2 \\ \dot{y}_2 &= \frac{1}{m + A_\infty}(F_{exc}(t) - F_m(t) - F_f(t) - F_{end}(t) - S y_1 - \mathbf{C}\cdot\mathbf{y}_3) \\ \dot{\mathbf{y}}_3 &= \mathbf{A}\cdot\mathbf{y}_3 + \mathbf{B}\cdot y_2 \\ \dot{y}_4 &= \frac{\beta}{V_{A0} - A_p y_1}(q_{A1} + q_{A2} + A_p y_2) \\ \dot{y}_5 &= \frac{\beta}{V_{B0} - \alpha A_p y_1}(q_{B1} + q_{B2} - \alpha A_p y_2) \\ \dot{y}_6 &= \frac{1}{J_m}((P_{HP} - P_{LP}) D_m - R_g y_6 - \tau_l) \\ \dot{y}_7 &= -q_{A1} - q_{B1} - q_m \\ y_8 &= q_{A1} + q_{B1} + q_m \end{aligned} \tag{21}$$

Here, the variables q_{A1}, q_{B1}, q_{A2} and q_{B2} are the flows through the check valves as shown in Fig. 2.

The empirical flow formula proposed by Borutzky et al. (2002) is used for the valves in this paper. The flow equations for the check valves with diameter of D_{val} can be expressed as

$$\begin{aligned} q_{A1} &= -\left(c_{turb} A_{val} \sqrt{\frac{2}{\rho}\max(P_{HP} - P_A, 0) + \left(\frac{\eta R_t}{2 c_{turb} D_{val}}\right)^2} - A_{val}\eta\frac{R_t}{2D_{val}}\right) \\ q_{A2} &= \left(c_{turb} A_{val} \sqrt{\frac{2}{\rho}\max(P_{LP} - P_A, 0) + \left(\frac{\eta R_t}{2 c_{turb} D_{val}}\right)^2} - A_{val}\eta\frac{R_t}{2D_{val}}\right) \\ q_{B1} &= -\left(c_{turb} A_{val} \sqrt{\frac{2}{\rho}\max(P_B - P_{HP}, 0) + \left(\frac{\eta R_t}{2 c_{turb} D_{val}}\right)^2} - A_{val}\eta\frac{R_t}{2D_{val}}\right) \\ q_{B2} &= \left(c_{turb} A_{val} \sqrt{\frac{2}{\rho}\max(P_{LP} - P_B, 0) + \left(\frac{\eta R_t}{2 c_{turb} D_{val}}\right)^2} - A_{val}\eta\frac{R_t}{2D_{val}}\right) \end{aligned} \tag{22}$$

Here, c_{turb} is the discharge coefficient for the turbulent flow, A_{val} is the cross section area of the valve, η is the kinematic viscosity of the liquid, ρ is the density of the fluid and R_t is the Reynolds number at which the linear characteristic intersects with the constant value of c_{turb}.

In Eq. (21), q_m is the fluid flow rate into the diving chambers of the hydraulic motor. It depends on the shaft angular velocity ω_m. In the linear wave theory, the excitation force $F_{exc}(t)$ can be obtained by linear superposition. The forces $F_m(t)$, $F_f(t)$ and $F_{end}(t)$ are described by Eqs. (7), (13) and (14), respectively. Finally, the accumulator pressures P_{HP} and P_{LP} can be obtained by using Eq. (18) with parameters of the respective accumulators.

From Eq. (21), we can see that the power-take off system of the WECs is strongly non-linear, so a frequency domain analysis is not applicable. The model can be dealt with by a time domain analysis.

Note that a number of assumptions that are typically satisfied in this studied case have been made for the derivation of this non-linear model:

- The internal leakage of the cylinder is neglected.
- The masses of the piston and the piston rod, in addition to the fluid in the cylinder and pipeline, are not considered.
- The cylinder walls, accumulator walls, piston and rod are rigid.
- The relation between the density and pressure is linear when considering the compressibility of the hydraulic oil.
- Possible dynamic behaviour of the pressure in the pipelines between the valves and the cylinder is assumed to be negligible.

The neglected effects can, however, be added if they appear to be essential for special purposes.

3. Natural frequency of the hydraulic system

The hydraulic fluid in the cylinder chamber is compressible and can thus be considered to be a very stiff spring. The stiffness of the spring is a function of the fluid bulk modulus β, piston area A_p, piston area ratio α and chamber volume V. For the cylinder with two chambers full of fluid, the fluid spring stiffness K_{fluid} is based on the two hydraulic springs connected in series and can be calculated as

$$K_{fluid} = \beta\left(\frac{{A_P}^2}{V_A} + \frac{(\alpha A_P)^2}{V_B}\right) \tag{23}$$

Suppose that the piston in the cylinder is situated in the mid-position at the initial time, then

$$\begin{aligned} V_{A0} &= A_P L \\ V_{B0} &= \alpha A_P L \end{aligned} \tag{24}$$

where L is the half length of the cylinder.

Substituting Eqs. (10, 24) into Eq. (23), the fluid spring stiffness can now be described as

$$K_{fluid} = \beta\left(\frac{A_P}{L-X} + \frac{\alpha A_P}{L+X}\right) \tag{25}$$

Eq. (25) demonstrates that fluid stiffness changes as a function of the cylinder geometry. If the geometric parameters are known, then K_{fluid} is a non-linear function of piston position X. Fig. 5 shows how the fluid stiffness changes as a function of X for an asymmetric pump, i.e. $\alpha \neq 1$. The stiffness is much larger when the cylinder is near to being fully retracted than when it is near to being fully extended. Note that if $\alpha=1$, then K_{fluid} is an even function of X and symmetric about $X=0$.

Minimum stiffness will occur at the position

$$X_{\min} = 2\frac{\sqrt{\alpha}-(1+\alpha)}{2(1-\alpha)}L \tag{26}$$

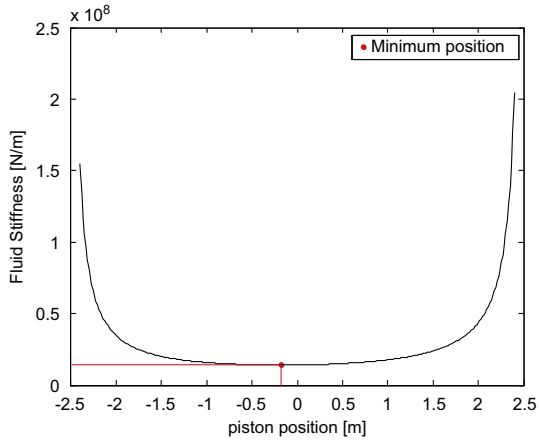

Fig. 5. Fluid stiffness as a function of piston position. The bulk modulus is taken as 1.4e9 Pa, the cylinder length is 5 m, the inner diameter of the cylinder D is 0.16 m and the area ratio α is 0.75. The solid red dot represents the piston position at which minimum fluid stiffness occurs.

The above calculation assumes rigid hydraulic tubing between the control valve and the cylinder. Hence, the stiffness is only related to the hydraulic stiffness.

We again consider the buoy oscillating in heave and driving a hydraulic cylinder that pumps HP oil into a hydraulic circuit. The single direction valves work in such a way that liquid is pumped from the cylinder into the HP accumulator when the pressure in the cylinder is larger than that in the HP accumulator ($\max[P_A, P_B] > P_{HP}$), and is sucked from the LP accumulator into the opposite side of the cylinder with a positive pressure difference between them ($\min[P_A, P_B] < P_{LP}$). If this is not the case, then there will be no flow pumped or sucked. Due to the compressibility of the oil, the velocity of the body is not zero at this moment. For the sake of simplicity, if we neglect the mass of the piston/rod and the fluid in the chambers, the natural frequency of the buoy at this position X is

$$\omega_n = \sqrt{\frac{(K_{fluid}+S)}{(m+A_\infty)}} \tag{27}$$

Since K_{fluid} is a function of the piston position X, the natural frequency ω_n is also dependent on X. The minimum natural frequency can therefore be described by combining Eqs. (25–27). In order to depict the characteristic of ω_n, we fix the cylinder volume V and piston area ratio α. Since the piston area A_p and the cylinder half length L now are related through $A_p=V/(2L)$, the stiffness K_{fluid} is only a function of one variable L (or A_p). According to Eqs. (25) and (27), the natural frequency ω_n will be changed with the cylinder length. Table 1 gives the cylinder geometric parameters as the half length L and inner diameters D. The minimum natural frequency ω_{min} and corresponding piston position X_{min} for different cylinder lengths are also shown in this table.

At the piston position X with no fluid pumped or sucked, the buoy tends to oscillate at the frequency given by Eq. (27), in combination with variations associated with a change in excitation and radiation forces. Compared with the incident wave, the frequencies of this oscillation are much higher (see Table 1). In this paper, we consider it as HFO. This type of cyclical motion was numerically tested for a semi-submerged sphere with a radius of $r=5$ m, a mass of $m=2.7\times10^5$ kg and an added mass at infinite frequency $A_\infty=1.35\times10^5$ kg, which is equal to half the mass of the sphere. To conduct simulations of irregular waves,

Table 1
The minimum fluid stiffness K_{min} and natural frequency ω_{min} corresponding to the piston position X_{min} with different cylinder parameters. The cylinder volume is fixed at 0.1005 m^3. L is the half length and D is the inner diameter of the cylinder, respectively.

L (m)	1.0	1.5	2.0	2.5	3.0	3.5	4.0
D (m)	0.2530	0.2066	0.1789	0.1600	0.1461	0.1352	0.1265
X_{min} (m)	−0.0718	−0.1077	−0.1436	−0.1795	−0.2154	−0.2513	−0.2872
K_{min} (1e7 N/m)	8.7513	3.8895	2.1878	1.4002	0.9724	0.7144	0.5470
ω_{min} (rad/s)	14.77	9.90	7.48	6.04	5.10	4.43	3.93

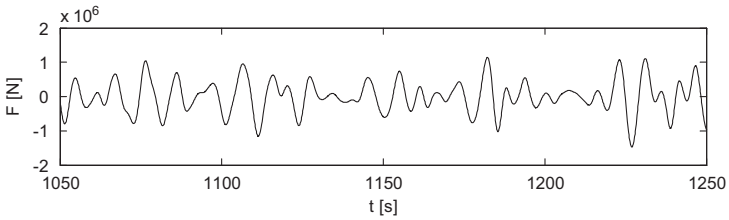

Fig. 6. Excitation force on the heaving sphere produced by incident waves in a sea state with $H_s=4.25$ m and $T_p=9.5$ s.

Bretschneider spectrum (e.g. Michel, 1999) is used. This spectrum was discretized into 225 equally spaced ($\Delta\omega$=0.01 rad/s) sinusoidal harmonics in the range between $0.25 \le \omega \le 2.5$ rad/s. The random phase angles are uniformly distributed between 0 and 2π and constant with time. The state-space Eq. (21) was numerically integrated in the time domain with a total simulation time of 1500 s. For H_s=4.25 m, T_p=9.5 s, Fig. 6 gives the time variation of the excitation force $F_{exc}(t)$ produced by incident waves in the interval $1050 \le t \le 1250$ s. For a cylinder type with L=2.5 m and D=0.16 m, Fig. 7a–e shows the buoy excursion $X(t)$ and velocity $\dot{X}(t)$ in the same time interval. These simulation results of Fig. 7a and b are obtained by integrating the dynamic equations without considering the compressibility of the oil in the cylinder as done by Falcão (2007). From the two figures, we can see that at some time, when the excitation force $F_{exc}(t)$ on the buoy is insufficient and no fluid is pumped into the accumulators, the buoy will remain stationary (flat line in Fig. 7a). This time period is called blocked period and denoted by T_{block}. Fig. 7c and d gives the corresponding buoy excursion and velocity by considering the fluid compressibility in the cylinder. Compared with Fig. 7a, we

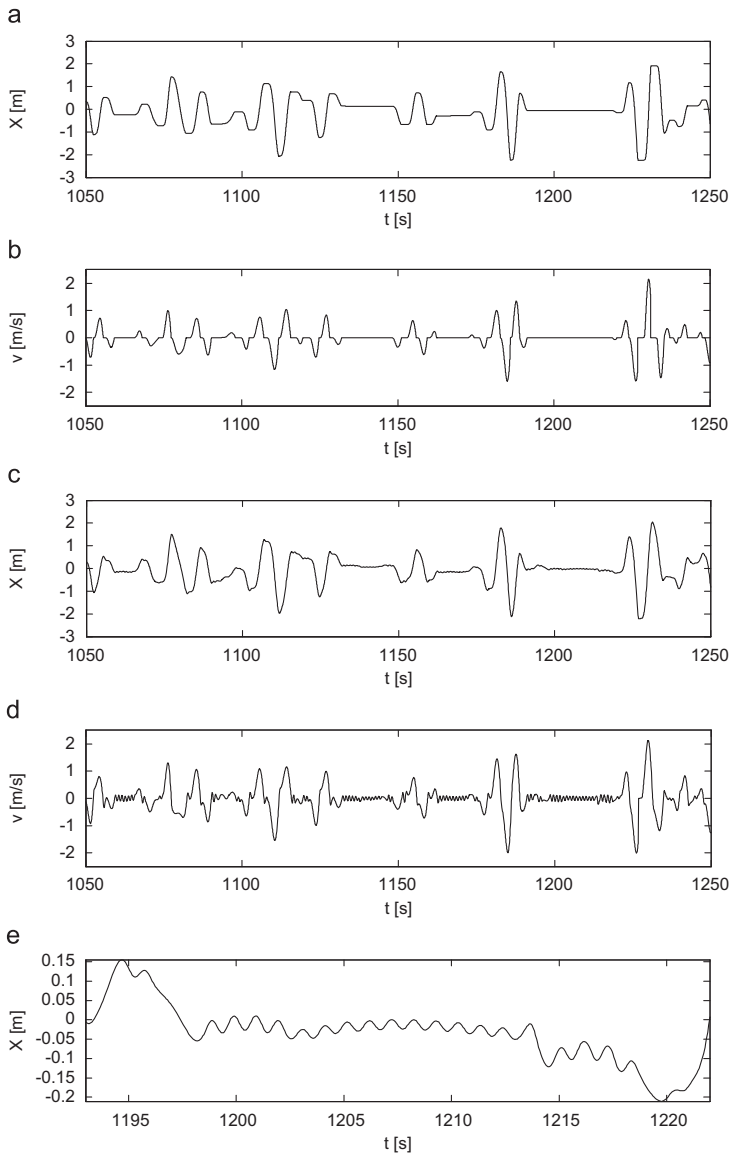

Fig. 7. Plot curves on top of each other for comparison: (a–b) Time variation for the buoy excursion $X(t)$ and velocity $v(t)$ for r=5 m, H_s=4.25 m, T_p=9.5 s, L=2.5 m. Compressibility of the fluid in the WEC system is not considered (see also Falcão, 2007). (c–d) As in Fig. 7a and b, but compressibility of the fluid in the WEC system is considered (see Eq. (19) in Section 2). (e) Buoy excursion for a short time interval in order to give a clear display of the HFO observed in Fig. 7c.

can see that the reciprocating motion of the buoy as shown in Fig. 7c mainly includes two parts: one occurs when the hydraulic fluid pumped or sucked from the cylinder, i.e., $\max[P_A, P_B] > P_{HP}$ or $\min[P_A, P_B] < P_{LP}$. It is the useful motion for energy absorption. The motion amplitudes are consistent with the results shown in Fig. 7a. It is found that this type of motion oscillates at or below the incident wave frequency (see Yang et al., 2009). In this paper, we define this motion as wave and lower frequency motion, which is used to distinguish the HFO; the other one is the HFO with relatively small amplitudes. This kind of motion is due to the compressibility of the fluid in the cylinder and occurs during the blocked period T_{block} (compared with the motionless part shown in Fig. 7a). In these time intervals, as mentioned above, the buoy can be considered as a simple mechanical oscillator in the form of a mass–spring–damper system. Compared with the mass of inertia ($m+A_\infty$) and the stiffness ($K_{fluid}+S$), the dissipating friction force F_f and the hydrodynamic damping force are very low at high frequencies. Therefore, the oscillations are lightly damped out which can be seen in Fig. 7c and e. In this paper, the damping of the system due to leakage past the piston and hydrodynamic viscous losses have not been taken into account and are expected to give an increased damping of the HFOs. It is not expected, however, that this would undermine the importance of the observed effect.

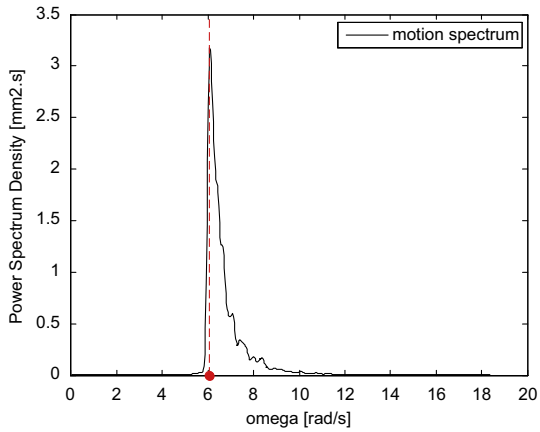

Fig. 8. The power spectrum of HFO with H_s=4.25 m, T_p=9.5 s and L=2.5 m. The solid red dot is the corresponding minimum natural frequency ω_{min} for this type of cylinder as shown in Table 1.

Let us reconsider the HFO shown in Fig. 7c; this process can be considered as a stiffness-controlled dynamic problem due to the high natural frequency compared to the frequency of excitation force. Fig. 7e is a locally enlarged figure for a time interval including a blocked period T_{block} and HFO is clearly shown. By filtering out the low frequencies of the motion before using the Fast Fourier Transform (FFT), Fig. 8 shows the power spectrum density for this high frequency motion (The time series used for the Fourier Transformation was taken from an interval between 500 and 1500 s). From the figure, we can see that the frequencies reside beyond the minimum natural frequency ω_{min}=6.04 rad/s (shown in Table 1), which seems reasonable for this system. Due to the variation in fluid stiffness according to piston position X, the natural frequencies at which the buoy oscillates will be above ω_{min}, which can be easily seen in Fig. 8.

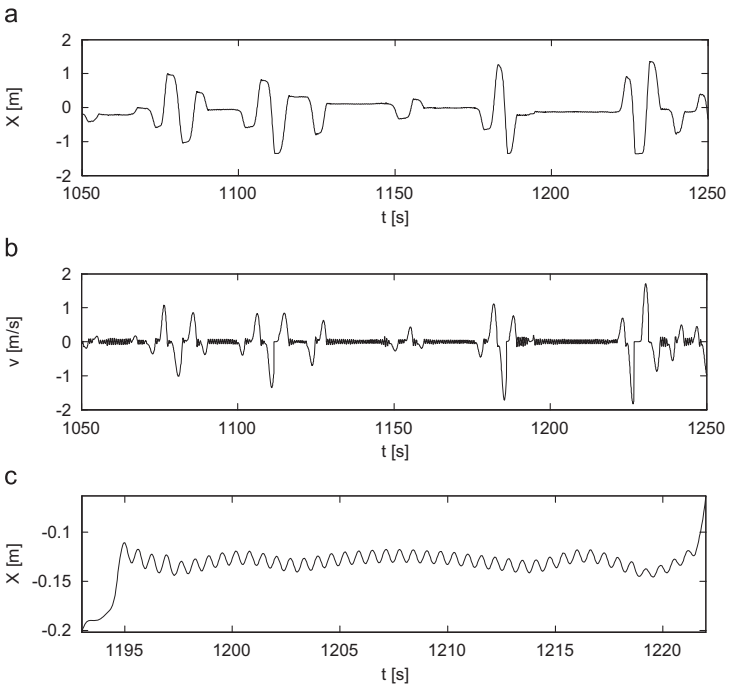

Fig. 9. Same case as for Fig. 7c–e, but with cylinder half length L=1.5 m.

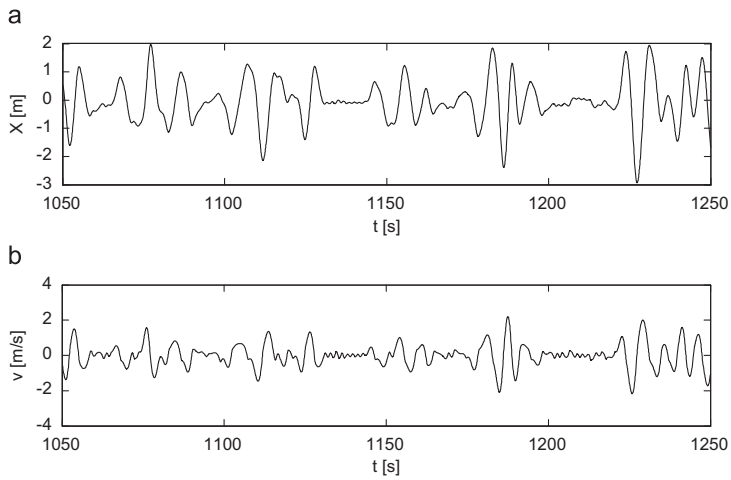

Fig. 10. Same case as for Fig. 7c–d, but with cylinder half length $L=4.0$ m.

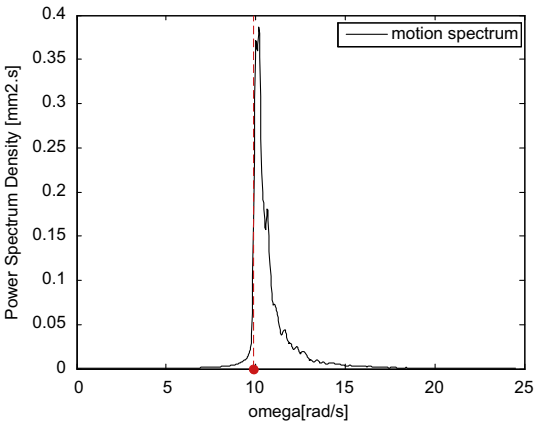

Fig. 11. As in Fig. 8, but with $L=1.5$ m.

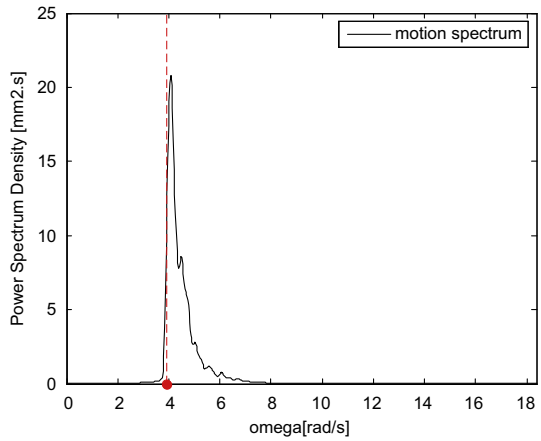

Fig. 12. As in Fig. 8, but with $L=4.0$ m.

Figs. 9(a–c) and 10(a–b) show corresponding curves of $X(t)$ and $\dot{X}(t)$ for smaller ($L=1.5$ m) and larger ($L=4$ m) half cylinder lengths for an identical floating buoy with the force shown in Fig. 6. In the case of the former, the fluid flow is blocked for a much larger period of time, and the oscillating frequency in this time interval is much higher. (This HFO is not quite clear in the position response shown in Fig. 9a. Here we supply a corresponding velocity response in Fig. 9b and a detailed position response for a certain time interval shown in Fig. 9c, which serve our purpose better.) The reason for this is that the cylinder with smaller length has a relatively larger cross section area, i.e., the force $F_m(t)$ defined in Eq. (7), is larger (with the same pressure input) which will resist the buoy motion. On the contrary, in the case of $L=4$ m, the characteristic dynamics will be changed in the opposite direction. We can follow the same way to analyze the problem.

Table 1 gives the minimum fluid stiffness for the various types of cylinders and shows that stiffness due to fluid compressibility is decreasing with L, i.e., the oscillating frequency varies with the cylinder length. Figs. 7c, 9c and 10a show these oscillations in the time domain for different cylinder types. The oscillating frequencies of HFOs are consistent with the previous analysis. Compared to the restoring coefficient S (for a sphere a radius of $r=5$ m, $S\approx 7.9\times 10^5$ N/m) of the spherical buoy, the fluid stiffness K_{fluid} has a relative large value (Fig. 5). For this reason, the body oscillates at a much higher frequency during the time period T_{block} than otherwise. This characteristic can be easily seen in Figs. 7, 9 and 10. Figs. 11 and 12 give the analysis of the power spectrum for the high frequency motion with $L=1.5$ and 4.0 m, respectively. The minimum frequencies ω_{min} for these sizes of the cylinder are presented in Table 1, and shown in Figs. 8, 11 and 12 as solid red dots.

4. Wear damage analysis for the piston ring and cylinder bore

From the analysis in the previous section, HFO with small amplitudes (Figs. 7c, 9a and 10a) occurs due to the compressibility of the oil in the cylinder. This type of motion can have an adverse

effect on the surface damage between the two contacting surfaces in the piston and cylinder system. At the contact areas, the lubricating oil will be squeezed out when the velocity is small or vanishing, resulting in surface-to-surface contact. Because a low amplitude motion does not permit the contact area to be re-lubricated, serious wear may occur for both the piston ring and cylinder bore. This progressive damage and material loss can have economic consequences which involve not only the costs of replacement but also the expenses involved in machine downtime and lost production. As a result, the design of pump is a highly important task for this WEC system, and it is necessary to make a detailed analysis of the wear under HFOs.

Several wear mechanisms contribute to the wear progression of a reciprocating hydraulic system. Different types of wear, such as adhesion, abrasion, corrosion, surface fatigue and impact wear, have been reported in the piston ring and cylinder bore system (Peterson and Winer, 1980). As reviewed by Becker and Ludema (1999), the three most important wear mechanisms mentioned over the years are corrosion, abrasion and adhesion. Corrosion is common when the components exposed to a variety of process fluids or other products that are chemically active. Abrasion results from the cutting and plowing action of hard particles. Adhesion is usually described as occurring when the oil film between the ring and the bore is so thin that surface contact occurs. Generally,

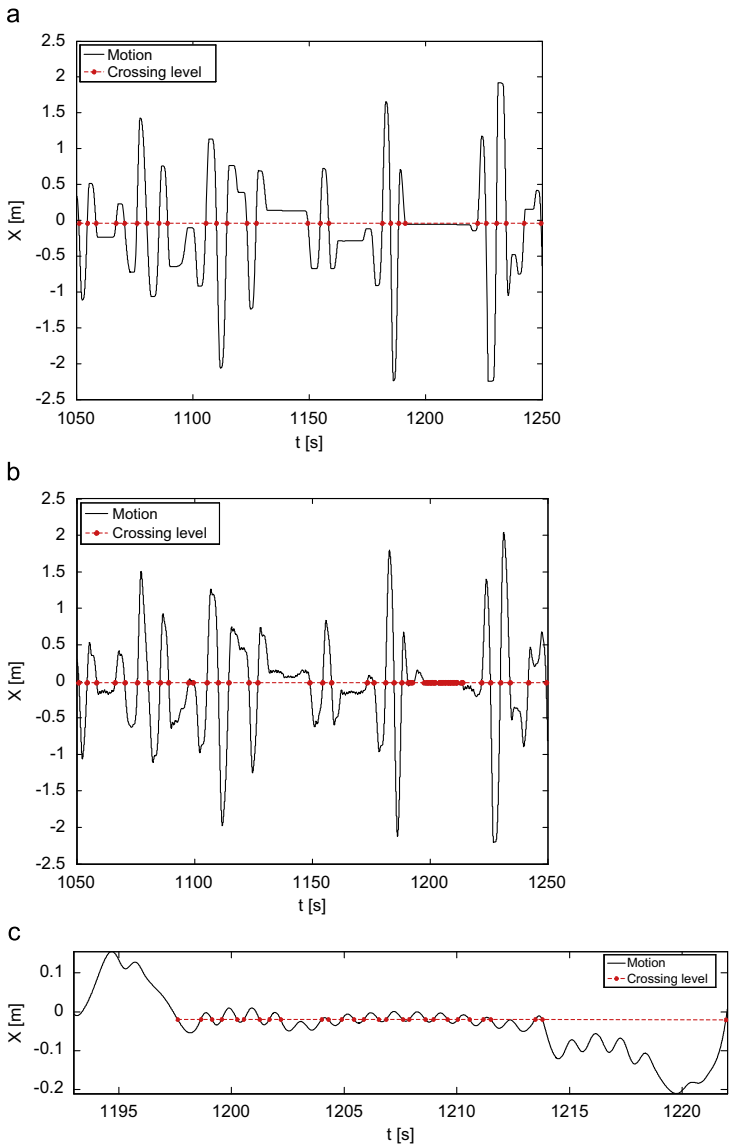

Fig. 13. A sample of the crossings for the performance shown in Fig. 7a, c and e.

corrosion can be reduced by the choice of material for various hydraulic fluids (Müller and Nau, 1998). Adhesion is common during the running-in period because of the surface roughness of both contact surfaces. Once running-in is complete, the system would attain a steady state and abrasive wear is generally considered to be a dominant wear mechanism for the reciprocating hydraulic system (Tung and Huang, 2004). Whatever the main wear mechanisms are for a specific piston ring and cylinder bore system, the total wear loss for both the ring and bore is the sum of the contributions from each mechanism that is observed. Detailed analysis of the piston ring and cylinder bore wear can be seen from Yang and Moan (submitted for publication).

The most commonly used model for wear on sliding contact surfaces states that the wear volume loss WeV is proportional to the normal load N and the sliding distance s, according to

$$WeV = kNs \tag{28}$$

where k is the wear coefficient. This model is often referred to as Archard's wear law (Archard and Hirst, 1956). The wear coefficient, k, is a function of the interacting materials, their surface topography, the lubricant and operating conditions. For lubricated tribo-pairs (here are the piston ring and cylinder bore), the wear volume loss also depends on the lubrication regime and surface roughness as described by the Stribeck curve, which is defined by a dimensionless film thickness λ (the ratio between the oil film thickness and the composite surface roughness). Assuming a pressure $P(t)$ uniformly distributed along the interface with area A, the total normal load N on the contact region is

$$N(t) = P(t)A \tag{29}$$

Combining Eqs. (28) and (29), the wear depth h can be written as

$$h = k\,P(t)\,s \tag{30}$$

For the cylinder bore, the sliding distance s_b can be calculated considering that during one ring crossing any segment of the bore is slid by a distance equal to the ring thickness, t_R (Fig. 4). If we assume that there is a linear damage accrual rule, the total wear depth $h_b(X)$ of the cylinder bore at position X for a reciprocating motion during a time interval T with $n(X)$ crossings can be expressed as

$$h_b(X) = \sum_{i=1}^{n(X)} k_i(X)P_i(X)t_R \tag{31}$$

For a flat faced ring (Fig. 4), the contact pressure $P(t)$ between the ring and the bore can be approximated by using the sealed pressure P_{cyl} (Nikas, 2003). This sealed pressure is assumed to be the larger of P_A and P_B. Therefore

$$P(t) \approx P_{cyl} = \max[P_A, P_B] \tag{32}$$

Since our system has only been defined on a conceptional level (the material, lubricant and operational conditions are unknown), we assume that the wear coefficient k is independent of time t. Eq. (31) can then be expressed as

$$h_b(X) = k(X)t_R n(X)\overline{P}(X) \tag{33}$$

where $\overline{P}(X)$ is the average pressure at piston position X.

Eq. (33) shows that the cylinder bore wear depth is proportional to the crossing times $n(X)$. We again study the simulation results obtained in Section 3. Using the buoy excursion $X(t)$, which neglects the HFO shown in Fig. 7a, a sample of the ring crossings at the level of $X=-0.02$ is given in Fig. 13a. Fig. 13b shows the corresponding ring crossings at the same level for simulation results including the HFO (Fig. 7c). Fig. 13c is a detailed plot of the crossings in a time interval with HFOs. It is easy to find that the crossing number $n(-0.02)$ is much larger in Fig. 13b than in Fig. 13a. Introducing the crossing rate $\kappa(X)$ which is defined as the ratio of the crossing numbers $n(X)$ to the corresponding time interval T, Eq. (33) can be rewritten as

$$h_b(X) = k(X)\overline{P}(X)\kappa(X)t_R T \tag{34}$$

Therefore, the cylinder bore wear damage rate $\dot{h}_b(X)$ can be expressed as

$$\dot{h}_b(X) = \frac{h_b(X)}{T} = k(X)\overline{P}(X)\kappa(X)t_R \tag{35}$$

The values of $\kappa(X)$ along the cylinder bore are given in Fig. 14 for the two cases; one neglects the fluid compressibility and only considers low frequency motion, the other includes the effect of the oil compressibility and the induced HFO. Generally speaking, the crossing rates along the cylinder bore are larger when considering the fluid compressibility than with the assumption of incompressible oil, but the difference is small far from the cylinder midpoint. On the contrary, a large difference is observed around the midpoint of the cylinder ($X=0$), which indicates that most of the HFOs occur in this region.

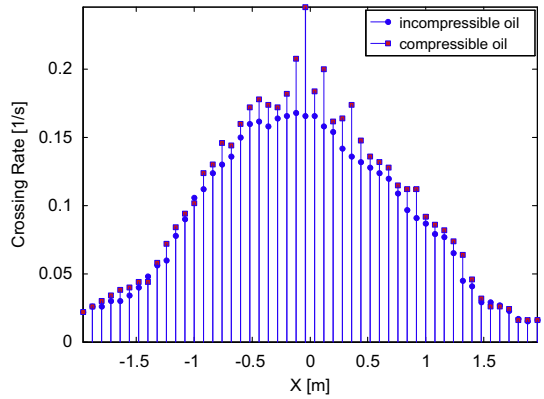

Fig. 14. Plot of crossing rate of motion response along the cylinder bore for $H_s=4.25$ m, $T_p=9.5$ s and $L=2.5$ m. The analysis has been done for the time interval between [500, 1500] s. The solid blue dots represent the WEC model with incompressible oil and the solid red squares represent the WEC model with compressible oil. (For interpretation of the references to colour in this figure legend, the reader is referred to the web version of this article.)

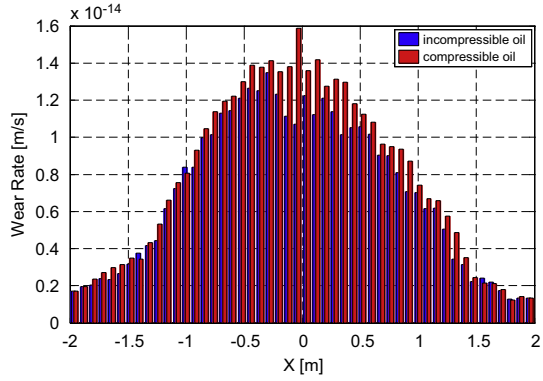

Fig. 15. Plot of wear damage rate along the cylinder bore for $H_s=4.25$ m, $T_p=9.5$ s and $L=2.5$ m. The ring thickness t_R is set as 3 mm and wear coefficient $K=1\times10^{-18}$ m^2/N. The blue bars represent the case which neglects the fluid compressibility while the red bars are the results obtained by considering the compressible fluid. (For interpretation of the references to colour in this figure legend, the reader is referred to the web version of this article.)

A ring with a thickness t_R=3 mm is used for case study. If the bore wear coefficient $k(X)$ is assumed to be equal to 1×10^{-18} m^2/N, the wear damage rate $\dot{h}_b(X)$ can be predicted by using Eq. (35). Fig. 15 gives the distribution wear damage rate for the two cases with and without considering the fluid compressibility in the WEC model. According to the results, the wear damage of the cylinder bore will be underestimated if we neglect the fluid compressibility. This effect reaches maximum when $X=-0.02$ m. (The wear damage rate at this position is 1.58×10^{-14} m/s with fluid compressibility included, while it is equal to 1.07×10^{-14} m/s with incompressible fluid as shown in Fig. 15.) In practice, for the wear of cylinder bore, local wear damage is usually dominating. Cylinder repair is generally carried out when the maximum wear of the internal surface approaches a specific limit. To predict the position of the bore where the maximum accumulated wear occurs is a critical issue. Fig. 15 shows that HFO induced by the fluid compressibility not only affects the amount of wear damage but also the repair position. Fig. 16 gives the relative wear difference for the two cases. The largest difference occurs around the middle of the cylinder and can reach almost 50%. This increment could lead to a reduction in life of the cylinder bore. To sum up, HFO contributes significantly to the bore wear damage in this WEC system and it should therefore be given thorough consideration.

Since the amplitudes of HFOs are usually very small (Figs. 7c, d, 9a, c and 10a), it is difficult to catch all the oscillation cycles by using discrete crossing levels. Additionally, as indicated by Giorgio et al. (2007), the severe wear usually occurs at or near the positions when the piston velocity is equal to 0. Hence, zero-crossing rate of the velocity is an important index for the bore wear. In order to estimate the contributions of these HFOs to the wear damage, we consider the velocity response $\dot{X}(t)$ instead of the position $X(t)$. At the turning points of $X(t)$, we have

$$\dot{X}(t)=0 \tag{36}$$

We can count the number of zero-crossings (the crossing level is equal to 0) for the time series of the velocity. This zero-crossing number (we can also use a corresponding variable named zero-crossing rate) includes all the motion periods along the cylinder bore. The zero-crossing rates for different cylinder designs are shown in Fig. 17. The rates decrease with increase in cylinder length. In addition, based on the simulation results of Falcão (2007) for a floating heaving buoy equipped with such a power take-off, the maximum value of average power was found to occur for a machinery force with a certain value $F_{m,opt}$ in each sea state.

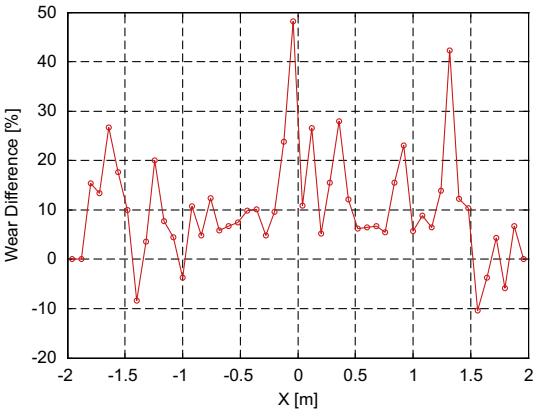

Fig. 16. Plot of relative wear difference along the cylinder bore for H_s=4.25 m, T_p=9.5 s and L=2.5 m. Calculations are carried out for a same case as for Fig. 15.

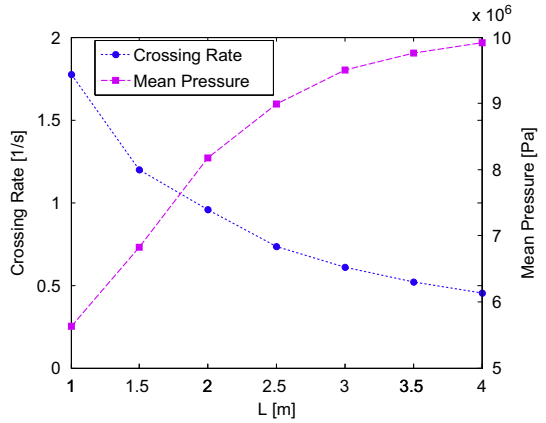

Fig. 17. Plot of zero-crossing rates of velocity response and mean pressure between the piston ring and cylinder bore for fixed cylinder volume V and varying cylinder half length L. The sea state parameters were H_s=1.5 m and T_p=9.5 s. The effect of fluid compressibility is considered for different cylinder types.

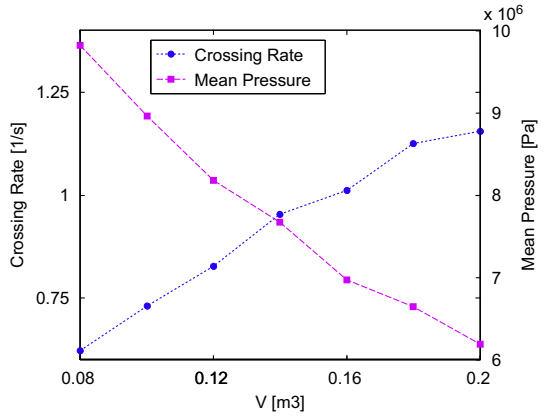

Fig. 18. Plot of zero-crossing rates of velocity response and mean pressure between the piston ring and cylinder bore for fixed cylinder half length L and varying cylinder volume V. The sea state parameters were H_s=1.5 m and T_p=9.5 s. The effect of fluid compressibility is considered for different cylinder types.

For a WEC system, the main function is to convert power. From this point, we should choose the optimum force $F_{m,opt}$ as the main parameter for this system. Eq. (7) shows that F_m is related to the piston area and pressure difference. For a constant value of $F_{m,opt}$, a larger piston area means a smaller pressure difference, i.e., a smaller $\overline{P}(X)$ in Eq. (34). Fig. 17 also gives the variation of $\overline{P}(X)$ with cylinder length L. As opposed to κ, the mean pressure $\overline{P}(X)$ is an increasing function of L. In order to find a minimum cylinder bore wear damage, we need comprehensive consideration of all the parameters mentioned in Eq. (34), including the crossing rate κ and average interface pressure$\overline{P}(X)$. Alternatively, we can choose the cylinder length first and then adjust the other variables of the cylinder, e.g. the cylinder volume V. The performances of WEC system for different cylinder volumes with fixed L=2.5 m are given by Fig. 18. We can follow the same path as we did for Fig. 17 to analyze these obtained results. We do not elaborate this any further here.

Similar to bore wear depth, ring wear depth can also be obtained from Eq. (30). The sliding distance of the ring can be obtained by

$$s_{ring} = \int_t |\dot{X}(t)|\, dt \tag{37}$$

The ring wear depth is:

$$h_{ring} = kP(t) \int_t |\dot{X}(t)|\, dt \tag{38}$$

A comparison of Fig. 7b and d shows that the HFOs cause an increase in the sliding distance, leading to increased wear as the result. Combined with the risk of poor lubrication at turning points mentioned before, it is clear that HFOs should be a matter of concern also for the piston ring wear.

5. Conclusions

A dynamic model, with the assumptions listed at the end of Section 2, has been presented for a heaving axisymmetric floating buoy, with a high-pressure hydraulic system for energy conversion. In particular, the compressibility of hydraulic fluid in the cylinder is included in the mathematic Wave Energy Converter (WEC) model. This hydraulic fluid acts likes a very stiff spring and, therefore influences the dynamics of the buoy. This work presents the effect of this type of fluid stiffness for an asymmetric cylinder ($\alpha \neq 1$) in different designs of the same volume. The minimum natural frequencies caused by fluid stiffness are presented for the different cylinder designs. The motion response of the floating buoy exposed to irregular waves is shown in time series where high frequency oscillations (HFOs) are observed. From an analysis of the power spectra, we can see that the main power of the HFOs resides beyond the estimated minimum natural frequency ω_{min}, which is reasonable for this system due to the variation of the piston position.

The wear model for piston ring and cylinder bore in the WEC system developed in Yang and Moan (submitted for publication) based on Archard's wear equation is applied to exemplify the contribution of the HFOs to the wear by numerical simulation of the heaving buoy model under a sea state characterized by $H_s = 4.25$ m and $T_p = 9.5$ s. Numerical results show that HFO strongly affects the wear of the cylinder bore, especially at the domain around the midpoint of the cylinder in the longitudinal direction. Simulation results combined with the analysis of Falcão (2007) indicate that there exists an optimum cylinder size which has minimum bore wear damage. As for the cylinder bore, the piston ring wear will be affected by the HFO. The HFOs can increase the sliding distance of the ring, which will lead to more ring wear. Although the increment of the sliding distance is not large, the surface to surface contact under this condition can also make a serious wear damage to the ring. To sum up, not only the low frequency motion, but also the high-frequency one can cause the ring and bore wear. Therefore, oil compressibility should be included in the mathematic model of this WEC system for the purpose of wear prediction. Otherwise, the wear damage of the ring and cylinder will be underestimated, which should be avoided both because of safety and durability reasons.

Acknowledgements

The authors wish to acknowledge the support of the Research Council of Norway through the Centre for Ships and Ocean Structures at the Norwegian University of Science and Technology in Trondheim, Norway.

References

Archard, J.F., Hirst, W., 1956. The wear of metals under unlubricated conditions. Proceedings of the Royal Society of London, Series A, Mathematical and Physical Science 236 (1206), 397–410.
Babarit, A., Duclos, G., Clement, A.H., 2004. Comparison of latching control strategies for a heaving wave energy device in random sea. Applied Ocean Research 26, 227–238.
Bjarte-Larsson, T., Falnes, J., 2006. Laboratory experiment on heaving body with hydraulic power take-off and latching control. Ocean Engineering 33, 847–877.
Becker, E.P., Ludema, K.C., 1999. A qualitative empirical model of cylinder bore wear. Wear 225–229 (Part I), 387–404.
Borutzky, W., Barnard, B., Thoma, J., 2002. An orifice flow model for laminar and turbulent conditions. Simulation Modeling Practice and Theory 10 (3–4), 141–152.
Budal, K., Falnes, J., 1982. Wave power conversion by point absorbers: a Norwegian project. International Journal of Ambient Energy 3 (2), 59–67.
Cummins, W., 1962. The impulse response function and ship motions. Schiffstechnik 9 (1661), 101–109.
Egeland, O., Gravdahl, J.T., 2002. Modeling and simulation for automatic control. Marine Cybernetics.
Eidsmoen, H., 1995. On the theory and simulation of heaving-buoy wave-energy converters with control. Ph.D. Thesis, NTH.
Evans, D.V., 1978. The oscillating water column wave energy device. Journal of the Institute of Mathematics and its Applications 22, 423–433.
Evans, D.V., 1981. Maximum wave-power absorption under motion constraints. Applied Ocean Research 3, 200–203.
de O Falcão, A.F., 2007. Modelling and control of oscillating-body wave energy converters with hydraulic power take-off and gas accumulator. Ocean Engineering 34, 2021–2032.
de O Falcão, A.F., 2008. Phase control through load control of oscillating-body wave energy converters with hydraulic PTO system. Ocean Engineering 35, 358–366.
Falnes, J., Budal, K., 1978. Wave-power conversion by point absorbers. Norwegian Maritime Research 6, 2–11.
Falnes, J., 2002. Ocean Waves and Oscillating Systems. Cambridge University Press, Cambridge.
Faltinsen, O.M., 1990. Sea Loads on Ships and Offshore Structures. Cambridge University Press, Cambridge.
French, M.J., Bracewell, R., 1986. Heaving point absorbers reacting against an internal mass. In: Evans, D.V, de, A.F, Falcão, O. (Eds.), Hydrodynamics of Ocean-wave Energy Utilization. IUTAM Symposium, Lisbon, Portugal (1985). Springer Verlag, Berlin, pp. 247–255.
Giorgio, M., Guida, M., Pulcini, G., 2007. A wear model for assessing the reliability of cylinder liners in marine diesel engines. IEEE Transactions on Reliability 56 (1), 158–166.
Hals, J., Taghipour, R., Moan, T., 2007. Dynamics of a force compensated two-body wave energy converter in heave with hydraulic power take-off subject to phase control. In: Proceedings of the Seventh European Wave and Tidal Energy Conference, Porto, Portugal.
Jelali, M., Kroll, A., 2003. Hydraulic Servo-systems: Modelling, Identification and Control. Springer, London, ISBN: 1-85233-692-7.
Karnopp, D.C., Margolis, D.L., Rosenberg, R.C., 2006. System Dynamics: Modelling and Simulation of Mechatronic Systems. John Wiley &Sons.
Lopes, M.F.P., Hals, J., Gomes, R.P.F., Moan, T., Gato, L.M.C., Falcão, A.F., de, O., 2009. Experimental and numerical investigation of non-predictive phase-control strategies for a point-absorbing wave energy converter. Ocean Engineering 36, 386–402.
Michel, W.H., 1999. Sea spectra revisited. Marine Technology and SNAME News 36 (4), 211–227.
Müller, H.K., Nau, B.S., 1998. Fluid Sealing Technology: Principles and Applications. Marcel Dekker, New York.
Nikas, G.K., 2003. Elastohydrodynamics and mechanics of rectangular elastomeric seals for reciprocating piston rods. Journal of Tribology 125 (1), 60–69.
Peterson, M.B., Winer, W.O., 1980. Wear Control Handbook. The American Society of Mechanical Engineers, New York.
Pizer, D.J., 1993. Maximum wave-power absorption of point absorbers under motion constraints. Applied Ocean Research 15 (4), 227–234.
Priest, M., Dowson, D., Taylor, C.M, 1999. Predictive wear modelling of lubricated piston rings in a diesel engine. Wear 231, 89–101.
Taghipour, R., Perez, T., Moan, T., 2008. Hybrid frequency time domain models for dynamic response analysis of marine structures. Ocean Engineering 35, 685–705.
Thoma, J., 1970. Modern Hydraulic Engineering. Trade and Technical Press, London.
Ting, L.L., Mayer, J.E., 1974. Piston ring lubrication and cylinder bore wear analysis: Part I-Theory. American Society of Mechanical Engineers, Journal of Lubrication Technology 96, 305–314.
Tung, S., Huang, Y., 2004. Modeling of abrasive wear in a piston ring and engine cylinder bore system. Tribology Transactions 47, 17–22.
Vantorre, M., Banasiak, M., Verhoeven, R., 2004. Modelling of hydraulic performance and wave energy extraction by a point absorber in heave. Applied Ocean Research 26, 61–72.
WAMIT, 2006. WAMIT User Manual. Version 6.3 〈http://www.wamit.com〉.
Yang, L.M., Hals, J., Moan, T., 2009. A wear model for assessing the reliability of wave energy converter in heave with hydraulic power take-off. In: Proceedings of the Eighth European Wave and Tidal Energy Conference, Uppsala, Sweden.
Yang, L.M., Moan, T.. Analysis of wear in seals of a wave energy converter with hydraulic power take-off under random loads. Tribology Transactions, submitted for publication.

Paper B

Cylinder bore wear damage analysis of a heaving-buoy wave energy converter with hydraulic power take-off

Published in

Proceedings of the ASME 29th International Conference of Offshore Mechanics and Arctic Engineering, OMAE2010-20164, Shanghai, China, June 6-11, 2010.

Is not included due to copyright

Paper C

Numerical modeling of wear damage in seals of a wave energy converter with hydraulic power take-off under random loads

Published in

Tribology Transactions, Vol. 54, No. 1, pp. 44-56, 2011.

Is not included due to copyright

Paper D

Dynamic analysis of wave energy converter by incorporating the effect of hydraulic transmission lines

Submitted for publication, 2010.

Is not included due to copyright

Paper E

Comparable study of bond graph models of hydraulic transmission lines with transient flow dynamics

Submitted for publication, 2010.

Is not included due to copyright

R A P P O R T E R
UTGITT VED
INSTITUTT FOR MARIN TEKNIKK
(tidligere: FAKULTET FOR MARIN TEKNIKK)
NORGES TEKNISK-NATURVITENSKAPELIGE UNIVERSITET

Report No.	Author	Title
	Kavlie, Dag	Optimization of Plane Elastic Grillages, 1967
	Hansen, Hans R.	Man-Machine Communication and Data-Storage Methods in Ship Structural Design, 1971
	Gisvold, Kaare M.	A Method for non-linear mixed -integer programming and its Application to Design Problems, 1971
	Lund, Sverre	Tanker Frame Optimalization by means of SUMT-Transformation and Behaviour Models, 1971
	Vinje, Tor	On Vibration of Spherical Shells Interacting with Fluid, 1972
	Lorentz, Jan D.	Tank Arrangement for Crude Oil Carriers in Accordance with the new Anti-Pollution Regulations, 1975
	Carlsen, Carl A.	Computer-Aided Design of Tanker Structures, 1975
	Larsen, Carl M.	Static and Dynamic Analysis of Offshore Pipelines during Installation, 1976
UR-79-01	Brigt Hatlestad, MK	The finite element method used in a fatigue evaluation of fixed offshore platforms. (Dr.Ing. Thesis)
UR-79-02	Erik Pettersen, MK	Analysis and design of cellular structures. (Dr.Ing. Thesis)
UR-79-03	Sverre Valsgård, MK	Finite difference and finite element methods applied to nonlinear analysis of plated structures. (Dr.Ing. Thesis)
UR-79-04	Nils T. Nordsve, MK	Finite element collapse analysis of structural members considering imperfections and stresses due to fabrication. (Dr.Ing. Thesis)
UR-79-05	Ivar J. Fylling, MK	Analysis of towline forces in ocean towing systems. (Dr.Ing. Thesis)
UR-80-06	Nils Sandsmark, MM	Analysis of Stationary and Transient Heat Conduction by the Use of the Finite Element Method. (Dr.Ing. Thesis)
UR-80-09	Sverre Haver, MK	Analysis of uncertainties related to the stochastic modeling of ocean waves. (Dr.Ing. Thesis)
UR-81-15	Odland, Jonas	On the Strength of welded Ring stiffened cylindrical Shells primarily subjected to axial Compression

UR-82-17	Engesvik, Knut	Analysis of Uncertainties in the fatigue Capacity of Welded Joints
UR-82-18	Rye, Henrik	Ocean wave groups
UR-83-30	Eide, Oddvar Inge	On Cumulative Fatigue Damage in Steel Welded Joints
UR-83-33	Mo, Olav	Stochastic Time Domain Analysis of Slender Offshore Structures
UR-83-34	Amdahl, Jørgen	Energy absorption in Ship-platform impacts
UR-84-37	Mørch, Morten	Motions and mooring forces of semi submersibles as determined by full-scale measurements and theoretical analysis
UR-84-38	Soares, C. Guedes	Probabilistic models for load effects in ship structures
UR-84-39	Aarsnes, Jan V.	Current forces on ships
UR-84-40	Czujko, Jerzy	Collapse Analysis of Plates subjected to Biaxial Compression and Lateral Load
UR-85-46	Alf G. Engseth, MK	Finite element collapse analysis of tubular steel offshore structures. (Dr.Ing. Thesis)
UR-86-47	Dengody Sheshappa, MP	A Computer Design Model for Optimizing Fishing Vessel Designs Based on Techno-Economic Analysis. (Dr.Ing. Thesis)
UR-86-48	Vidar Aanesland, MH	A Theoretical and Numerical Study of Ship Wave Resistance. (Dr.Ing. Thesis)
UR-86-49	Heinz-Joachim Wessel, MK	Fracture Mechanics Analysis of Crack Growth in Plate Girders. (Dr.Ing. Thesis)
UR-86-50	Jon Taby, MK	Ultimate and Post-ultimate Strength of Dented Tubular Members. (Dr.Ing. Thesis)
UR-86-51	Walter Lian, MH	A Numerical Study of Two-Dimensional Separated Flow Past Bluff Bodies at Moderate KC-Numbers. (Dr.Ing. Thesis)
UR-86-52	Bjørn Sortland, MH	Force Measurements in Oscillating Flow on Ship Sections and Circular Cylinders in a U-Tube Water Tank. (Dr.Ing. Thesis)
UR-86-53	Kurt Strand, MM	A System Dynamic Approach to One-dimensional Fluid Flow. (Dr.Ing. Thesis)
UR-86-54	Arne Edvin Løken, MH	Three Dimensional Second Order Hydrodynamic Effects on Ocean Structures in Waves. (Dr.Ing. Thesis)
UR-86-55	Sigurd Falch, MH	A Numerical Study of Slamming of Two-Dimensional Bodies. (Dr.Ing. Thesis)
UR-87-56	Arne Braathen, MH	Application of a Vortex Tracking Method to the Prediction of Roll Damping of a Two-Dimension

		Floating Body. (Dr.Ing. Thesis)
UR-87-57	Bernt Leira, MK	Gaussian Vector Processes for Reliability Analysis involving Wave-Induced Load Effects. (Dr.Ing. Thesis)
UR-87-58	Magnus Småvik, MM	Thermal Load and Process Characteristics in a Two-Stroke Diesel Engine with Thermal Barriers (in Norwegian). (Dr.Ing. Thesis)
MTA-88-59	Bernt Arild Bremdal, MP	An Investigation of Marine Installation Processes – A Knowledge - Based Planning Approach. (Dr.Ing. Thesis)
MTA-88-60	Xu Jun, MK	Non-linear Dynamic Analysis of Space-framed Offshore Structures. (Dr.Ing. Thesis)
MTA-89-61	Gang Miao, MH	Hydrodynamic Forces and Dynamic Responses of Circular Cylinders in Wave Zones. (Dr.Ing. Thesis)
MTA-89-62	Martin Greenhow, MH	Linear and Non-Linear Studies of Waves and Floating Bodies. Part I and Part II. (Dr.Techn. Thesis)
MTA-89-63	Chang Li, MH	Force Coefficients of Spheres and Cubes in Oscillatory Flow with and without Current. (Dr.Ing. Thesis
MTA-89-64	Hu Ying, MP	A Study of Marketing and Design in Development of Marine Transport Systems. (Dr.Ing. Thesis)
MTA-89-65	Arild Jæger, MH	Seakeeping, Dynamic Stability and Performance of a Wedge Shaped Planing Hull. (Dr.Ing. Thesis)
MTA-89-66	Chan Siu Hung, MM	The dynamic characteristics of tilting-pad bearings
MTA-89-67	Kim Wikstrøm, MP	Analysis av projekteringen for ett offshore projekt. (Licenciat-avhandling)
MTA-89-68	Jiao Guoyang, MK	Reliability Analysis of Crack Growth under Random Loading, considering Model Updating. (Dr.Ing. Thesis)
MTA-89-69	Arnt Olufsen, MK	Uncertainty and Reliability Analysis of Fixed Offshore Structures. (Dr.Ing. Thesis)
MTA-89-70	Wu Yu-Lin, MR	System Reliability Analyses of Offshore Structures using improved Truss and Beam Models. (Dr.Ing. Thesis)
MTA-90-71	Jan Roger Hoff, MH	Three-dimensional Green function of a vessel with forward speed in waves. (Dr.Ing. Thesis)
MTA-90-72	Rong Zhao, MH	Slow-Drift Motions of a Moored Two-Dimensional Body in Irregular Waves. (Dr.Ing. Thesis)
MTA-90-73	Atle Minsaas, MP	Economical Risk Analysis. (Dr.Ing. Thesis)
MTA-90-74	Knut-Aril Farnes, MK	Long-term Statistics of Response in Non-linear Marine Structures. (Dr.Ing. Thesis)
MTA-90-	Torbjørn Sotberg, MK	Application of Reliability Methods for Safety

75		Assessment of Submarine Pipelines. (Dr.Ing. Thesis)
MTA-90-76	Zeuthen, Steffen, MP	SEAMAID. A computational model of the design process in a constraint-based logic programming environment. An example from the offshore domain. (Dr.Ing. Thesis)
MTA-91-77	Haagensen, Sven, MM	Fuel Dependant Cyclic Variability in a Spark Ignition Engine - An Optical Approach. (Dr.Ing. Thesis)
MTA-91-78	Løland, Geir, MH	Current forces on and flow through fish farms. (Dr.Ing. Thesis)
MTA-91-79	Hoen, Christopher, MK	System Identification of Structures Excited by Stochastic Load Processes. (Dr.Ing. Thesis)
MTA-91-80	Haugen, Stein, MK	Probabilistic Evaluation of Frequency of Collision between Ships and Offshore Platforms. (Dr.Ing. Thesis)
MTA-91-81	Sødahl, Nils, MK	Methods for Design and Analysis of Flexible Risers. (Dr.Ing. Thesis)
MTA-91-82	Ormberg, Harald, MK	Non-linear Response Analysis of Floating Fish Farm Systems. (Dr.Ing. Thesis)
MTA-91-83	Marley, Mark J., MK	Time Variant Reliability under Fatigue Degradation. (Dr.Ing. Thesis)
MTA-91-84	Krokstad, Jørgen R., MH	Second-order Loads in Multidirectional Seas. (Dr.Ing. Thesis)
MTA-91-85	Molteberg, Gunnar A., MM	The Application of System Identification Techniques to Performance Monitoring of Four Stroke Turbocharged Diesel Engines. (Dr.Ing. Thesis)
MTA-92-86	Mørch, Hans Jørgen Bjelke, MH	Aspects of Hydrofoil Design: with Emphasis on Hydrofoil Interaction in Calm Water. (Dr.Ing. Thesis)
MTA-92-87	Chan Siu Hung, MM	Nonlinear Analysis of Rotordynamic Instabilities in Highspeed Turbomachinery. (Dr.Ing. Thesis)
MTA-92-88	Bessason, Bjarni, MK	Assessment of Earthquake Loading and Response of Seismically Isolated Bridges. (Dr.Ing. Thesis)
MTA-92-89	Langli, Geir, MP	Improving Operational Safety through exploitation of Design Knowledge - an investigation of offshore platform safety. (Dr.Ing. Thesis)
MTA-92-90	Sævik, Svein, MK	On Stresses and Fatigue in Flexible Pipes. (Dr.Ing. Thesis)
MTA-92-91	Ask, Tor Ø., MM	Ignition and Flame Growth in Lean Gas-Air Mixtures. An Experimental Study with a Schlieren System. (Dr.Ing. Thesis)
MTA-86-92	Hessen, Gunnar, MK	Fracture Mechanics Analysis of Stiffened Tubular

		Members. (Dr.Ing. Thesis)
MTA-93-93	Steinebach, Christian, MM	Knowledge Based Systems for Diagnosis of Rotating Machinery. (Dr.Ing. Thesis)
MTA-93-94	Dalane, Jan Inge, MK	System Reliability in Design and Maintenance of Fixed Offshore Structures. (Dr.Ing. Thesis)
MTA-93-95	Steen, Sverre, MH	Cobblestone Effect on SES. (Dr.Ing. Thesis)
MTA-93-96	Karunakaran, Daniel, MK	Nonlinear Dynamic Response and Reliability Analysis of Drag-dominated Offshore Platforms. (Dr.Ing. Thesis)
MTA-93-97	Hagen, Arnulf, MP	The Framework of a Design Process Language. (Dr.Ing. Thesis)
MTA-93-98	Nordrik, Rune, MM	Investigation of Spark Ignition and Autoignition in Methane and Air Using Computational Fluid Dynamics and Chemical Reaction Kinetics. A Numerical Study of Ignition Processes in Internal Combustion Engines. (Dr.Ing. Thesis)
MTA-94-99	Passano, Elizabeth, MK	Efficient Analysis of Nonlinear Slender Marine Structures. (Dr.Ing. Thesis)
MTA-94-100	Kvålsvold, Jan, MH	Hydroelastic Modelling of Wetdeck Slamming on Multihull Vessels. (Dr.Ing. Thesis)
MTA-94-102	Bech, Sidsel M., MK	Experimental and Numerical Determination of Stiffness and Strength of GRP/PVC Sandwich Structures. (Dr.Ing. Thesis)
MTA-95-103	Paulsen, Hallvard, MM	A Study of Transient Jet and Spray using a Schlieren Method and Digital Image Processing. (Dr.Ing. Thesis)
MTA-95-104	Hovde, Geir Olav, MK	Fatigue and Overload Reliability of Offshore Structural Systems, Considering the Effect of Inspection and Repair. (Dr.Ing. Thesis)
MTA-95-105	Wang, Xiaozhi, MK	Reliability Analysis of Production Ships with Emphasis on Load Combination and Ultimate Strength. (Dr.Ing. Thesis)
MTA-95-106	Ulstein, Tore, MH	Nonlinear Effects of a Flexible Stern Seal Bag on Cobblestone Oscillations of an SES. (Dr.Ing. Thesis)
MTA-95-107	Solaas, Frøydis, MH	Analytical and Numerical Studies of Sloshing in Tanks. (Dr.Ing. Thesis)
MTA-95-108	Hellan, Øyvind, MK	Nonlinear Pushover and Cyclic Analyses in Ultimate Limit State Design and Reassessment of Tubular Steel Offshore Structures. (Dr.Ing. Thesis)
MTA-95-109	Hermundstad, Ole A., MK	Theoretical and Experimental Hydroelastic Analysis of High Speed Vessels. (Dr.Ing. Thesis)
MTA-96-110	Bratland, Anne K., MH	Wave-Current Interaction Effects on Large-Volume Bodies in Water of Finite Depth. (Dr.Ing. Thesis)

MTA-96-111	Herfjord, Kjell, MH	A Study of Two-dimensional Separated Flow by a Combination of the Finite Element Method and Navier-Stokes Equations. (Dr.Ing. Thesis)
MTA-96-112	Æsøy, Vilmar, MM	Hot Surface Assisted Compression Ignition in a Direct Injection Natural Gas Engine. (Dr.Ing. Thesis)
MTA-96-113	Eknes, Monika L., MK	Escalation Scenarios Initiated by Gas Explosions on Offshore Installations. (Dr.Ing. Thesis)
MTA-96-114	Erikstad, Stein O., MP	A Decision Support Model for Preliminary Ship Design. (Dr.Ing. Thesis)
MTA-96-115	Pedersen, Egil, MH	A Nautical Study of Towed Marine Seismic Streamer Cable Configurations. (Dr.Ing. Thesis)
MTA-97-116	Moksnes, Paul O., MM	Modelling Two-Phase Thermo-Fluid Systems Using Bond Graphs. (Dr.Ing. Thesis)
MTA-97-117	Halse, Karl H., MK	On Vortex Shedding and Prediction of Vortex-Induced Vibrations of Circular Cylinders. (Dr.Ing. Thesis)
MTA-97-118	Igland, Ragnar T., MK	Reliability Analysis of Pipelines during Laying, considering Ultimate Strength under Combined Loads. (Dr.Ing. Thesis)
MTA-97-119	Pedersen, Hans-P., MP	Levendefiskteknologi for fiskefartøy. (Dr.Ing. Thesis)
MTA-98-120	Vikestad, Kyrre, MK	Multi-Frequency Response of a Cylinder Subjected to Vortex Shedding and Support Motions. (Dr.Ing. Thesis)
MTA-98-121	Azadi, Mohammad R. E., MK	Analysis of Static and Dynamic Pile-Soil-Jacket Behaviour. (Dr.Ing. Thesis)
MTA-98-122	Ulltang, Terje, MP	A Communication Model for Product Information. (Dr.Ing. Thesis)
MTA-98-123	Torbergsen, Erik, MM	Impeller/Diffuser Interaction Forces in Centrifugal Pumps. (Dr.Ing. Thesis)
MTA-98-124	Hansen, Edmond, MH	A Discrete Element Model to Study Marginal Ice Zone Dynamics and the Behaviour of Vessels Moored in Broken Ice. (Dr.Ing. Thesis)
MTA-98-125	Videiro, Paulo M., MK	Reliability Based Design of Marine Structures. (Dr.Ing. Thesis)
MTA-99-126	Mainçon, Philippe, MK	Fatigue Reliability of Long Welds Application to Titanium Risers. (Dr.Ing. Thesis)
MTA-99-127	Haugen, Elin M., MH	Hydroelastic Analysis of Slamming on Stiffened Plates with Application to Catamaran Wetdecks. (Dr.Ing. Thesis)
MTA-99-128	Langhelle, Nina K., MK	Experimental Validation and Calibration of Nonlinear Finite Element Models for Use in Design of Aluminium Structures Exposed to Fire. (Dr.Ing.

		Thesis)
MTA-99-129	Berstad, Are J., MK	Calculation of Fatigue Damage in Ship Structures. (Dr.Ing. Thesis)
MTA-99-130	Andersen, Trond M., MM	Short Term Maintenance Planning. (Dr.Ing. Thesis)
MTA-99-131	Tveiten, Bård Wathne, MK	Fatigue Assessment of Welded Aluminium Ship Details. (Dr.Ing. Thesis)
MTA-99-132	Søreide, Fredrik, MP	Applications of underwater technology in deep water archaeology. Principles and practice. (Dr.Ing. Thesis)
MTA-99-133	Tønnessen, Rune, MH	A Finite Element Method Applied to Unsteady Viscous Flow Around 2D Blunt Bodies With Sharp Corners. (Dr.Ing. Thesis)
MTA-99-134	Elvekrok, Dag R., MP	Engineering Integration in Field Development Projects in the Norwegian Oil and Gas Industry. The Supplier Management of Norne. (Dr.Ing. Thesis)
MTA-99-135	Fagerholt, Kjetil, MP	Optimeringsbaserte Metoder for Ruteplanlegging innen skipsfart. (Dr.Ing. Thesis)
MTA-99-136	Bysveen, Marie, MM	Visualization in Two Directions on a Dynamic Combustion Rig for Studies of Fuel Quality. (Dr.Ing. Thesis)
MTA-2000-137	Storteig, Eskild, MM	Dynamic characteristics and leakage performance of liquid annular seals in centrifugal pumps. (Dr.Ing. Thesis)
MTA-2000-138	Sagli, Gro, MK	Model uncertainty and simplified estimates of long term extremes of hull girder loads in ships. (Dr.Ing. Thesis)
MTA-2000-139	Tronstad, Harald, MK	Nonlinear analysis and design of cable net structures like fishing gear based on the finite element method. (Dr.Ing. Thesis)
MTA-2000-140	Kroneberg, André, MP	Innovation in shipping by using scenarios. (Dr.Ing. Thesis)
MTA-2000-141	Haslum, Herbjørn Alf, MH	Simplified methods applied to nonlinear motion of spar platforms. (Dr.Ing. Thesis)
MTA-2001-142	Samdal, Ole Johan, MM	Modelling of Degradation Mechanisms and Stressor Interaction on Static Mechanical Equipment Residual Lifetime. (Dr.Ing. Thesis)
MTA-2001-143	Baarholm, Rolf Jarle, MH	Theoretical and experimental studies of wave impact underneath decks of offshore platforms. (Dr.Ing. Thesis)
MTA-2001-144	Wang, Lihua, MK	Probabilistic Analysis of Nonlinear Wave-induced Loads on Ships. (Dr.Ing. Thesis)
MTA-2001-145	Kristensen, Odd H. Holt, MK	Ultimate Capacity of Aluminium Plates under Multiple Loads, Considering HAZ Properties. (Dr.Ing. Thesis)

MTA-2001-146	Greco, Marilena, MH	A Two-Dimensional Study of Green-Water Loading. (Dr.Ing. Thesis)
MTA-2001-147	Heggelund, Svein E., MK	Calculation of Global Design Loads and Load Effects in Large High Speed Catamarans. (Dr.Ing. Thesis)
MTA-2001-148	Babalola, Olusegun T., MK	Fatigue Strength of Titanium Risers – Defect Sensitivity. (Dr.Ing. Thesis)
MTA-2001-149	Mohammed, Abuu K., MK	Nonlinear Shell Finite Elements for Ultimate Strength and Collapse Analysis of Ship Structures. (Dr.Ing. Thesis)
MTA-2002-150	Holmedal, Lars E., MH	Wave-current interactions in the vicinity of the sea bed. (Dr.Ing. Thesis)
MTA-2002-151	Rognebakke, Olav F., MH	Sloshing in rectangular tanks and interaction with ship motions. (Dr.Ing. Thesis)
MTA-2002-152	Lader, Pål Furset, MH	Geometry and Kinematics of Breaking Waves. (Dr.Ing. Thesis)
MTA-2002-153	Yang, Qinzheng, MH	Wash and wave resistance of ships in finite water depth. (Dr.Ing. Thesis)
MTA-2002-154	Melhus, Øyvin, MM	Utilization of VOC in Diesel Engines. Ignition and combustion of VOC released by crude oil tankers. (Dr.Ing. Thesis)
MTA-2002-155	Ronæss, Marit, MH	Wave Induced Motions of Two Ships Advancing on Parallel Course. (Dr.Ing. Thesis)
MTA-2002-156	Økland, Ole D., MK	Numerical and experimental investigation of whipping in twin hull vessels exposed to severe wet deck slamming. (Dr.Ing. Thesis)
MTA-2002-157	Ge, Chunhua, MK	Global Hydroelastic Response of Catamarans due to Wet Deck Slamming. (Dr.Ing. Thesis)
MTA-2002-158	Byklum, Eirik, MK	Nonlinear Shell Finite Elements for Ultimate Strength and Collapse Analysis of Ship Structures. (Dr.Ing. Thesis)
IMT-2003-1	Chen, Haibo, MK	Probabilistic Evaluation of FPSO-Tanker Collision in Tandem Offloading Operation. (Dr.Ing. Thesis)
IMT-2003-2	Skaugset, Kjetil Bjørn, MK	On the Suppression of Vortex Induced Vibrations of Circular Cylinders by Radial Water Jets. (Dr.Ing. Thesis)
IMT-2003-3	Chezhian, Muthu	Three-Dimensional Analysis of Slamming. (Dr.Ing. Thesis)
IMT-2003-4	Buhaug, Øyvind	Deposit Formation on Cylinder Liner Surfaces in Medium Speed Engines. (Dr.Ing. Thesis)
IMT-2003-5	Tregde, Vidar	Aspects of Ship Design: Optimization of Aft Hull with Inverse Geometry Design. (Dr.Ing. Thesis)

IMT-2003-6	Wist, Hanne Therese	Statistical Properties of Successive Ocean Wave Parameters. (Dr.Ing. Thesis)
IMT-2004-7	Ransau, Samuel	Numerical Methods for Flows with Evolving Interfaces. (Dr.Ing. Thesis)
IMT-2004-8	Soma, Torkel	Blue-Chip or Sub-Standard. A data interrogation approach of identity safety characteristics of shipping organization. (Dr.Ing. Thesis)
IMT-2004-9	Ersdal, Svein	An experimental study of hydrodynamic forces on cylinders and cables in near axial flow. (Dr.Ing. Thesis)
IMT-2005-10	Brodtkorb, Per Andreas	The Probability of Occurrence of Dangerous Wave Situations at Sea. (Dr.Ing. Thesis)
IMT-2005-11	Yttervik, Rune	Ocean current variability in relation to offshore engineering. (Dr.Ing. Thesis)
IMT-2005-12	Fredheim, Arne	Current Forces on Net-Structures. (Dr.Ing. Thesis)
IMT-2005-13	Heggernes, Kjetil	Flow around marine structures. (Dr.Ing. Thesis
IMT-2005-14	Fouques, Sebastien	Lagrangian Modelling of Ocean Surface Waves and Synthetic Aperture Radar Wave Measurements. (Dr.Ing. Thesis)
IMT-2006-15	Holm, Håvard	Numerical calculation of viscous free surface flow around marine structures. (Dr.Ing. Thesis)
IMT-2006-16	Bjørheim, Lars G.	Failure Assessment of Long Through Thickness Fatigue Cracks in Ship Hulls. (Dr.Ing. Thesis)
IMT-2006-17	Hansson, Lisbeth	Safety Management for Prevention of Occupational Accidents. (Dr.Ing. Thesis)
IMT-2006-18	Zhu, Xinying	Application of the CIP Method to Strongly Nonlinear Wave-Body Interaction Problems. (Dr.Ing. Thesis)
IMT-2006-19	Reite, Karl Johan	Modelling and Control of Trawl Systems. (Dr.Ing. Thesis)
IMT-2006-20	Smogeli, Øyvind Notland	Control of Marine Propellers. From Normal to Extreme Conditions. (Dr.Ing. Thesis)
IMT-2007-21	Storhaug, Gaute	Experimental Investigation of Wave Induced Vibrations and Their Effect on the Fatigue Loading of Ships. (Dr.Ing. Thesis)
IMT-2007-22	Sun, Hui	A Boundary Element Method Applied to Strongly Nonlinear Wave-Body Interaction Problems. (PhD Thesis, CeSOS)
IMT-2007-23	Rustad, Anne Marthine	Modelling and Control of Top Tensioned Risers. (PhD Thesis, CeSOS)
IMT-2007-24	Johansen, Vegar	Modelling flexible slender system for real-time simulations and control applications
IMT-	Wroldsen, Anders Sunde	Modelling and control of tensegrity structures. (PhD

2007-25		Thesis, CeSOS)
IMT-2007-26	Aronsen, Kristoffer Høye	An experimental investigation of in-line and combined inline and cross flow vortex induced vibrations. (Dr. avhandling, IMT)
IMT-2007-27	Gao, Zhen	Stochastic Response Analysis of Mooring Systems with Emphasis on Frequency-domain Analysis of Fatigue due to Wide-band Response Processes (PhD Thesis, CeSOS)
IMT-2007-28	Thorstensen, Tom Anders	Lifetime Profit Modelling of Ageing Systems Utilizing Information about Technical Condition. (Dr.ing. thesis, IMT)
IMT-2008-29	Berntsen, Per Ivar B.	Structural Reliability Based Position Mooring. (PhD-Thesis, IMT)
IMT-2008-30	Ye, Naiquan	Fatigue Assessment of Aluminium Welded Box-stiffener Joints in Ships (Dr.ing. thesis, IMT)
IMT-2008-31	Radan, Damir	Integrated Control of Marine Electrical Power Systems. (PhD-Thesis, IMT)
IMT-2008-32	Thomassen, Paul	Methods for Dynamic Response Analysis and Fatigue Life Estimation of Floating Fish Cages. (Dr.ing. thesis, IMT)
IMT-2008-33	Pákozdi, Csaba	A Smoothed Particle Hydrodynamics Study of Two-dimensional Nonlinear Sloshing in Rectangular Tanks. (Dr.ing.thesis, IMT)
IMT-2007-34	Grytøyr, Guttorm	A Higher-Order Boundary Element Method and Applications to Marine Hydrodynamics. (Dr.ing.thesis, IMT)
IMT-2008-35	Drummen, Ingo	Experimental and Numerical Investigation of Nonlinear Wave-Induced Load Effects in Containerships considering Hydroelasticity. (PhD thesis, CeSOS)
IMT-2008-36	Skejic, Renato	Maneuvering and Seakeeping of a Singel Ship and of Two Ships in Interaction. (PhD-Thesis, CeSOS)
IMT-2008-37	Harlem, Alf	An Age-Based Replacement Model for Repairable Systems with Attention to High-Speed Marine Diesel Engines. (PhD-Thesis, IMT)
IMT-2008-38	Alsos, Hagbart S.	Ship Grounding. Analysis of Ductile Fracture, Bottom Damage and Hull Girder Response. (PhD-thesis, IMT)
IMT-2008-39	Graczyk, Mateusz	Experimental Investigation of Sloshing Loading and Load Effects in Membrane LNG Tanks Subjected to Random Excitation. (PhD-thesis, CeSOS)
IMT-2008-40	Taghipour, Reza	Efficient Prediction of Dynamic Response for Flexible amd Multi-body Marine Structures. (PhD-thesis, CeSOS)
IMT-2008-41	Ruth, Eivind	Propulsion control and thrust allocation on marine vessels. (PhD thesis, CeSOS)

IMT-2008-42	Nystad, Bent Helge	Technical Condition Indexes and Remaining Useful Life of Aggregated Systems. PhD thesis, IMT
IMT-2008-43	Soni, Prashant Kumar	Hydrodynamic Coefficients for Vortex Induced Vibrations of Flexible Beams, PhD thesis, CeSOS
IMT-2009-43	Amlashi, Hadi K.K.	Ultimate Strength and Reliability-based Design of Ship Hulls with Emphasis on Combined Global and Local Loads. PhD Thesis, IMT
IMT-2009-44	Pedersen, Tom Arne	Bond Graph Modelling of Marine Power Systems. PhD Thesis, IMT
IMT-2009-45	Kristiansen, Trygve	Two-Dimensional Numerical and Experimental Studies of Piston-Mode Resonance. PhD-Thesis, CeSOS
IMT-2009-46	Ong, Muk Chen	Applications of a Standard High Reynolds Number Model and a Stochastic Scour Prediction Model for Marine Structures. PhD-thesis, IMT
IMT-2009-47	Hong, Lin	Simplified Analysis and Design of Ships subjected to Collision and Grounding. PhD-thesis, IMT
IMT-2009-48	Koushan, Kamran	Vortex Induced Vibrations of Free Span Pipelines, PhD thesis, IMT
IMT-2009-49	Korsvik, Jarl Eirik	Heuristic Methods for Ship Routing and Scheduling. PhD-thesis, IMT
IMT-2009-50	Lee, Jihoon	Experimental Investigation and Numerical in Analyzing the Ocean Current Displacement of Longlines. Ph.d.-Thesis, IMT.
IMT-2009-51	Vestbøstad, Tone Gran	A Numerical Study of Wave-in-Deck Impact usin a Two-Dimensional Constrained Interpolation Profile Method, Ph.d.thesis, CeSOS.
IMT-2009-52	Bruun, Kristine	Bond Graph Modelling of Fuel Cells for Marine Power Plants. Ph.d.-thesis, IMT
IMT 2009-53	Holstad, Anders	Numerical Investigation of Turbulence in a Sekwed Three-Dimensional Channel Flow, Ph.d.-thesis, IMT.
IMT 2009-54	Ayala-Uraga, Efren	Reliability-Based Assessment of Deteriorating Ship-shaped Offshore Structures, Ph.d.-thesis, IMT
IMT 2009-55	Kong, Xiangjun	A Numerical Study of a Damaged Ship in Beam Sea Waves. Ph.d.-thesis, IMT/CeSOS.
IMT 2010-56	Kristiansen, David	Wave Induced Effects on Floaters of Aquaculture Plants, Ph.d.-thesis, IMT/CeSOS.
IMT 2010-57	Ludvigsen, Martin	An ROV-Toolbox for Optical and Acoustic Scientific Seabed Investigation. Ph.d.-thesis IMT.
IMT 2010-58	Hals, Jørgen	Modelling and Phase Control of Wave-Energy Converters. Ph.d.thesis, CeSOS.

IMT IMT 2010- 59	Shu, Zhi	Uncertainty Assessment of Wave Loads and Ultimate Strength of Tankers and Bulk Carriers in a Reliability Framework. Ph.d. Thesis, IMT.
IMT 2010-60	Shao, Yanlin	Numerical Potential-Flow Studies on Weakly-Nonlinear Wave-Body Interactions with/without Small Forward Speed, Ph.d.thesis, IMT.
IMT 2010-61	Califano, Andrea	Dynamic Loads on Marine Propellers due to Intermittent Ventilation. Ph.d.thesis, IMT.
IMT 2010-62	El Khoury, George	Numerical Simulations of Massively Separated Turbulent Flows, Ph.d.-thesis, IMT
IMT 2010-63	Seim, Knut Sponheim	Mixing Process in Dense Overflows with Emphasis on the Faroe Bank Channel Overflow. Ph.d.thesis, IMT
IMT 2010-64	Jia, Huirong	Structural Analysis of Intect and Damaged Ships in a Collission Risk Analysis Perspective. Ph.d.thesis CeSoS.
IMT 2010-65	Jiao, Linlin	Wave-Induced Effects on a Pontoon-type Very Large Floating Structures (VLFS). Ph.D.-thesis, CeSOS.
IMT 2010-66	Abrahamsen, Bjørn Christian	Sloshing Induced Tank Roof with Entrapped Air Pocket. Ph.d.thesis, CeSOS.
IMT 2011-67	Karimirad, Madjid	Stochastic Dynamic Response Analysis of Spar-Type Wind Turbines with Catenary or Taut Mooring Systems. Ph.d.-thesis, CeSOS.
IMT - 2011-68	Erlend Meland	Condition Monitoring of Safety Critical Valves. Ph.d.-thesis, IMT.